SAND76-0081
Unlimited Release
UC-21

Laser-Fusion Research Progress Report January-December 1975

Directorate of Physical Research

Prepared by Sandia Laboratories, Albuquerque, New Mexico 87115 and Livermore, California 94550 for the United States Energy Research and Development Administration under Contract AT(29-1)-789

Printed June 1976

Sandia Laboratories

SF 2900 Q(7-73)

When printing a copy of any digitized SAND Report, you are required to update the markings to current standards.

Issued by Sandia Laboratories, operated for the United States Energy Research and Development Administration by Sandia Corporation.

NOTICE

This report was prepared as an account of work sponsored by the United States Government. Neither the United States nor the United States Energy Research and Development Administration, nor any of their employees, nor any of their contractors, subcontractors, or their employees, makes any warranty, express or implied, or assumes any legal liability or responsibility for the accuracy, completeness or usefulness of any information, apparatus, product or process disclosed, or represents that its use would not infringe privately owned rights.

SAND76-0081
Unlimited Release
Printed June 1976

Distribution
Category
UC-21

LASER-FUSION RESEARCH PROGRESS REPORT
JANUARY-DECEMBER 1975

Directorate of Physical Research 5200
Sandia Laboratories
Albuquerque, New Mexico 87115

Printed in the United States of America

Available from
National Technical Information Service
U. S. Department of Commerce
5285 Port Royal Road
Springfield, Virginia 22161
Price: Printed Copy $6.00; Microfiche $2.25

CONTENTS

Page

LASER FUSION (J. B. Gerardo) 9

INTRODUCTION (J. B. Gerardo) 9

HF LASER PROGRAM 10

Electron-Beam-Initiated HF Laser (R. A. Gerber and E. L. Patterson) 10

Pilot-Beam Experiments on the Electron-Beam-Initiated HF Laser (J. M. Hoffman and G. C. Tisone) 15

Transverse-Electron Beam Excitation of an HF Laser (E. L. Patterson and R. A. Gerber) 18

Computer Modeling of Electron-Beam-Initiated H_2-F_2 Laser (J. B. Moreno) 20

Kinetic Studies Related to the HF Laser (M. K. Matzen and M. E. Riley) 21

Stability Studies of Multiatmosphere H_2-F_2-O_2 Mixtures (F. K. Truby) 24

10-Atmosphere H_2-F_2 Laser Experiment (G. N. Hays) 27

Use of Optical Absorbers with HF Lasers (G. N. Hays and G. A. Fisk) 27

Gain Control in Vibrational-Rotational Lasers (J. B. Moreno) 32

Pressure Rundown in the H_2-F_2 Laser (J. B. Moreno) 34

IODINE LASER PROGRAM 34

Mode-Locked Iodine Oscillator (E. D. Jones and M. A. Palmer) 34

Large-Iodine-Laser System (R. E. Palmer and T. D. Padrick) 38

Chemical Kinetic Studies of the Iodine-Photodissociation Laser (T. D. Padrick and R. E. Palmer) 40

NOBLE-GAS-HALIDE LASER PROGRAM 42

High-Power Ultraviolet Lasers (A. K. Hays, G. C. Tisone, and J. M. Hoffman) 42

Spectroscopic Studies of Diatomic Noble-Gas Halides: Analysis of Spontaneous and Stimulated Emission from XeCl (J. M. Hoffman, G. C. Tisone, A. K. Hays, and Joel Tellinghuisen) 47

CONTENTS
(cont.)

	Page
LASER-DEVELOPMENT-RELATED STUDIES	53
Electron Beam Excitation of Neon/D_2 Mixtures (J. K. Rice)	53
Hg-Noble Gas Spectra (J. R. Woodworth)	55
Flashlamp Research (M. A. Gusinow)	56
Xenon-Excimer Formation Rates (J. B. Gerardo and A. Wayne Johnson)	58
Electron-Beam Excitation of Rate Gas Mixtures (J. K. Rice and A. Wayne Johnson)	61
Relativistic E-Beam Energy Deposition in Gases (E. J. McGuire)	62
Gas Discharge Physics (E. J. McGuire)	62
Space Charge Effects in Gas Discharges (E. J. McGuire)	62
Computer Modeling of Traveling-Wave-Excitation in the N_2 Laser (J. B. Moreno)	63
The Characterization and Calibration of Nonlinear Optical Susceptibilities (A. Owyoung)	63
LASER-EXCITATION-SOURCE DEVELOPMENT	66
Long Pulsewidth Electron Beams for Laser Excitation (J. R. Woodworth, J. B. Bagg, and D. L. Johnson)	66
Radically Converging Electron Beams (K. R. Prestwich)	67
Excitation of Rare Gases in a High-Voltage, Electron-Beam-Controlled Discharge (F. W. Bingham)	70
2-MeV, 200-kA Electron-Beam Facility (J. C. Bagg)	71
LASER-FUSION RELATED STUDIES	72
Sandia Glass Laser System (J. P. Anthes)	72
Plasma and Solid Conductivity (J. S. Pearlman)	74
Blast-Shutter Experiment (M. A. Duguay, M. A. Palmer, and R. E. Palmer)	77
REFERENCES	78
PUBLICATIONS	81
PRESENTATIONS	85

LASER-FUSION RESEARCH PROGRESS REPORT

JANUARY-DECEMBER 1975

LASER FUSION

INTRODUCTION

The United States laser-fusion program is a multilaboratory effort, with both government laboratories and privately owned laboratories contributing to the multifaceted program. The Sandia Laboratories laser-fusion program is mainly directed to the development of advanced laser systems suitable for laser-fusion applications. A secondary objective of our laser-fusion program is to explore and develop applications of high-power lasers that are of national interest; this includes, but is not limited to, nuclear weapon simulation and weapon effect studies.

Laser-fusion studies are being pursued on an international scale. The goal of this international program is the production of energy by inertial confinement of laser-heated fusionable materials. Laser systems can now be built which should be capable of determining the scientific feasibility of this energy-production scheme, but a new, more efficient laser system needs to be developed in order for laser fusion to be a serious competitor for commercial power generation. The laser system in a commercial laser-fusion power plant will be required to deliver about 10^5 joules of laser energy in about 1-ns pulses, with a pulse repetition rate of about 100 pulses per second. The efficiency of the laser system will need to be near 10%; the laser wavelength should be in the visible or near-ultraviolet regions; and the system must be reliable and require low maintenance. The Sandia laser-fusion program is directed to the development of the laser systems that are required for both near-term and long-term laser-fusion applications.

A laser that satisfies the criteria for the laser-fusion power plant has probably not yet been discovered; and, if it has been discovered, it certainly has not been demonstrated as possessing all the required characteristics. The near-term goals of our program are: (1) to identify lasers that can be useful for near-term and for long-term laser-fusion applications, (2) to increase the peak-power capability and efficiency of existing lasers, and (3) to develop the technology to increase the repetition rate and reliability of high-power lasers.

During this reporting period, several major advances have been made in our effort to identify, evaluate, and improve high-power laser systems:

1. Laser radiation in excess of 4000 joules and power greater than 10^{11} watts were obtained by exciting a chemical chain reaction in H_2/F_2 mixtures with electron beam. Peak electrical efficiencies greater than 180% and peak chemical efficiencies greater than 11% were realized in this electron-beam-excited HF-laser study. During the next report period, our HF-laser program will emphasize: (1) an accurate evaluation of the laser beam quality that can be obtained with the HF laser, (2) an evaluation of schemes to shorten the pulse width to about 1 ns, (3) development of technology to improve system reliability, and (4) evaluation of the prospects of fast-repetition-rate operation.

2. Also, during this report period, we made several contributions to the identification and evaluation of the newly discovered noble-gas halide lasers. Although this class of laser was discovered less than 8 months ago, we have already obtained 100 joules of laser energy from both KrF (2484 Å) and ArF (1920 Å) lasers. While these lasers have high-gain cross sections, which limit their utility for laser-fusion applications, they may find wide application as photon sources to excite other low-gain lasers. Certainly they will be useful for applications that require lower power than is necessary for laser fusion; for example, laser isotope separation.

3. The iodine laser and the CO_2 laser are the only lasers that can presently be considered as possible high-repetition-rate lasers for laser-fusion studies. We have met all our milestones during this report period in our program to evaluate the capability of the photodissociation iodine laser (1.315 μm). A 7-cm-diameter, 4-m-long iodine-laser amplifier was fully assembled,

and initial tests were begun on this amplifier. This amplifier stores about 100 J of extractable laser energy. A short-pulse oscillator that produces pulses as short as 160 ps (FWHM) also became operational. During the next report period, we will: (1) determine the maximum efficiency of this laser using standard flashlamps as pump sources, (2) evaluate energy extraction, (3) evaluate pulse distortion, and (4) evaluate the effect of anomalous dispersion on beam quality under saturated-gain conditions. Later experiments will focus on improving the efficiency of the laser and on increasing the pulse-repetition rate.

4. The oxygen laser ($^1S \rightarrow {}^1D$ transition) is the most promising known laser for laser-fusion applications. It is possible that this laser will satisfy all of the laser requirements for the laser-fusion power plant. The program to evaluate the capability of this future-generation laser is still in its infancy. We have assembled the pulse-power systems and the diagnostic capability to fully evaluate this promising laser. Detailed studies of different excitation schemes will be accelerated during the next report period.

5. Electron-beam excitation of gas lasers has several characteristics that make this excitation scheme promising for high-power gas lasers. Several different electron-beam configurations and different electrical-system designs are being evaluated for excitation of large-volume lasers. There is probably no single best electron-beam scheme for laser excitation: the electron-beam system must be matched to the particular laser. It is also important to develop technology to improve the reliability and the pulse-repetition rate of electron-beam systems. These efforts will be substantially increased during the next report period.

HF LASER PROGRAM

Electron-Beam-Initiated HF Laser

The second-generation H_2-F_2 laser experiment using REBA was completed and analyzed. Mixtures of F_2, O_2, and H_2 at pressure ratios of 1/0.3/0.25 with F_2 pressures up to 800 torr were initiated with the REBA electron beam, and a parametric study of laser emission was performed. In one series of studies, the F_2 and O_2 pressures were held constant while the hydrogen pressure was varied up to stoichiometric. Under some conditions, SF_6 or He was added to the above mixtures. A maximum laser energy of 4.2 kJ was measured at the higher pressures. Chemical and electrical efficiencies of up to 11.4% and 180%, respectively, were obtained. Each of these efficiencies has been found to be dependent upon the gas pressure and composition. The measured laser energy was found to be proportional to the measured electron-beam energy deposited in the gas. Addition of an unstable resonator provided a laser beam with a 4-mrad divergence.

The experimental arrangement is shown in Fig. 1. The operating voltage of the REBA electron-beam machine for this experiment was 2 MeV with 50 kA delivered in a 70-ns FWHM pulse. The electrons, after passing through a 100-μ-thick titanium anode, passed through a low-pressure (1 torr) drift region and then passed through a 127-μ-thick stainless-steel diaphragm into the laser mixture. The electrons were magnetically guided into the laser cell. It has been experimentally determined that less than 5% of the electron beam energy fails to traverse the bend when using this magnetic injection scheme. A magnetic field of 3 kG was used to guide the electrons from the REBA diode to the far end of the laser cell. A transverse magnetic field near the far end of the laser cell guided the remaining electrons into the wall of the laser cell, thus preventing window damage by the high-energy electrons. The stainless-steel laser cell has an active length of 185 cm. The diameter of the cell is 14.9 cm, giving an active volume of 32.3 liters. A rupture foil separated the laser cell from the pressure relief tank. The foil was burst by the pressure pulse produced during the chemical-chain reaction. The pressure relief tank was evacuated through a soda-lime trap to remove the excess F_2.

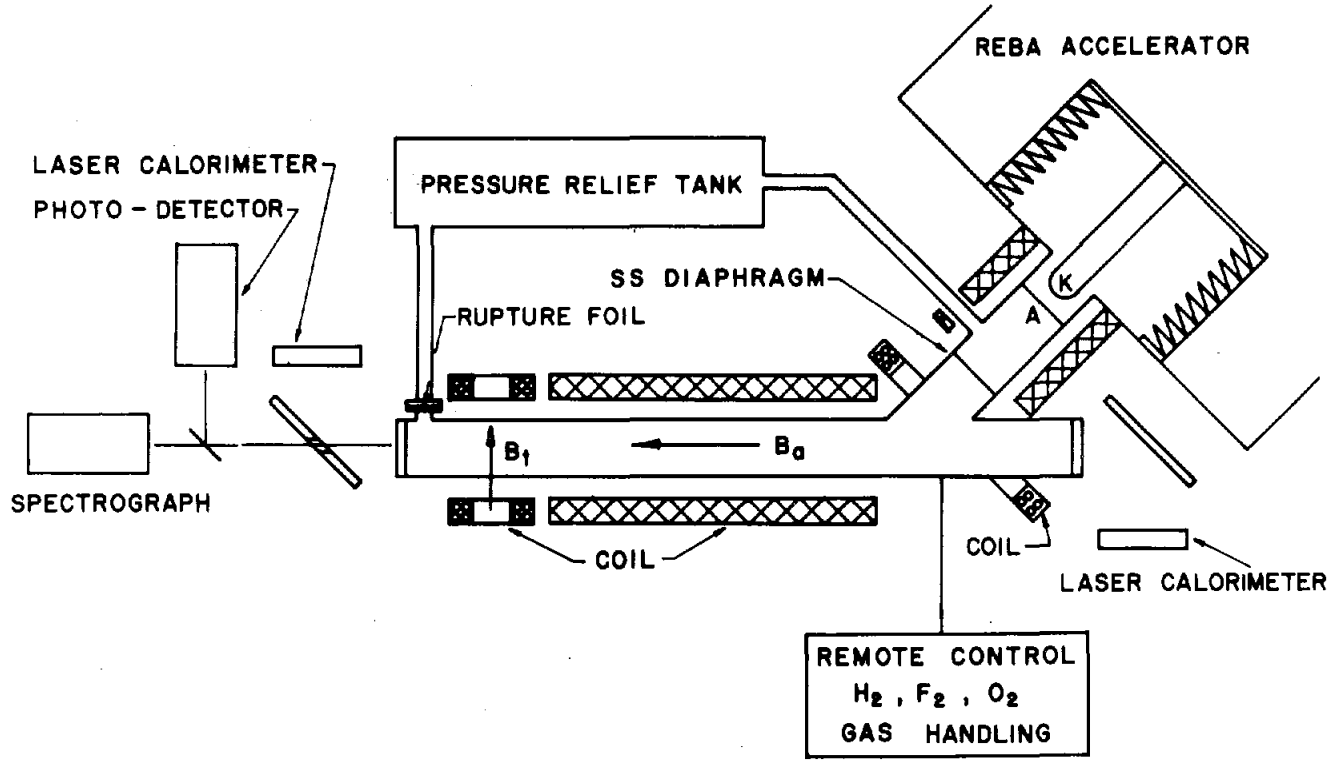

Fig. 1. Schematic diagram of the experimental apparatus.

A remotely controlled gas-handling system was used to evacuate the laser cell (10^{-6} torr), for passivation with fluorine, and to fill the laser cell with F_2, O_2, H_2, and other gases before each shot. Fluorine gas pressures up to 800 torr was added first; this was followed by SF_6 or He (when used), which in turn was followed by oxygen. Oxygen was used to reduce spontaneous explosions during the mixing process. Hydrogen was turbulently injected through four separate fill lines shortly before the accelerator was pulsed.

Four different optical arrangements were used. For most of the experiments, a planar high-loss cavity was formed using flat sapphire windows as indicated in Fig. 1. In one series of experiments, unstable optics were used on the cell. The confocal-unstable resonator had a magnification of two and a length of 2.5 m. The third configuration consisted of a 10-m radius-of-curvature mirror and a sapphire flat. The fourth arrangement consisted of flat windows on each end mounted on 5-degree wedges to reduce feedback along the optical axis. With this latter configuration, the amplified spontaneous emission was measured.

The laser diagnostics included a measurement of the laser energy from each end of the laser cell using Model 36-0801 Scientech calorimeters. Lucite beam splitters were used to reduce the energy impinging on the calorimeters to prevent damage to the absorbing surface.

Gold-doped germanium detectors with a time response of about 1 ns were used to record the temporal history of the laser radiation. A spectrograph was used to determine the time-integrated spectra. The divergence of the radiation was obtained by focusing a portion of the laser energy onto a segmented carbon calorimeter located at the focal point of a spherical mirror. The angle was obtained from the spot size by using the approximate formula $2\theta \simeq$ spot size/focal length of mirror.

The electron-beam energy deposition was measured using a segmented carbon calorimeter. The electron-beam deposition at each pressure was obtained by subtracting the value of the measured energy at that pressure from the value obtained using 20-torr N_2. With 20-torr N_2 the electron-beam energy was transported through the laser cell with the highest efficiency. The measurements gave an upper bound to the true deposition because any increased scattering to the walls when the pressure is increased is counted as deposition and not as scattering.

Laser energy as a function of fluorine pressure for a fixed F_2:O_2:H_2 pressure ratio of 1:0.3:0.25 is shown by the lower curve in Fig. 2. The upper curve shows the energy measured for mixtures with the same pressure ratios to which 100 torr of SF_6 has been added. The planar cavity was used for all the energy measurements presented here. In general, the unstable resonator and hemispherical cavity yielded 90% as much energy as the planar cavity. The cavity with 5-degree wedges on each end produced 20% as much energy as the planar cavity under the same conditions. Measurements with the unstable resonator were limited to laser energies of 2 kJ and less because of damage to the convex mirror at the higher energies.

As shown by the lower curve in Fig. 2, the laser energy initially increases nearly linearly with pressure. Calculations predict that the energy should increase with pressure as long as the rate of dissociation increases proportionally with pressure and the percentage of dissociation remains constant. The electron deposition for the conditions shown in Fig. 2 is shown by the curves in Fig. 3. The lower curve of Fig. 3 demonstrates that within experimental error, the deposition is linear for equivalent F_2 pressures up to 800 torr. The fact that the laser energy shown by the lower curve of Fig. 2 begins to level off at the higher pressures is because the laser pulsewidth plus the initial delay time is decreasing. Therefore, at the higher pressures, some of the electon-beam energy is not deposited until after the termination of the laser pulse.

The upper curve of Fig. 2 indicates that the laser energy saturates abruptly at about 4 kJ for F_2 pressures above 400 torr. This result can be understood by using the energy deposition curves of Fig. 3. When 100 torr of SF_6 is used with the mixture using 500 torr of F_2, 3.3 kJ of electron beam energy is deposited in the gas. Increasing the mixture pressure to the value corresponding to 800 torr of F_2 increases the deposition only slightly because there is a total of only 3.8 kJ of beam energy available for deposition. This result suggests that the effect

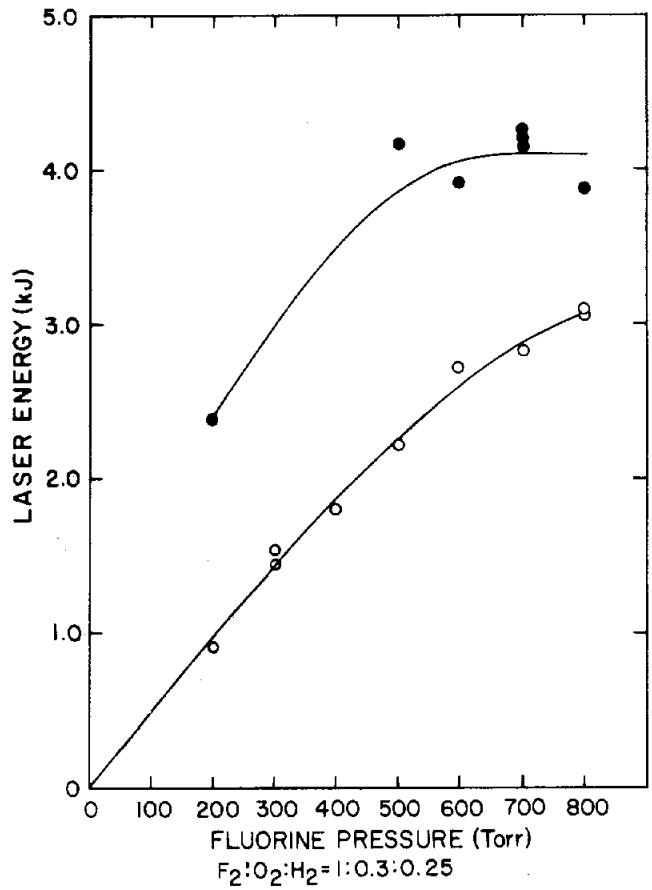

Fig. 2. Laser energy as a function of fluorine pressure with a composition of F_2:O_2:H_2 equal to 1:0.3:0.25. The lower curve is for data when no SF_6 was used; the upper curve represents data when 100 torr of SF_6 is added to each mixture.

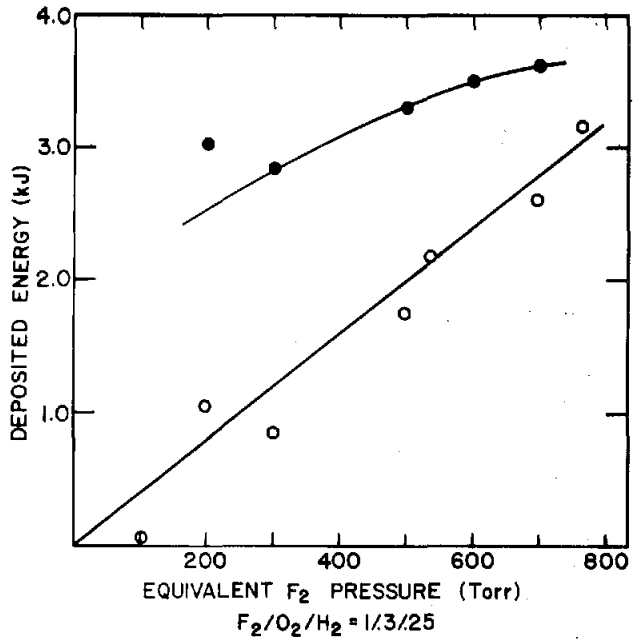

Fig. 3. Electron-energy deposition measurements for the same conditions as those in Fig. 2. Nitrogen, at the same density as that of $F_2 + O_2 + H_2$, was used to simulate the laser mixture.

of adding SF_6 is to increase the energy deposited in the gas. This conclusion is supported by the observation that the increased laser energy when 100 torr of SF_6 is added corresponds to the increased energy deposition. For the F_2:O_2:H_2 mixtures with no SF_6, the laser pulsewidths (FWHM) decreased from 42 ns to 20 ns as the F_2 pressure was increased from 200 to 600 torr. The pulsewidths from 600 to 800 torr remained constant at about 20 ns. The pulsewidth using 100 torr of SF_6 was about 5 ns longer than those without SF_6 for a given F_2-H_2 mixture.

In order to show that the observations were the same with and without SF_6, except for the change due to the increased electron-beam deposition, the SF_6 pressure was varied at constant F_2, O_2, and H_2 pressures of 500, 150, and 125 torr, respectively. These data are shown by the upper curve in Fig. 4. The laser energy increases with SF_6 pressure up to 100 torr where the energy saturates at about 4 kJ. The effect of adding SF_6 to this mixture is to increase the laser energy by a factor of 1.9. The electron-beam deposition, given by the lower curve in Fig. 4, shows that the increase in energy deposition with 100 torr of SF_6 is a factor of 1.8 higher than that with no SF_6. The laser energy evidently saturates when all the available e-beam energy is deposited in the gas. Figures 2, 3, and 4 show that the laser energy obtained in this experiment correlates with the amount of electron-beam energy that can be deposited. Adding SF_6 increases the deposition rate which, in turn, increases the number of fluorine atoms produced by the electron beam.

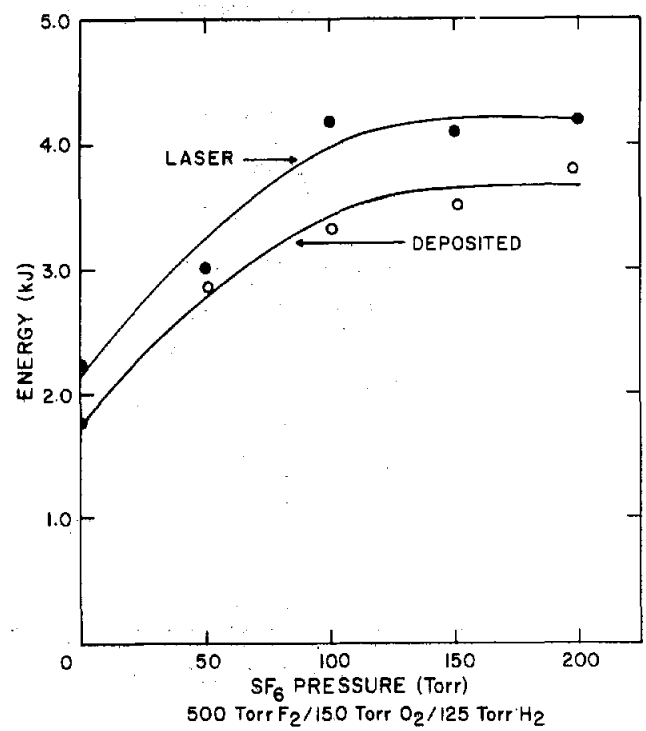

Fig. 4. Laser energy and deposited electron-beam energy as a function of SF_6 pressure for a mixture of 500 torr F_2, 150 torr O_2 and 125 torr H_2. Deposited energy was measured with the given pressures of SF_6 and a nitrogen density equal to the $F_2 + O_2 + H_2$ density.

The divergence angle of the laser radiation for three different optical arrangements is shown in Fig. 5. Because of the material blow-off of the calorimeter, which can permit heat transfer between individual elements, these measurements give an upper limit to the divergence. The occurrence of blow-off also makes absolute energy measurements impossible. The full angle at half maximum is about 35 mrad for the planar and hemispherical cavities and about 4 mrad for the unstable resonator. It is apparent that this laser with its high gain and specific energy (> 60 J/ℓ) is effectively controlled by feedback optics.

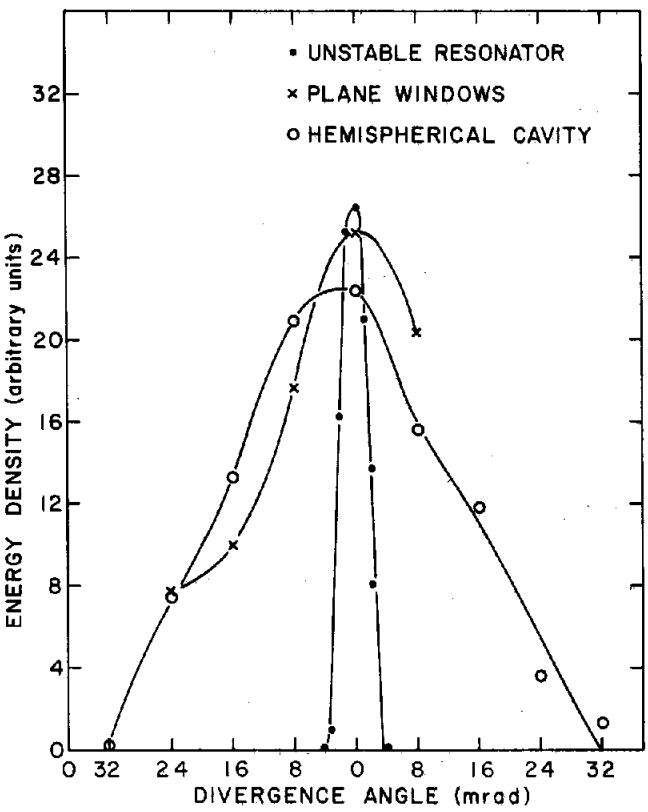

Fig. 5. Energy density as a function of divergence angle for three different cavity configurations.

The time-integrated spectra were obtained at various pressures and concentrations. Because of the high laser intensity, it was difficult to accurately separate some of the transitions, but a minimum of 40 were observed. The spectra did not appear to change drastically when SF_6 was added or when the hydrogen concentration was varied. P_1, P_2, P_3, P_4, P_5, and P_6 transitions were observed. The majority of the energy was contained in P_1, P_2, and P_3 transitions.

In this study, one of the objectives was to determine the energy scalability of the HF laser. Of primary importance are the electrical and chemical efficiencies of such a laser. The electrical efficiency as used here is defined as the ratio of the laser energy output to the electron-beam energy deposited in the lasing medium. The chemical efficiency is defined as the percentage of the total available exothermic energy contained in the laser tube (based on the hydrogen content) that appears as laser radiation.

Figure 6 shows the chemical and electrical efficiency for a fluorine pressure of 300 torr and an oxygen pressure of 90 torr. A chemical efficiency of 11.4% was attained at a hydrogen pressure of 10 torr. This value represents the highest chemical efficiency reported for a pulsed laser operating on the H_2-F_2 chain. As the hydrogen pressure is increased, the chemical efficiency decreases to a value of about 1% when the mixture is stoichiometric. The electrical efficiency increases to 180% for a stoichiometric mixture.

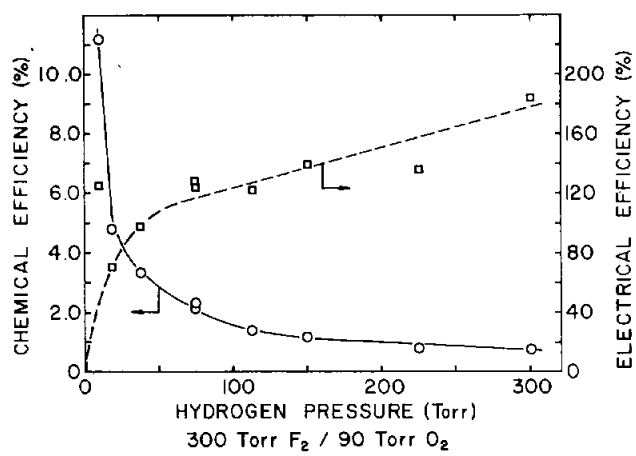

Fig. 6. Chemical and electrical efficiencies as a function of hydrogen pressure with 300 torr F_2 and 90 torr O_2.

The chemical and electrical efficiencies as a function of laser energy are shown in Fig. 7. All the data in Fig. 7 are for an F_2:O_2:H_2 pressure ratio of 1:0.3:0.25. The data shown by the open circles are for mixtures without SF_6, and the solid points are those in which 100 torr of SF_6 was used. The lower graph shows that the electrical efficiency is constant at about 110% for these conditions. This shows that, for a given F_2, O_2, and H_2 mixture, the laser energy depends strongly on the amount of energy that can be deposited in the gas. The chemical efficiency, as a function of laser energy, is shown by the upper graph. Since the chemical efficiency is based on the hydrogen content, adding SF_6 to the mixture increases the chemical efficiency, because it increases the laser energy. The most dramatic improvement in chemical efficiency with added SF_6 is in those cases where not all the electron-beam energy is deposited in the gas. The efficiency in this case is about 5%. The efficiency with no SF_6 is about constant at 2%. The conditions shown in Fig. 7 have not been optimized for either efficiency. However, this graph does show that, as the energy is scaled up, the efficiencies remain nearly constant. This implies that laser energy could be scaled up by using a more energetic electron beam.

Pilot-Beam Experiments on the Electron-Beam-Initiated HF Laser

Recent HF laser experiments have shown that it is possible to obtain multikilojoule output optical energies in about a 20-ns pulse from electron-initiated mixtures of H_2 and F_2. The preceding report demonstrates that it is possible to produce an output beam of low divergence using an unstable resonator configuration. However, a major problem limits the use of an unstable resonator in a high-power laser: damage to the output coupling mirror of the resonator. If an HF laser is to be developed into a system for irradiation of fusion targets, higher power and shorter pulses than presently available must be produced. The only approach in which it appears possible to achieve energies greater than 10^4 joules in a 1-ns pulse is the Master Oscillator-Power Amplifier (MOPA) system. This technique is well established for Nd-glass and CO_2 lasers, but it has not been used on a high-gain, high-power, multiline laser such as HF. The development of a MOPA system for a high-gain system which does not store energy requires an understanding of the extraction of energy from an amplifier.

A computer model of the HF laser, developed here recently, has been used to investigate the extraction of energy from an HF amplifier using a low-power quasi-cw multiline oscillator. The results of this study indicate that use of a quasi-cw multiline oscillator with a total incident intensity of 10^4 watts cm^{-2} can substantially suppress backward radiation (backward radiation is defined as the radiation leaving the amplifier opposite to the direction in which the oscillator beam is propagated). Although the model cannot predict the divergences of the forward output beam, it is assumed that it will be essentially the same as the divergences of the oscillator optical beam.

For the purposes of the present study, the electron-beam-initiated HF laser described in the previous report was configured to operate as an amplifier. The amplifier had 15-cm-diameter sapphire windows with normals tilted 5 degrees from the laser axis to reduce feedback which might cause parasitic oscillations. The experimental arrangement for the MOPA experiment is shown in Figs. 8a and 8b. The HF oscillator shown in Fig. 8a was a commercially available laser operating with a mixture of H_2 and SF_6. The output of this laser is 0.5 to 1.0 joule in a pulse lasting 300 to 400 ns. The output spectrum consisted of 17 different vibrational lines: $P_1(3)$-$P_1(8)$, $P_2(3)$-$P_2(8)$, and $P_3(3)$-$P_3(7)$. The oscillator beam had a diameter of 3.8 cm and a divergence of 5 milliradians when the oscillator was operated with a stable resonator. The oscillator output was propagated into the amplifier using the series of mirrors shown in Figs. 8a and 8b. The distance from the oscillator to the input window of the amplifier was 11.5 m, and the oscillator

beam was allowed to diverge over this distance. The oscillator beam was 10 cm in diameter at the entrance to the amplifier. The amplified oscillator pulse in the forward direction and the amplified spontaneous emission (ASE) in the backward direction were monitored by the Au-Ge detectors shown in Fig. 8a.

The laser energy in the forward direction and that in the backward direction were measured using quartz beam splitters and calorimeters as indicated in Fig. 8b. In some measurements the calorimeter measuring the extracted energy in the forward direction was moved 2.5 m away from the amplifier output window. In this case, the energy from ASE was reduced because of its large beam divergence.

In order to determine the effect of the oscillator beam on the energy propagating in the forward and backward directions, measurements were made at the same gas mixture

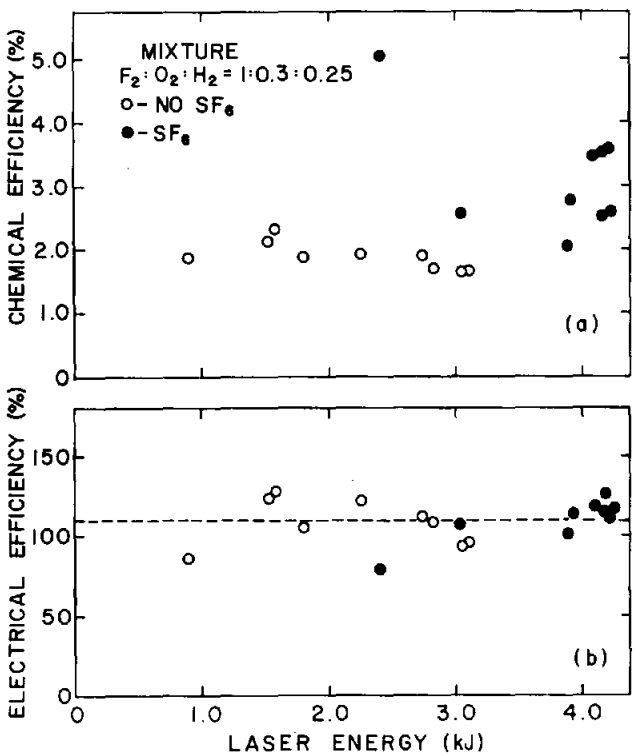

Fig. 7. Chemical efficiency (a) and electrical efficiency (b) as functions of laser energy.

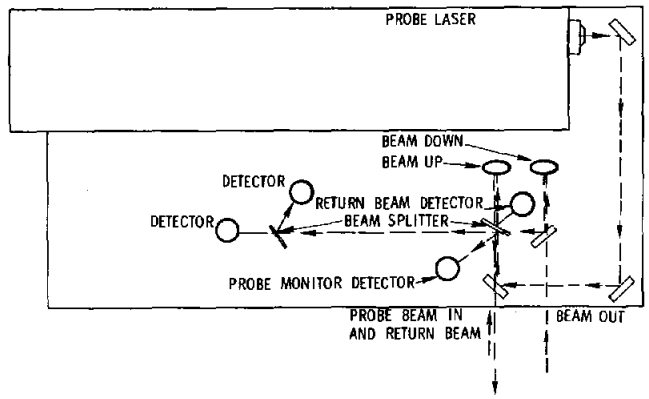

Fig. 8a. Diagram of laser probe-amplifier experiment. In 8(a) the beam from the probe laser is monitored and is reflected to change the height by several feet before entering the electron beam cell. Partial reflectors, and the detectors monitor the probe laser, the amplified beam, and the return beam.

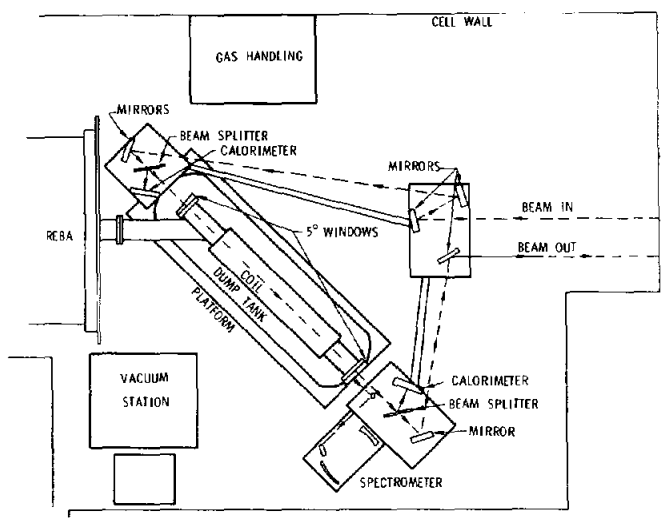

Fig. 8b. Diagram of laser probe-amplifier experiment. In 8(b) the path of the probe beam is shown. Forward and backward components from the amplifier are monitored by the beam splitters and the calorimeters.

with and without the oscillator. The difference between these two measurements was taken to be the energy extracted from the amplifier by the oscillator.

The energy extracted from the amplifier by the oscillator beam is shown in Fig. 9. The data marked E_{total}^{ASE} indicates the total energy (forward + backward) of the amplified spontaneous emission with no incident oscillator beam. These data were obtained with the sapphire window tilted 5 degrees from the normal. For an F_2 pressure of 400 torr and an optical cavity consisting of two parallel sapphire flats, a total energy of 1800 joules was obtained. This may be considered to be the total extractable energy which is generated in the amplifier.

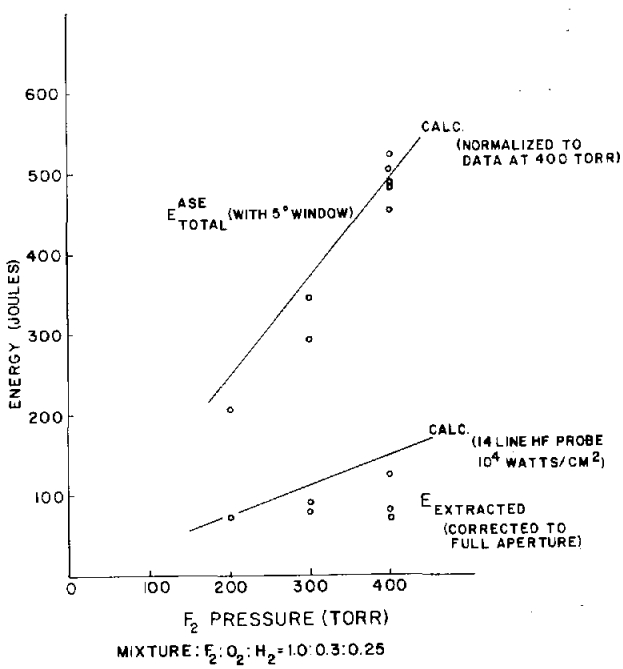

Fig. 9. Amplified spontaneous emission and probe extracted energy. The experimental points are shown by the circles and the theoretical prediction by the solid lines.

The lower data points indicate the energy extracted by the oscillator beam. These data have been scaled (by a factor of 2) to the full aperture of the amplifier so that a comparison can be made with the model calculations. Some data were taken with the amplifier windows tilted ~ 45 degrees to the laser axis. This gave a smaller input aperture, and the resulting data indicated that scaling to the full aperture was valid. Also shown in Fig. 9 are the calculations of the energy output with and without the oscillator beam. The calculations have been normalized to the total ASE at 400 torr F_2. With this normalization there is reasonable agreement between the model calculations and the experimental data. The experimental data for the energy extracted by the oscillator beam fall below the calculations at fluorine pressure of 400 torr. This disagreement between the model calculations and the data could be due to parasitic oscillations in the amplifier. Additional experiments will be required to determine whether this is a problem.

While we do not fully understand the experimental results, they do show that it is possible to use a low-power quasi-cw oscillator to extract energy from a large high-gain HF amplifier, and that the divergence of the amplifier beam is nearly the same as that of the oscillator. This latter observation was made using burn patterns. A comparison between normalized model calculations and experimental data shows reasonable agreement with the F_2 pressure dependence on the energy extracted from the amplifier. With only vibrational lines from the $v' = 1$, $v' = 2$, and $v' = 3$ levels contained in the oscillator output, the efficiency of energy extractions is estimated to be about 6%. This estimate is based on the assumption that the extractable energy is 1800 joules for an F_2 pressure of 400 torr. The model calculations indicate that, if a low-power (~ 10^4 watts cm^{-2}) quasi-cw oscillator with 77 lines from the $v' = 1$ through $v' = 6$ levels were used to extract energy, 23 percent of the generated energy could be extracted from the amplifier.

Transverse-Electron Beam Excitation of an HF Laser

All HF lasers at Sandia have thus far used axial electron beam excitation, where the electron beam travels parallel to the optical axis. An experiment is in progress to study the relative efficiency of transverse excitation. In this geometry the electron beam is injected into a high-pressure laser cell in a direction transverse to the optical axis. Figure 10 shows a schematic representation of the geometry used to study electron-beam deposition and the effects of an externally applied magnetic field on beam propagation. The 893 electron-beam accelerator was used for these studies. The cathode, which is shown here in cross-section, is 50 cm long. Either 25-, 50-, or 75-μm-thick titanium foils were used for the anode. The high-pressure-window support structure had a geometrical transmission of 85%. It consisted of a series of openings 2.5 cm wide by 7.5 cm high, separated by supports which were 1.2 cm long in the beam direction. The window was made of 125-μm-thick stainless steel. Each calorimeter array consisted of twenty-six 2.5- x 2.5-cm calorimeter elements, arranged in a straight line. The arrays could be arranged on a cylindrical surface bounding the laser volume or they could be positioned in a rectangular configuration which could be moved along the e-beam axis. The wall thickness of the stainless-steel cell and diode chamber was designed to allow the magnetic field to diffuse into the diode.

A series of measurements was performed to investigate the effect of the magnetic field on the operation of the diode and on the transmission of the e-beam through the support structure. Figure 11 shows the energy transmitted to the calorimeters located a distance of 3.5 cm from the anode. For these measurements, the gas was nitrogen at a pressure of 0.5 torr. The electron energy was varied from 0.9 to 1.5 MeV. These measurements gave no indication of pinching in the diode. The ratio of the diode current to the critical current for pinching in the diode was 0.36. The top curve shows the measured energy when only a 75-μm-thick anode

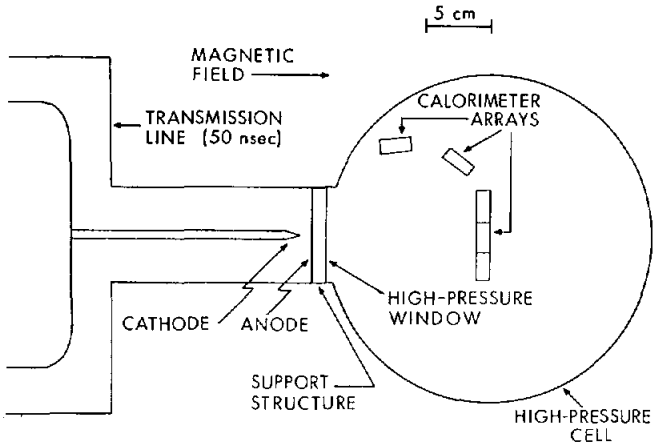

Fig. 10. Schematic representation of a transverse excitation geometry.

foil was used. A magnetic field as large as 2 kG had a negligible effect on the diode operation. The major portion of the increase in measured energy with higher electron energies is due to the diode operating at a higher power level. The middle curve of Fig. 11 gives the measured energy when the support structure was placed behind the 75-μm-thick anode. The data points at an electron energy of 1.5 MeV for a magnetic field of 0 and 2 kG are indistinguishable with or without a support structure. The 50% reduction in measured energy at 0.9 MeV is apparently due largely to the low-energy electrons, scattered by the anode, striking the support structure. A one-dimensional Monte Carlo calculation could not be used to evaluate the losses in the support structure. However, an experimental estimation of the effect of anode scattering on loss in the support structure was obtained by decreasing the anode thickness of 25 μm and measuring the transmitted energy. These measurements were done with both the high-pressure window and the support structure in place. At 0.9 MeV, the measured energy increased by 110%, while at 1.5 MeV the energy increased by 75%. Since the beam-loss in the anode for either thickness is small, it is apparent that anode scattering is a significant factor in the loss associated with the support structure. The lower curve in Fig. 11 shows the energy measured when the

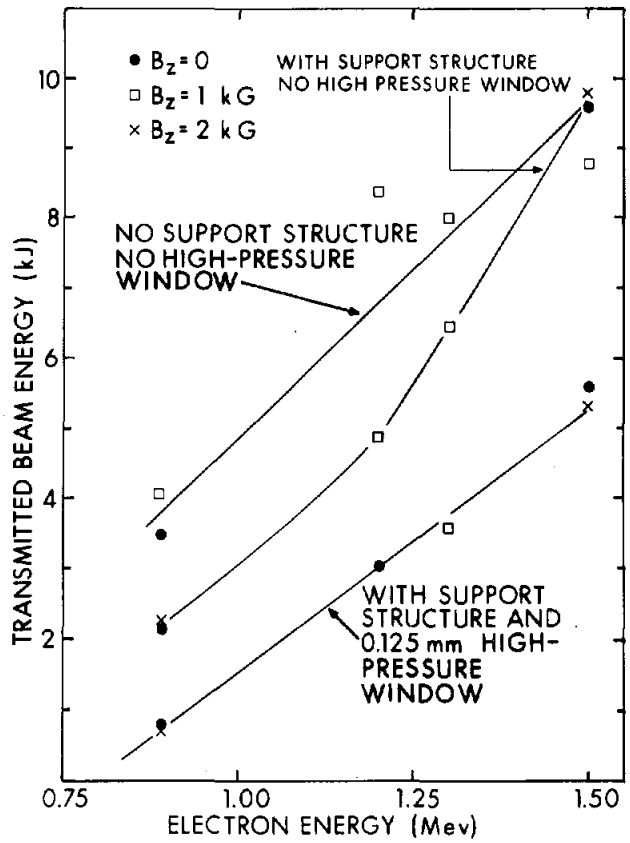

Fig. 11. Transmitted beam energy as a function of electron energy.

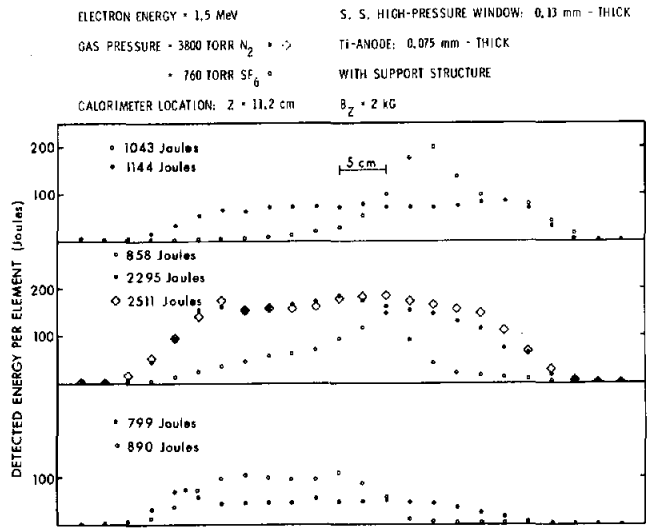

Fig. 12. Energy distribution in a plane normal to beam axis at a distance of 11.2 cm from anode.

high-pressure window was added. The loss introduced by the window at 0.9 MeV is 80% and at 1.5 MeV is ~ 45%. The one-dimensional calculations indicate that, for electrons arriving at normal incidence to the window, the losses should be 65% and 45% for 0.9- and 1.5-MeV electrons, respectively. The large losses measured experimentally are probably caused by the greater loss of energy by electrons with an average angular distribution greater than zero. Some of the discrepancy could also be caused by a portion of the electrons not being collected by the calorimeter. However, the energy distribution, as shown in Fig. 12, indicates that the beam energy density decreases rapidly off the diode axis. An applied magnetic field up to 2 kG did not make a measurable difference in the energy transmittal or in the energy distribution for any of the above conditions.

Figure 12 shows the spatial energy distribution of the electron beam measured at 11.2 cm from the anode. The dots and squares give the energy distribution using 3800 torr of N_2 for different shots. The open circles give the spatial distribution when the cell was filled with 760 torr of SF_6. With nitrogen, the energy is uniformly distributed along the laser axis. However, when SF_6 was used, the energy distribution became very nonuniform and the beam appears to have undergone a rotation about the original beam axis. This behavior may be caused by a rotation of the beam due to j x B forces. However, this same sort of distribution has been observed with SF_6 (at pressures between 1 and 4 atm) whether or not a magnetic field was applied. Conversely, it has never been observed when nitrogen was used (at pressures between 1 and 5 atm) with or without the applied magnetic field. Consequently, the peculiar behavior of the e-beam when SF_6 is used is probably caused by the electrical characteristics of the gas which can affect space charge and current neutralization of the beam.

The distribution of electron-beam energy along the diode axis is shown in Fig. 13. The dots and crosses are experimentally determined points showing the total energy collected by the calorimeter array. The squares are calculated values using the one-dimensional code and multiplying the result by 0.87 to normalize to the experiment at the surface of the high-pressure window. This adjustment is close to the 0.85 transparency of the support structure. The calculations and measurements at 5 atm of N_2 are in agreement with experimental error. However, there is a large discrepancy when SF_6 is used. The reason for this discrepancy is evidently related to the unusual propagation behavior of the electron beam in SF_6.

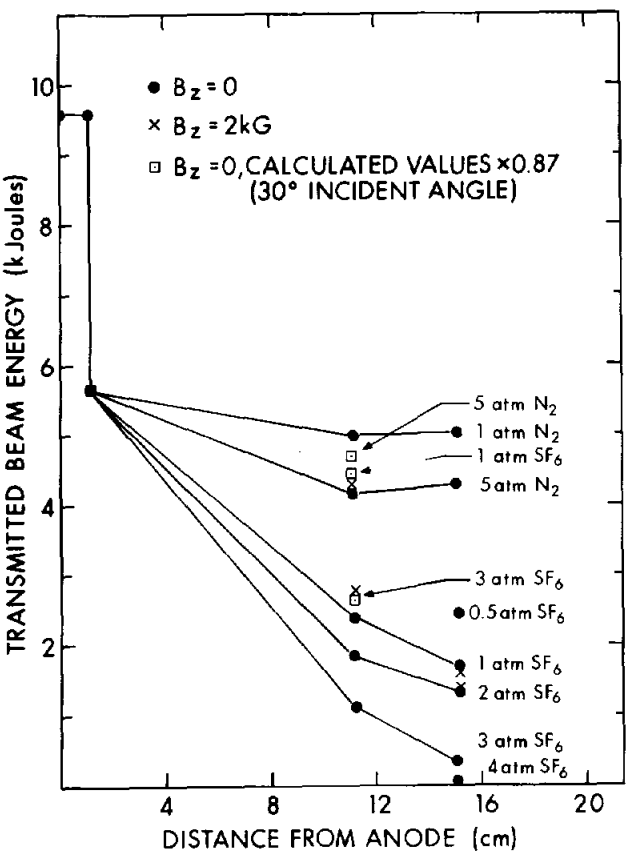

Fig. 13. Transmitted beam energy as a function of position along e-beam axis.

Distributions shown in Figs. 12 and 13 are typical of all those obtained, and the presence of a magnetic field did not significantly affect either the distribution or the total energy arriving at the calorimeter. An evaluation of the relative importance of the beam self-magnetic field and of electron-molecule scattering indicates that, for our conditions, the magnetic field should dominate. For these calculations, the Larmor radius was calculated using the actual self-magnetic field of the beam at its edge and assuming no magnetic neutralization. Since the beam's magnetic field has a maximum value of about 2.5 kG, the external magnetic field of 2 kG should adequately control the propagation. If, in reality, current neutralization were appreciable, the external magnetic field should dominate more strongly.

Following the electron-beam deposition measurements, HF laser experiments using SF_6 and H_2 will be done. Laser energy and thus electrical efficiencies will be obtained. These measurements will allow us to compare transverse and axial geometries for HF laser initiation. The results will be useful for other lasers as well.

Computer Modeling of Electron-Beam-Initiated H_2-F_2 Laser

The H_2-F_2 laser code has been improved in several important respects. First, the code has been extended in order to separately calculate amplified spontaneous emission (ASE) and amplified incident (probe) radiation. This makes it possible to predict the performance of the H_2-F_2 laser as an amplifier. Second, the boundary-condition restriction disallowing simultaneous incident radiation and reflecting windows has been removed without approximation. This permits assessment of the effects of regeneration on amplifier performance. Third, the code has been modified to allow incident pulses and pulse trains, in addition to steady incident radiation.

Comparison has been made between the model predictions and the most recent H_2-F_2 experiments at Sandia. The new experiments suggest that the active medium diameter is equal to the tube diameter, rather than to half this value, as previously thought. Such a change introduces a factor of up to four disagreement between predicted and measured output energy. This problem is a matter of current investigation. The trend of the disagreement, with mole fraction of H_2, is reminiscent of that observed in an Aerospace Corporation study where factors of up to 50 disagreement were found (using the RESALE code), under conditions different than considered here. Similar difficulties have been reported by AVCO and TRW. One of the possibilities suggested by these studies is that the influence of rotational-rotational (J-J) lasing may not be negligible. The H_2-F_2 code has been modified to admit lasing on all possible $\Delta J = -1$ transitions, and preliminary results indicate that J-J lasing is not important, at least for the conditions of the Sandia experiments. Another possibility suggested in the Aerospace study was that parasitic oscillations were affecting the measured output energy. Modifications of the H_2-F_2 code, to include the effects of transverse lasing off the tube walls, are presently under way.

In all other respects, agreement between theory and experiment is satisfactory. In the latest experiments, output power spiking is no longer observed, bringing the experimental and predicted time histories into agreement. The experiments show that misaligning the partially reflecting laser windows to suppress regeneration reduces the output energy by a factor of 3; the code predicts 2.6. In the amplifier-probe experiments, theory predicts that the 14-line probe at 10^4 w/cm^2 can extract about 1/3 the nonregenerative output, or about 1/8 the regenerative output. The measured result varies from 0 to about 40% less than these figures, with the difference probably attributable to experimental difficulties. Ten of the fourteen probe lines were sufficiently amplified to be detected, and the calculation correctly identified nine of these ten strongest lines.

Kinetic Studies Related to the HF Laser

The important chemical reactions in the electron-beam-initiated, high-pressure H_2-F_2 chemical laser system are contained in the highly exothermic linear chain reaction:

$$F + H_2 \rightarrow HF + H$$

and

$$H + F_2 \rightarrow HF + F \cdot$$

The chain reaction is initiated by a pulse of F atoms produced by the electron beam, herein referred to as the hot source atoms. The chemical reactions themselves, in turn, continually produce hot H and F atoms by way of their exothermicity. The HF laser modeling calculations usually assume that these H and F atoms thermalize before they react chemically. If thermalization does not occur, one may expect a tenfold increase in the rate constants for the reactions. The purpose of this work is to study the competition between thermalization and reaction of these atoms. Up to the present, experiments have been limited to a determination of the thermalized rates. From this study we obtain an estimate of the increase of the reaction rates due to the hot atoms and assess the importance of the enhancement caused by the hot source atoms as opposed to the effects of the hot atoms produced by the chemical reactions.

To study these effects, we solve the Boltzmann equation for the distribution functions of the H and F atoms. In order to solve this rather recalcitrant system, we must make some simplifying approximation. First, we assume that all distribution functions are homogeneous and isotropic. Classical trajectory calculations are used to calculate the reaction cross sections as a function of the relative collision velocity. The trajectories are also used to calculate a probability distribution of relative separation velocity of the products for each reaction. The nonreactive collisions which moderate the hot atoms are modeled through

an energy-dependent rigid-sphere cross section. This energy-dependent rigid-sphere model is determined by requiring its momentum-transfer cross section to agree with that of a realistic interaction potential. We further assume the background gases (H_2, F_2, plus moderators) are Maxwellian at the background temperature. The Boltzmann equation can now be written in a form which is linear in the H and F distribution functions and solved by rather straightforward numerical techniques.

To isolate the effects of the hot atoms produced by the exothermic reactions, we assume that the background temperature and the H_2 and F_2 densities remain fixed at their various initial values. With these restrictions, the effective reaction rates approach quasi-steady-state values (hereafter referred to as SS) which are independent of the initial F-atom energy and depend only upon temperature and mole fraction of the mixture. The SS distribution function for the F atoms in an equimolar background of H_2 and F_2 at a total density of 10^{20} molecules/cm^3 and T = 300 K is compared with its corresponding Maxwellian distribution in Fig. 14. The "hot tail" of the F-atom distribution at this SS limit reflects the continuous production of hot H and F atoms by the chain reaction.

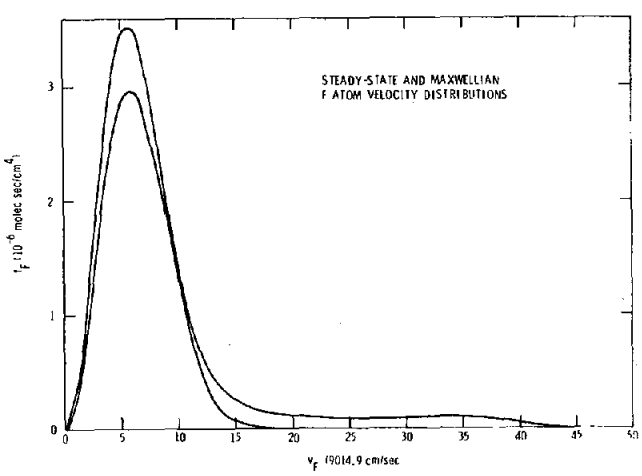

Fig. 14. The quasi-steady-state distribution of F atoms compared with a Maxwellian of the same density (0.219/cm^3) and background temperature (300 K). The H_2 and F_2 densities are 5×10^{19}/cm^3 (X_{F_2} = 1/2).

From these distribution functions we calculate the SS reaction rates k_F and k_H, as summarized in Fig. 15, for three temperatures. The thermal values of k_F (open circles) are the values of k_F at X_{F_2} = 1, so the increase above this value is due to hot atom enhancement. A similar enhancement of k_H (closed circles) over their thermal values (X_{F_2} = 0) is also shown. We note that these SS rate constants can be completely parameterized as functions of mole fraction and temperature. We further define a scaled quantity R_{HF} which is dimensionally a second-order rate constant and, therefore, defines the rate of production of HF molecules at specified background and atom densities. The SS values of R_{HE} are compared with the scaled thermal production rate in Fig. 16 as a function of temperature and mole fraction. We note that, at 300 K, the SS HF production rate shows nearly a factor of 2 increase over the thermal production rate. This was not as large an enhancement as first expected, but represents an effect which must be incorporated into the model.

To study the enhancement of the reaction rates due to the source F atoms, we allow for the time dependence of the H_2, F_2, and HF densities and their temperature. We also allow for a time-dependent F-atom source. In Fig. 17 we display the time dependence of the HF density for a mixture of H_2, F_2, and O_2 initially at partial pressures of 200, 800, and 240 torr, respectively, and 300 K. The source of the F atoms is taken to be monoenergetic and of the form $S_F = 2 \times 10^5 N_{F_2}$ (atoms/cm^3/sec). Detailed model calculations on the HF laser indicate that the time scale shown encompasses the important laser activity. A simple rate equation model with the thermal reaction rates (T) predicts a slow burn for the system. The burn rate initiated by source atoms of 1 eV and 4 eV as calculated by our theory is consideredly greater. The most surprising aspect of our calculations is the small increase of the 1-eV and 4-eV source atom burn rates over the burn rates calculated using the simple rate equation model and SS reaction rates. Obviously the source-F-atom energies do not play a crucial role

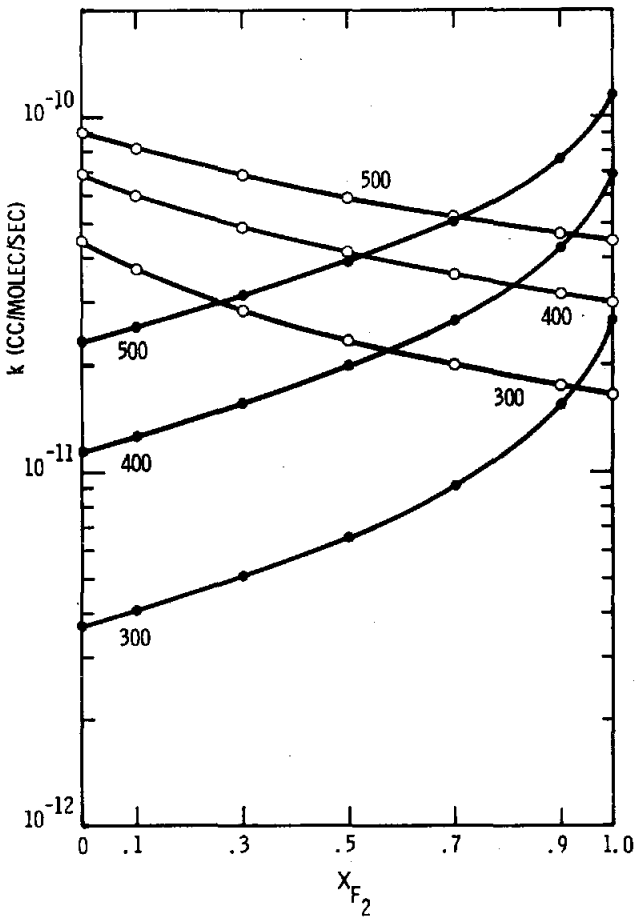

Fig. 15. The quasi-steady-state reaction rate constants as a function of temperature and mole fraction. The number of each curve is the temperature in K. The open circles are labeled k_F and the solid dots are labeled k_H. The $X_{F_2} = 0$ values of k_H and the $X_{F_2} = 1$ values of k_F are the thermalized rates.

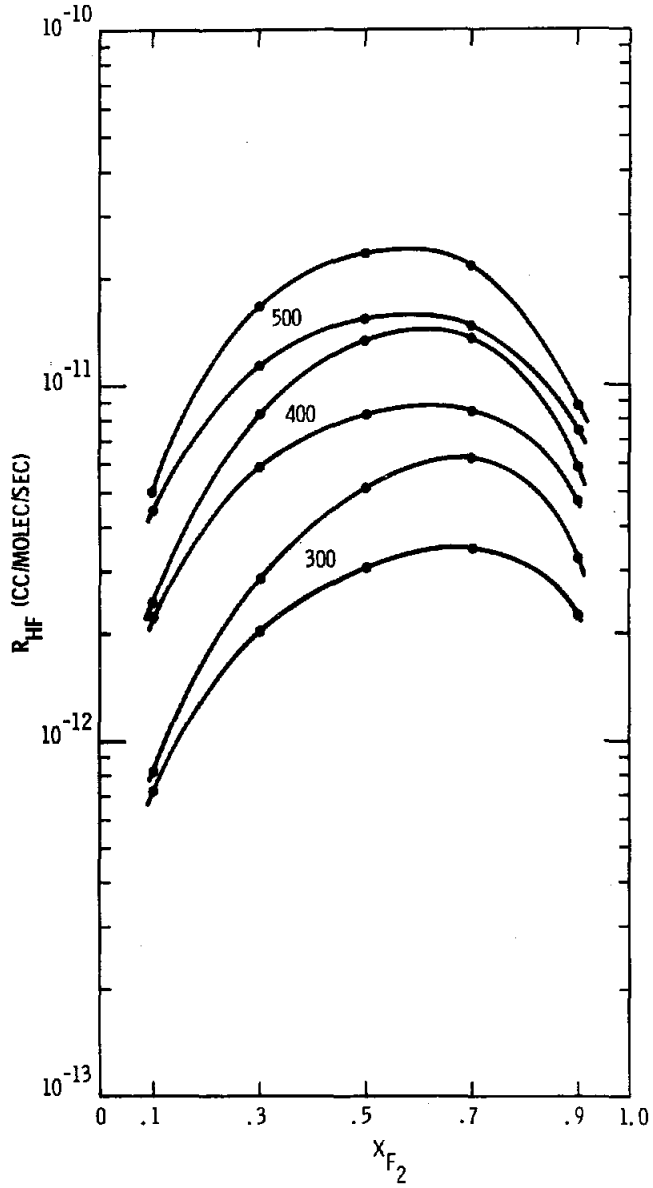

Fig. 16. The scaled rate of HF production as a function of temperature and mole fraction. The numbers between the pairs of curves represent the Kelvin temperature. The upper curve is the quasi-steady-state result and the lower curve is the thermalized result.

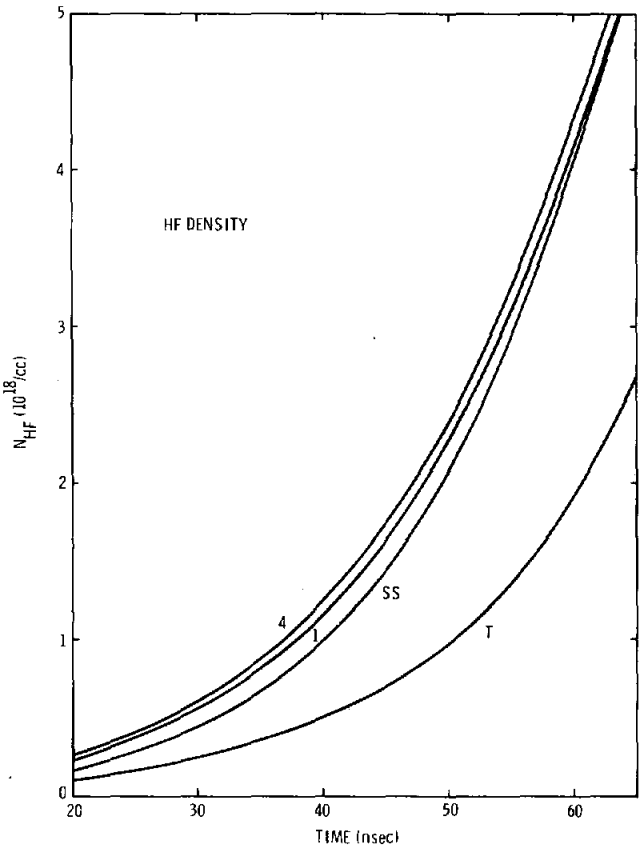

Fig. 17. Time dependence of the HF number density for an initial H_2, F_2, O_2 mixture of 200, 800, and 240 torr, respectively, at an initial temperature of 300 K. The effect of including source F atoms at 1 eV and 4 eV is compared with the thermal (T) and quasi-steady-state (SS) results.

in the non-Maxwellian burn rates for the H_2 and F_2 reactions.

In order to insert the results of our calculations into the kinetic modeling code, we developed a good two-temperature model of the H and F atom kinetics. This two-temperature model was calibrated against our Boltzmann equation solutions. The success of this rather elaborate model enabled us to write the rate constants for the chain reaction as effective functions of temperature and mole fraction.

Stability Studies of Multiatmosphere H_2-F_2-O_2 Mixtures

Extensive investigations concerning the stability of gas mixtures containing hydrogen, fluorine, and oxygen have been conducted. The purpose of this study is to determine procedures that are necessary to achieve short-term stability of these gases for use in high-pressure electron-beam-initiated HF lasers. The study has also established practical explosion limits determined as a function of gas pressure for a wide range of mole fraction of the gases involved. Studies concerning the removal of high-pressure H_2-F_2-O_2 mixtures from an explosion cell chamber without the occurrence of detonation were completed during the period covered by this report. A final phase of this program involves the study of the causes of unexpected detonations occurring at gas pressures lower than the normally observed explosion-limit pressures. As an outgrowth of this latter study, work has been initiated concerning changes in the condition of the explosion cell surfaces, which shift the observed explosion limits to higher pressures.

The mixing chamber used for this study was constructed of stainless steel and has an inside diameter of 15.2 cm and a length of 25 cm. The diameter is essentially identical to that used in some of the electron-beam-initiated HF laser studies being conducted at Sandia Laboratories. Thus, the data obtained in the current gas-mixing study should be applicable to the laser studies, since the heat transfer characteristics for the two sets of experiments are nearly identical.

Gas-mixing data for the case where short-term stability was achieved are shown in Fig. 18. Various partial pressures of oxygen were present as indicated in the figure. The vertical lines at given F_2 pressures indicate that H_2 was added to the F_2-O_2 mixture (already present in the cell) up to a pressure indicated by the horizontal dash at the top of each fill line without the occurrence of detonation. The cell temperature for these measurements was 287±3 K.

The data shown in Fig. 18 represent fill pressures which were actually achieved for various mixing experiments, but do not necessarily represent maximum filling pressures possible for any given oxygen partial pressure. Data presented in Table I, however, show filling pressures achieved which are close to the maximum filling pressures obtained in this study for short-term stability.

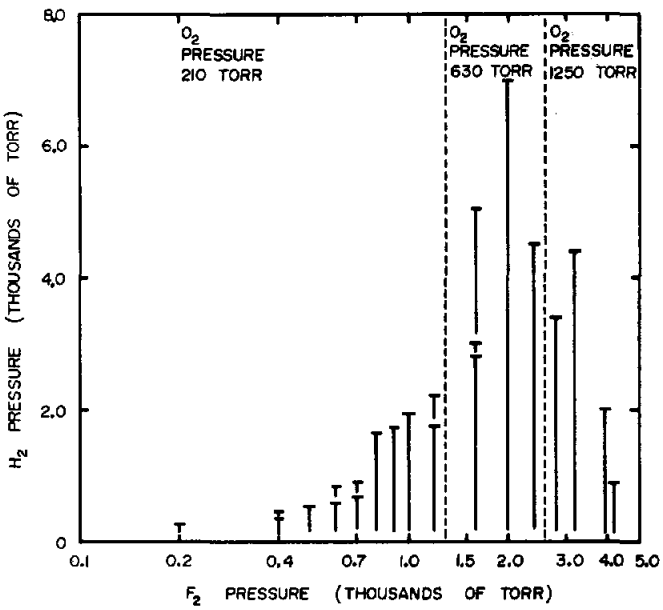

Fig. 18. Hydrogen filling pressures reached without detonation. The H_2 was added to the fluorine at pressures shown where O_2 at pressures of 210, 630, and 1250 torr were present.

TABLE I

High-Pressure H_2-F_2-O_2 Mixtures Which Have Exhibited Short-Term Stability*

$[O_2]$ (torr)	$[F_2]$ (torr)	$[H_2]$ (torr)	Total Pressure (atm)
210	1200	1200	4.75
630	2400	4500	9.91
1250	3900	2000	9.41

*Near maximum values under optimum filling conditions (see text).

If fill pressures of F_2 and H_2 are extended to higher values than those shown in Fig. 18, then, for any given O_2 pressure, detonation of the mixtures will occur. The observed explosion-pressure data are shown in Fig. 19 for various F_2 and H_2 pressures using O_2 partial pressures of 210, 630, 1250, and 2500 torr. Although the data shown in Fig. 2 (taken at 287±3 K) represent an essentially self-consistent set of data, the positions of the whole set of curves can shift, depending upon the purity of the gases and upon the condition of the explosion cell.

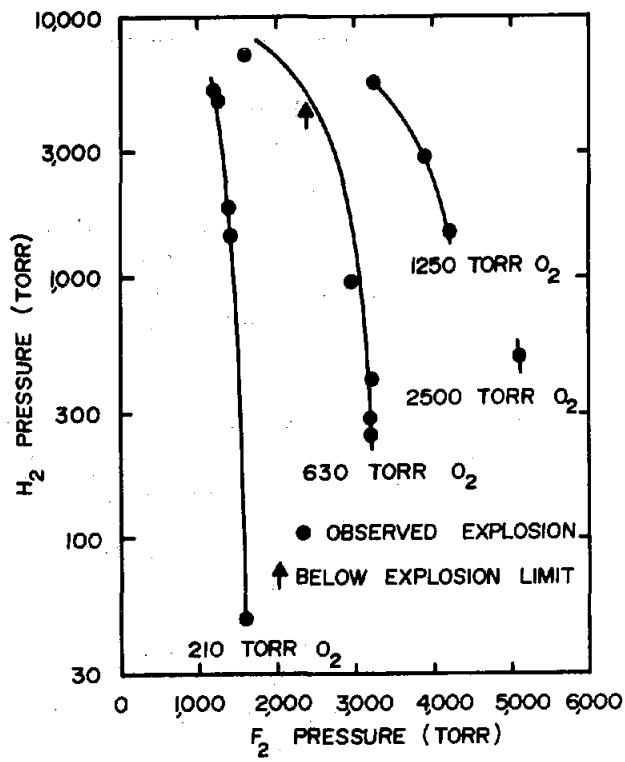

Fig. 19. Observed explosion limits for various O_2 partial pressures. Explosions occur at H_2 of F_2 pressures which lie above or to the right of each of the curves shown.

As seen from the data in Fig. 19, the explosion limits do not increase linearly with increasing O_2 pressure. This observation is more clearly shown in Fig. 20 where explosion limits for various $[F_2]/[H_2]$ ratios are given for F_2 pressure as a

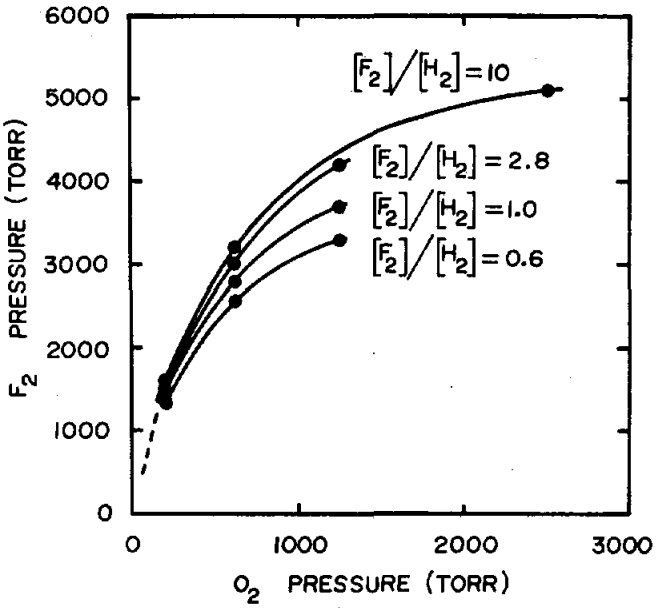

Fig. 20. Observed explosion-limit curves for different $[F_2]/[H_2]$ ratios as a function of F_2 and O_2 pressure. The unstable region is above and to the left of each curve.

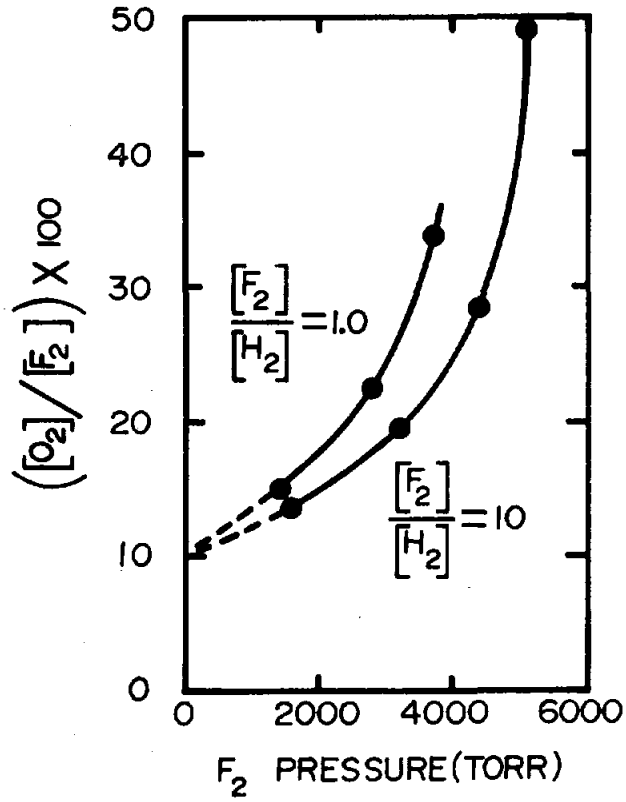

Fig. 21. Observed explosion-limit curves for a stoichiometric mixture $[F_2]/[H_2] = 1$ and for a fluorine-rich mixture $[F_2]/[H_2] = 10$. The unstable region lies below and to the right of each curve.

function of O_2 pressure. The figure shows that, even for the case where small amounts of H_2 are involved, e.g., $[F_2]/[H_2] = 10$, the effectiveness of O_2 in extending the explosion limits to higher F_2 pressures appears to approach a limiting value.

For a given F_2 pressure, the percentage of O_2 required to attain the observed explosion limits occurring for $[F_2]/[H_2] = 1$ is only slightly greater than that required for the case where $[F_2]/[H_2] = 10$. This effect becomes more pronounced at lower F_2 pressures as shown in Fig. 21 by the convergence of the $[F_2]/[H_2] = 10$ curve with the $[F_2]/[H_2] = 1$ curve as the F_2 pressure approaches lower values. Extrapolation of these curves to lower F_2 pressures suggests that the curves could intersect at $[F_2] = 0$ with an O_2 pressure of about $0.1[F_2]$. This extrapolation implies that the stability threshold for H_2-F_2-O_2 mixtures in the present case occurs with a minimum value for $[O_2]/[F_2] = 0.1$. It has been established in the literature that, for lower-pressure work, H_2-F_2-O_2 mixtures can remain stable above the second explosion limit with O_2 concentrations much less than that required in this study. Thus, the mechanism for reaching stability in the present case is not that encountered for stability above the second explosion limit modeled for gas-phase reactions in H_2-F_2-O_2 mixtures. From preliminary studies concerning the shift in the explosion-limit data (shown in Fig. 19) by treatment of the cell surfaces, it is concluded that the explosion limits as shown in Figs. 19 through 21 are associated with surface-initiated detonations rather than gas-phase processes alone.

Studies have shown that it is possible to remove high-pressure H_2-F_2-O_2 mixtures from the explosion cell without detonation, provided that the removal rate be kept below

certain critical values. However, hydrogen-rich mixtures appear to be more stable during removal than mixtures containing equal amounts of F_2 and H_2. Mixtures containing relatively large mole fractions of O_2 do not exhibit a higher degree of stability during pump-out than is observed for mixtures containing only enough oxygen to achieve stability.

This study has previously shown that detonations usually occur at extremely low filling pressures if the cell surfaces are contaminated prior to filling. It has now been determined that the position of the explosion curves as shown in Figs. 19 through 21 can be shifted quite drastically to higher H_2 and F_2 pressures by use of certain procedures in addition to the usual fluorine-passivation treatment. The usefulness of using such techniques to shift the explosion limits to higher total gas pressures for a given absolute amount of O_2 is currently under study.

10-Atmosphere H_2-F_2 Laser Experiment

In order to make the HF laser, or any very-high-gain laser, into a viable candidate for laser fusion, it is essential to provide a short output pulse (~ 1 ns) with a negligible prepulse. One approach to this problem is to tailor a longer pulse using saturable absorbers, electro-optic modulators, or some other fast-acting switch. Another technique is to rely on the chemical kinetics of the H_2-F_2 chain reaction at very high pressures. Calculations indicate that the burn time of this laser should approach 3 to 4 ns at a total pressure of 10 atmospheres, and even shorter times at correspondingly higher pressures. Chemical mixing experiments at Sandia have established the feasibility of obtaining very-high-pressure mixtures of H_2-F_2-O_2 without premature detonation. Experiments currently in progress will measure the laser pulse duration at these pressures with electron-beam-excitation times of about 3 ns.

The laser cell for these experiments is transverse-initiated with a 3-ns-wide electron beam containing 10-12 joules. The lasing volume is about 3 cm^3. Because of the small size of this cell relative to the incoming electron beam, a considerable portion of the e-beam energy is lost as a result of scattering to the cell walls; only about 1/4 or less of the energy is actually deposited in the gas. To accurately determine the energy deposited (using air-SF_6 mixtures to simulate the laser mixture), the scattered component of the e-beam was directly measured using a total stopping calorimeter as a function of total gas pressure. Using a second calorimeter, the total energy lost was monitored at the same time. In order to account for fluctuations in the incoming beam energy (which was typically equal to or larger than the deposited energy), a current probe was constructed to monitor the e-beam current in the drift region before the laser cell. The output was then calibrated against a calorimeter to provide an energy monitor.

The resultant energy deposition as a function of total gas density is shown in Fig. 22. Also shown is the result of a one-dimensional computer calculation. These measurements indicate that 1-2 joules will be deposited in the region of interest. High-pressure fluorine has not yet been introduced into the cell.

Use of Optical Absorbers with HF Lasers

The HF laser is currently being considered as a candidate for controlled nuclear fusion applications. It is thus appropriate to explore avenues which may facilitate construction and/or utilization of a large HF system. Optical absorbers in the HF spectral region, about 2.5 to 4 μm, can be used for two basically different jobs: (1) in low gain systems, absorbers can be used to introduce frequency selective loss within a laser cavity and, hence, control spectral distribution of laser output; and (2) saturable or bleachable absorbers can be used as fast-acting shutters. By way of introduction, we indicate why (1) and (2) are useful applications in the HF system. HF lasers typically radiate energy at many wavelengths in a complicated spectrum. In many applications an output spectrum containing only

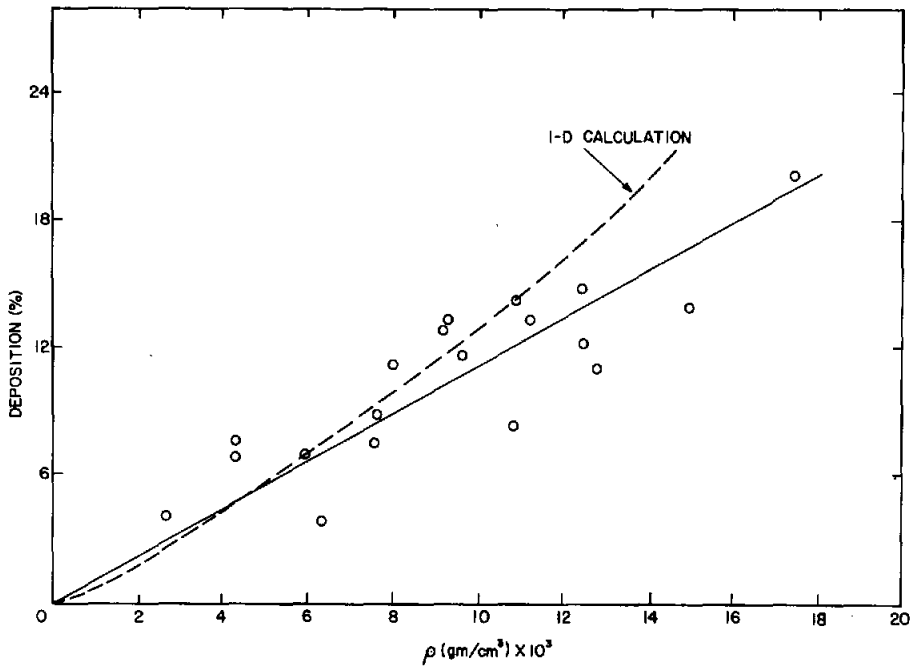

Fig. 22. Energy deposited in the region of interest (3 cm^3) expressed as percentage of incident energy for 440-kV electrons, for gas densities up to 17 mg/cm^3. The solid line is a linear least-squares fit through the origin. The dashed line is a result of a one-dimensional computer calculation.

a few lines is more useful than a many-lined one, especially if it can be obtained without a significant sacrifice in output energy. The rapid rotational relaxation present in even low-pressure HF systems makes it possible to extract laser energy relatively efficiently, even if only one vibration-rotation transition in each active vibrational manifold is allowed to lase. In designing and constructing a large HF oscillator-amplifier system, it will be important to determine the minimum number of lasing lines consistent with efficient operation. Use of optical absorbers for oscillator spectrum control will then allow the development of relatively simple systems operating at the required frequencies. The use of saturable or bleachable absorbers as fast shutters has obvious application. Such absorbers can serve to isolate amplifier stages from one another except during the passage of the pulse of interest, and they can protect the final target from low-intensity radiation preceding the main pulse. Applications (1) and (2) are clearly related: development and use of a large HF laser will, in practice, be simpler if it can be operated with reasonable efficiency on a few selected lines for which bleachable or saturable absorbers can be found.

In order to simplify an HF laser output spectrum, a frequency selective loss may be inserted in the cavity to lower the gain on certain lines below threshold. When an output spectrum containing several lines is required as in the case of the HF laser, the use of intracavity optical absorbers is an attractive technique, whereas single-line operation is generally accomplished with a grating. Ideally, one would add to the cavity a single absorbing species completely transparent to the desired lines and opaque to all others. In practice one is not likely to find such absorbers; one must determine the spectra of many compounds and mix them in appropriate proportions to generate the desired overall effects.

We have determined the absorption spectra of several gases and liquids. Conventional infrared absorption spectra of liquids show rather broad bands lacking in the frequency selectivity necessary for oscillator spectrum control. Spectra obtained using a small HF laser and a monochromator confirmed that liquids are not useful for spectrum control. Conventional infrared absorption spectra of gases are not very useful for this study because they lack necessary resolution, and the intensity information is not often quantitatively interpretable. Consequently, quantitative absorption spectra were obtained using a double-beam spectrometer assembled from standard optical components and using a grating-tuned single-line HF laser as the light source. Spectra were obtained for several gases including CO_2, CH_3OH (methanol), and $(CH_3)_2CO$ (acetone). Figure 23 presents effective cross section, σ_{eff}, for absorption of HF(P_2(4)) radiation as a function of CO_2 pressure at 300 K. The effective absorption cross section is defined by the relation

$$\sigma_{eff} = (n\ell)^{-1} \ln(I_o/I) \quad ,$$

where n is the overall (or bulk) number density in the sample cell, ℓ is the sample cell length, and I_o/I is the ratio of incident to transmitted intensities. The actual molecular absorption cross section is related to σ_{eff} through multiplication by the appropriate partition function. For the data presented in Fig. 23, the CO_2 transition is an R12 and $\sigma_{mol} \approx 30\ \sigma_{eff}$. The pressure dependence exhibited by the data is that expected when the frequency of the probing radiation and that of the absorbing transitions are displaced by more than Dopper width at zero pressure. The zero pressure limit of σ_{eff} is $\approx$ zero, and σ_{eff} initially increases rapidly with pressure as the wing of the broadened CO2 line begins to overlap the HF line. At higher pressures, the CO_2 linewidth is larger than the zero pressure HF-CO_2 line separation. Consequently, the HF line may be regarded as close to the center of the CO_2 line and increasing the pressure further reduces σ_{eff}.

Data similar to those presented in Fig. 23 allow one to determine the loss inserted on various lines when a certain quantity of a

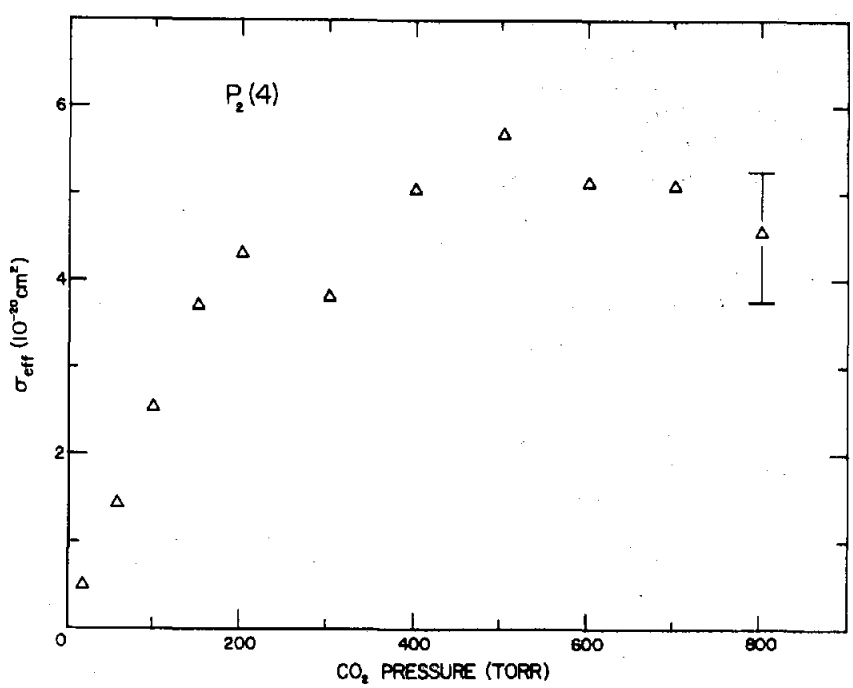

Fig. 23. Effective cross section, σ_{eff}, of CO_2 for absorption of HF (P_2(4)) laser radiation.

gas is placed in an HF oscillator cavity. It is then possible to predict semiquantitatively the resulting change in output spectrum. Rotational relaxation effects make exact prediction of spectrum change with absorber pressure impossible without resorting to elaborate calculations. As a test case, a cell containing CO_2 was placed in the cavity of a small, electric-discharge-initiated HF laser. The laser gas mixture was H_2/SF_6 with He as a diluent. Continuous flow was used, and operating pressure was ≈ 20 torr. The laser operated predominantly on $V = 2 \rightarrow V = 1$ and $V = 1 \rightarrow V = 0$ transitions. The total energy output per pulse in multiline operation was ≈ 150 μJ and the overall pulse-width was about 1/2 μs. Individual lines radiated for shorter times, typically 200 ns. When the laser was operated on a single line through use of a grating, typical small signal gain was ≈ 0.25/cm.

Figure 24 illustrates the variation of σ_{eff} with wavelength and CO_2 pressure and shows the effect on the laser output spectrum of 600 torr CO_2 contained in a 29-cm-long intracavity cell. The spectrum obtained with CO_2 in the cell is simpler than that observed with the cell empty. As expected, the surviving lines are predominantly those with small values of σ_{eff}. It is important to note that, with CO_2 in the absorption cell, much more energy was radiated into the surviving lines than was radiated into these same lines when the cell was empty. This indicates that rapid rotational relaxation feeds energy from transitions below threshold into lines having appreciable gain. Decrease in overall energy output is small, only $\approx 20\%$ in the case shown.

One of the goals of this project was to use optical absorbers to collapse the HF laser output spectrum to essentially one line per vibrational manifold, with only minor contributions from other lines. The data in Fig. 24 clearly indicate that this is not possible using CO_2 alone; for CO_2, the σ_{eff} values are too small for at least three lines in the $V = 2 \rightarrow V = 1$ manifold. Figure 25 shows the effect of an intracavity absorber composed of CO_2, $(CH_3)_2CO$, and CH_3OH.

The two strong lines are $P_1(4)$ and $P_2(6)$ with a minor contribution from $P_2(7)$. Approximately 50% of the total energy radiated in the unperturbed spectrum shown in Fig. 25a appears in the $P_1(4)$ and $P_2(6)$ lines in Fig. 25b. These lines carried only about 20% of the energy in the unperturbed case. As was the case for the data presented in Fig. 23, rapid rotational relaxation channels energy to transitions having appreciable gain so that use of an intracavity absorber to simplify the output spectrum does not entail great intensity loss. An exhaustive study of absorber mixtures was not carried out, and the mixture discussed above was not optimal on two counts.

$$\sigma_{eff}(10^{-21}\,cm^2) = \frac{10^{21}}{nl} \ln\left(\frac{I_0}{I}\right)$$

P(TORR) \ λ(μ)	2.64	2.67	2.71	2.73	2.74	2.76	2.78	2.79	2.83	2.87	2.91
	$P_1(4)$	$P_1(5)$	$P_1(6)$	$P_2(3)$	$P_1(7)$	$P_2(4)$	$P_1(8)$	$P_2(5)$	$P_2(6)$	$P_2(7)$	$P_2(8)$
70						13					
110	~0	5.1				19					
270	~0	8.9	2.1	~0	3.0		2.2	4.2	0.5	~0	~0
600			3.6	0.4	4.9		3.4	5.5	~0	0.1	~0

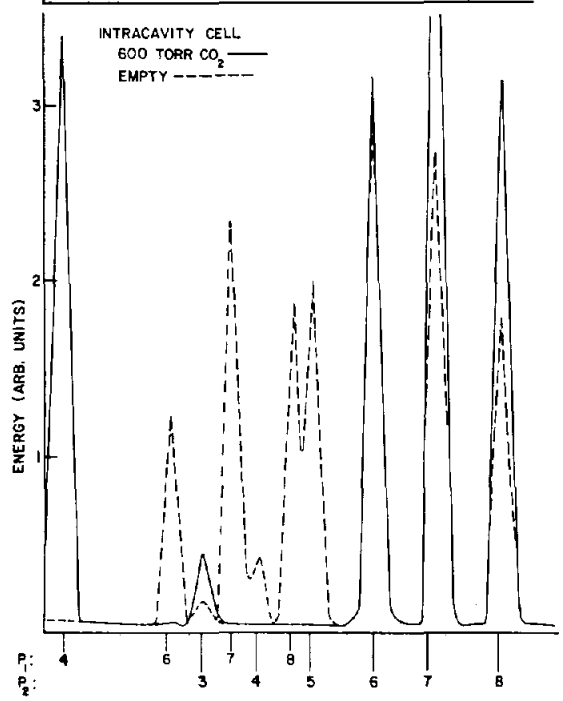

Fig. 24. Dependence of σ_{eff} (CO_2) on wavelength and pressure, and effect of intracavity CO_2 sample on output spectrum of HF laser.

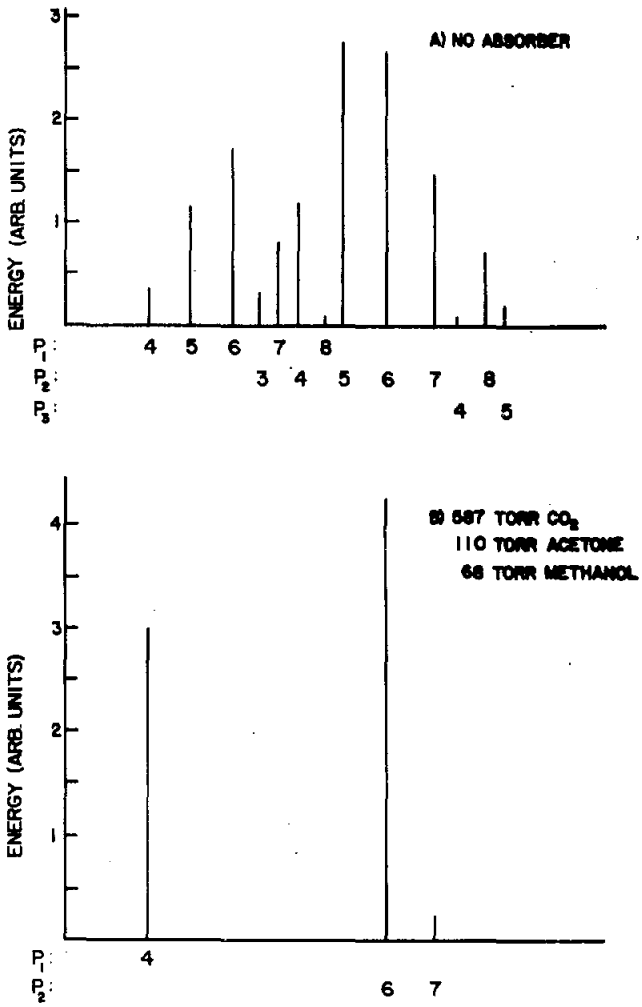

Fig. 25. Effect of intracavity absorber [mixture of CO_2, $(CH_3)_2CO$, and CH_3OH] on output spectrum of HF laser. A) No absorber in sample cell. B) 587 torr CO_2, 110 torr $(CH_3)_2CO$, 68 torr CH_3OH in sample cell. Total output energy for B is approximately 50 percent that for A.

First, not all of the species in the mixture were completely transparent to HF $P_1(4)$ and $P_2(6)$ transitions. Second, rotational relaxation would presumably have more efficiently coupled internal energy into radiation had $P_1(6)$ been chosen as the surviving line in V = 1 V = O manifold.

The technique of using intracavity optical absorbers for HF laser spectrum control has been shown to be feasible. Rotational relaxation is fast enough that the technique does not require the acceptance of severe intensity loss. Use of optical absorbers should prove valuable in designing an oscillator for a large HF laser system based on an oscillator-amplifier chain.

As mentioned earlier, optical absorbers can also be used for isolation of laser amplifier stages and for target protection. In principle, absorbers could also be used in oscillators as Q switches if the relation $\sigma_{mol} > \sigma_{stim}$ could be satisfied, where σ_{mol} is the molecular absorption cross section of the absorber and σ_{stim} is the HF stimulated emission cross section. We have been unable to find any absorber satisfying $\sigma_{mol} > \sigma_{stim}$ and have thus not pursued Q switching. In searching for saturable or bleachable absorbers, one need not be restricted by the inequality above. Rather, one finds that, for a two-stage absorber with very short relaxation time, τ, there is a characteristic saturation intensity I_s defined by

$$I_s = (2\sigma_{mol}\tau)^{-1} \quad . \qquad (1)$$

For incident flux $I \ll I_s$, classical Beer-Lambert absorption is predicted, but for $I \gtrsim I_s$ the absorber will transmit better than predicted by the Beer-Lambert law. The above remarks are valid for $\tau \ll \tau_p$, where τ_p is the incident light pulse length; in this time regime, saturable absorption is observed and the degree of saturation is strictly intensity dependent. For $\tau > \tau_p$, the decrease in absorptivity becomes an energy-dependent effect and a strongly irradiated absorber is said to be bleached rather than saturated.

Liquid and gases have been examined for evidence of saturation or bleaching. The broad-band nature of liquid infrared absorption spectra is a potentially desirable feature when searching for a system which will absorb over the entire HF spectral region. Unfortunately, a broad absorption feature is usually associated with a small σ_{mol}, and vibrational relaxation times are

very short in condensed phases. Reasonable estimates of σ_{mol} and τ, when used in Eq. (1), indicate that I_s would typically be $\geq 10^{14}$ W/cm^2 in the HF spectral region. These saturation levels are too large to be interesting. We found experimentally that, for pure liquids (such as acetone) and for solutions (such as infrared absorbing dyes dissolved in acetone), the Beer-Lambert absorption law was obeyed at low flux levels. At flux levels of about 1 MW/cm^2, deviations from the Beer-Lambert law were observed, but they were attributed to thermal effects. No evidence of saturated absorption was found for any liquid studied. Unless some anamolous transition with very large σ_{mol} and very long τ can be found, it is not worthwhile pursuing liquids further. The type of anomalous transition one might hope to find is a very-low-frequency electronic transition resulting from some solute-solvent interaction. Except for this postulated transition, the solution under investigation must be transparent throughout the HF region.

After eliminating liquids as saturable absober candidates, we initiated a preliminary investigation of gases. A line-by-line approach must be taken with gases because of the narrow absorption features; we relied heavily on our previously determined absorption cross sections in selecting a prototype system for study. CO_2 was the most interesting absorber candidate. As indicated in Fig. 23, $\sigma_{eff}(CO_2)$ for HF radiation is very large for the HF $P_2(4)$ line. Use of data from Fig. 23 and reasonable estimates of τ indicate [from Eq. (1)] that I_s should be in the neighborhood of 1 MW/cm^{-2} for absorption of (HF $P_2(4)$) radiation by CO_2. CO_2 is not a simple two-level system, and the relation $\tau \ll \tau_p$ is not well satisfied, so Eq. (1) can be used only as a rough guide.

A preliminary CO_2 absorption experiment was performed using a Lumonics HF laser in grating-tuned single-line operation on HF $P_2(4)$. By focusing the output, fluxes of ≈ 20 MW/cm^{-2} could be obtained; lower flux levels were obtained by attenuation. A sample cell containing 800 torr CO_2 was placed at the output focus, and transmission was determined as a function of incident flux level. The percent transmission was independent of intensity at low flux levels but increased with intensity at higher flux levels. At the highest intensities obtained, transmission was about 100% greater than is was at low intensity. Higher intensities than so far attained will be necessary to characterize adequately the transmission versus intensity curve for this system, but it seems clear that CO_2 is either a bleachable or saturable absorber for HF $P_2(4)$ radiation. The pressure dependence of σ_{eff} exhibited in Fig. 23, together with the assumption $\tau \propto P(CO_2)^{-1}$, suggests that I_s will increase with CO_2 pressure for pressures $\gtrsim 500$ torr. Thus, pressure is a convenient parameter for control of the intensity at which saturation effects become important.

This work demonstrates that bleachable or saturable absorbers of HF radiation can be found and that saturation effects occur at reasonably low incident intensities. Further work should result in identification of appropriate absorbers for many HF lines, and these absorbers are likely to be simple gases.

Gain Control in Vibrational-Rotational Lasers

As an outgrowth of the rotational-rotational lasing study for the H_2-F_2 laser, a novel technique for gain control has been devised. The diagram shown in Fig. 26 is helpful. The ordinate measures the ratio of adjacent rotational-state fractional populations for a diatomic molecule. The abscissa measures the ratio of adjacent vibrational-level populations. It is assumed for simplicity that $f_{J,V} \approx f_J$. Using the known functional dependence of V-J, P-branch gain, and J-J gain, one can delineate regions of absorption and amplification on the diagram, as shown. The point P represents a typical partially inverted operating condition. Since this is in the J-J absorbing region, irradiation by J-J transition radiation can move the operating point towards P′, thus crossing into the V-J absorbing region. In this way, gain control occurs. An important

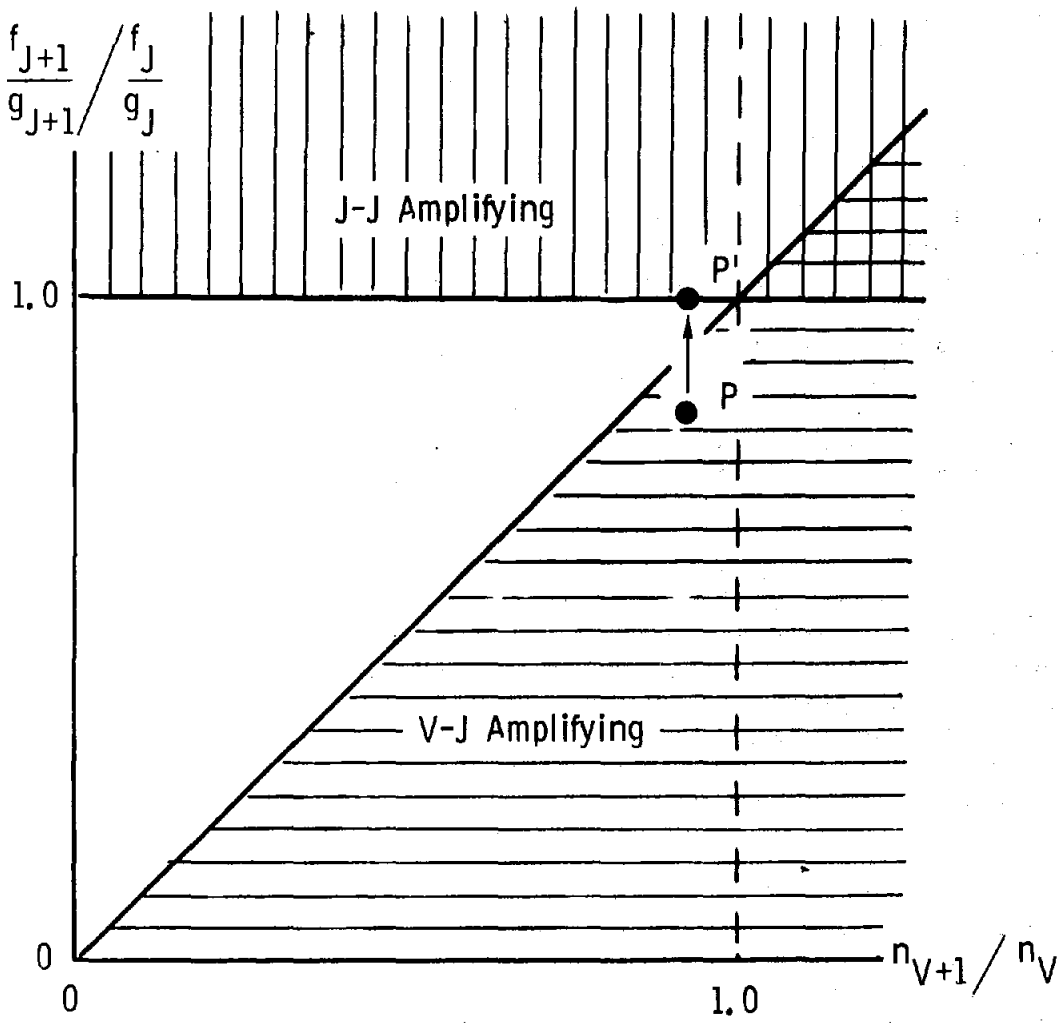

Fig. 26. V-J gain control by J-J irradiation.

consideration is that V-J photons may be much more energetic than J-J photons, so that control is energetically inexpensive. The H_2-F_2 code, modified as described in the previous section, has been used to explore this concept. Preliminary results show a ratio of controlled V-J power-output to J-J power-input in excess of 100.

Pressure Rundown in the H_2-F_2 Laser

The question has arisen as to the effect of various pressure-relief-tank configurations on pressure rundown after burn in the two-pi-irradiated H_2-F_2 laser. Pressure time-histories must be known in order to design electron-beam windows that will not rupture after each burn. Using calculations generated by the two-dimensional code CSQ, pressure rundown has been estimated for a number of dump-tank configurations.

The reaction chamber for the laser is a cylinder of length L and radius R. The electron-beam machines surrounding the laser are annular devices stacked so that their inner radii form the cylindrical wall of the reaction chamber. The H_2-F_2-O_2 mixture within the chamber is ignited by e-beam irradiation to produce a more or less uniform cylinder of HF, F_2, O_2, and minor amounts of other species, at nominally 3000 K and 100-atmosphere pressure. These changes occur in tens of nanoseconds, so that the reacted gas can be considered to be initially motionless. The problem then is to relieve the pressure before it causes the e-beam windows to rupture. Using cylindrical burst diaphragms opening into pressure-relief tanks, one can expect to observe an initial quiescent dwell time, during which the diaphragms open, followed by pressure rundown as the gas expands into the tanks. A number of tank configurations were considered. In all cases, the dump tanks were annular, with cylindrical burst diaphragms at the inner radius constituting part of the reaction-chamber wall. The first scheme places a single tank at one end of the chamber. The second places a tank at each end. A third scheme intersperses tanks and e-beam machines.

The results show that interspersing offers no significant advantage over the simpler configurations, for dimensions of current interest. In either case, the overpressure is relieved in a time of the order of 1 millisecond.

IODINE LASER PROGRAM

Mode-Locked Iodine Oscillator

The first mode-locking experiment on a CF_3I laser oscillator was reported by Ferrar,[1] who observed 3- to 4-ns mode-locked pulses. Subsequently, using similar mode-locking techniques, other researchers achieved mode-locked pulses as short as 700 ps.[2] Since it is estimated that pulsewidths in the 200-ps range are required for laser fusion, research into the problem of generating these pulsewidths by the iodine photodissociation laser was initiated. The following is a discussion of the techniques which have led to pulsewidths as short as 160 ps from a high-pressure oscillator system.

The oscillator system was simultaneously Q-switched and mode-locked. The advantages of such a configuration have been previously discussed.[3] The arrangement for the 1.5-m optical cavity consisted of the following: (1) A planar-planar mirror configuration with an output mirror reflectivity R = 80%; (2) a 0.8- x 100-cm quartz tube with a high-pressure window assembly containing the C_3F_7I-Ar mixture; (3) a pulsed fused-quartz acousto-optic mode-locker (ν = 49.40 MHz); (4) a quarter-wave voltage Q-switch assembly consisting of a KD*P Pockels cell and a Glan polarizer; and (5) an adjustable iris to provide single-transverse mode operation. The windows of the high-pressure quartz-tube assembly were canted at an angle of 0.5 degree from the normal to the lasing axis in order to prevent spurious reflections. All optical components inside the laser cavity had antireflection coatings at 1.315 μm. The two 1.5-cm-diameter, 100-cm-long xenon-filled (40 torr) flashlamps were discharged

in parallel, such that the resulting magnetic field was nearly zero. With the use of the Pockels cell Q-switch, the mode-locked pulse train could be generated for times as long as 50 μs after the flashlamp discharge. Hence, a fast-discharge flashlamp was needed[4] and the flashlamp time was relatively long (FWHM $\sim$ 10 μs). A separate capacitor-discharge power supply unit, operating at a maximum of 25 kV and 5 μF was utilized for each flashlamp. Simmer-current-mode operation was also employed. Pulsewidth data were taken near threshold ($V_t \simeq$ 15 kV).

The acousto-optic mode-locker was operated in a pulsed mode by using a gated rf generator. The gated rf generator was capable of delivering 80 W into 50 Ω with pulsewidths as short as 1 μs. The data presented in this note were taken at an rf power of 20 W and an rf pulse length of about 600 μs. Some laser pulsewidth data were taken at a fixed C_3F_7I-Ar pressure by varying the rf power to the modulator, and these results will be discussed briefly below; however, the majority of the data were taken at a fixed rf power of 20 W. The modulation index θ, as defined in Ref. 5, was measured under pulsed rf conditions and as a function of rf power at λ = 1.318 μ using an Nd;YAG CW oscillator. For example, at an rf power of 20 W, θ = 0.93, while at 80 W, θ = 1.52. At these high rf power levels, the predicted power dependence of $\theta \alpha$ (power)$^{1/2}$ (Ref. 5) was not obeyed. This is presumably due to the effect of exceeding elastic limits in the transducer and/or fused-quartz modulator.

The Q-switch assembly was operated in such a manner that a small amount of prelasing occurred before the Q-switch was triggered. This mode of operation is necessary for generating a stable pulsewidth for the mode-locked pulse.[3,6]

The energy content of the laser pulse was measured using a Molectron J3-05 pyroelectric energy monitor. The temporal behavior of the mode-locked pulse train was recorded using an S1-photocathode vacuum photodiode and a fast oscilloscope. The time dependence of the mode-locked pulses was also recorded directly using an EPL ICC 512 streak camera with an S1 photocathode. The use of this camera at these wavelengths has been previously discussed by the authors.[3] The inherent resolution of the streak camera for the streak rates used for data presented in this note is 59 ps, thereby giving an estimated pulsewidth resolution of about 25 ps.

The acousto-optic mode-locker was adjusted such that it was operational for at least 300 μs prior to the flashlamp discharge and for about 100 μs after the KD*P Pockels cell in the Q-switch assembly was activated. The Pockels cell timing was adjusted to approximately 20 μs after the peak of the flashlamp current. No measurements were made of the time dependence or energy content of the pumping band at 2750 Å produced by the xenon flashlamps. No pulsewidth data for pressures greater than 6500 torr were made because of the pressure limitation of the 1-mm-thick, 8-mm-diameter quartz tubing containing the C_3F_7I-Ar mixture. It was felt that greater pressures might result in catastropic failure of the quartz tube. The window assemblies were tested to 10^4 torr and were not considered to be the limiting factor for the maximum gas pressure that could be handled.

A typical oscilloscope record of the temporal response of the simultaneously Q-switched mode-locked pulse train is shown in Fig. 27a. The time scale is 20 ns/cm. The spacing between mode-locked pulses is seen to be nearly 10 ns, corresponding to the 98.8-MHz frequency separation of the longitudinal modes of the laser cavity. The FWHM time duration of the mode-locked train was observed to be pressure-dependent, as expected, for fixed flashlamp voltages. Energy measurements made at 6100 torr and an 80:1 mix of Ar to C_3F_7I gave a total energy in the mode-locked train of approximately 5 mJ and an average energy per mode-locked pulse of about 300 μJ. The energy content of the mode-locked pulse train was found to be proportional to the amount of C_3F_7I contained in the mixture, indicating that the mixture is optically thin to the flashlamp pumping. However, a decrease in output energy was observed when

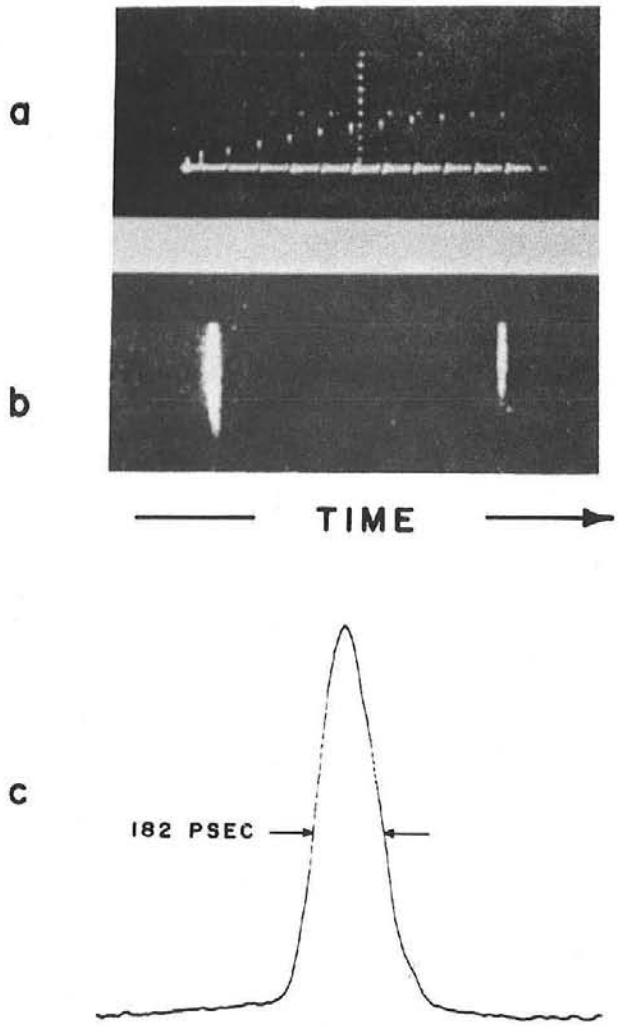

Fig. 27. Temporal and streak photographs of the mode-locked pulses. Fig. 27a is the temporal behavior of the mode-locked pulse train at 1.315 μ obtained by simultaneously Q-switching and acousto-optic mode-locking the optical cavity. The time scale is 20 ns/cm. Fig. 27b is the streak recording of two of the mode-locked pulses occurring about 80 ns into the mode-locked pulse train shown in Fig. 27a, and Fig. 27c, is an intensity vs. time profile for the second pulse shown in Fig. 27b. The recorded FWHM pulsewidth is indicated in the figure, and the deconvolved pulsewidth is 164 ps.

the C_3F_7I partial pressure was greater than 125 torr. Inversion density estimates based on standard Q-switching theory[7] indicate a 3% photolysis of the C_3F_7I in the mixture.

Pulsewidth data using the streak camera were taken in the pressure range of 1000 to 6500 torr for two ratios of Ar to C_3F_7I pressure: 80:1 and 60:1. Figure 27b is a typical streak record of two pulses near the middle of the mode-locked train shown in Fig. 27a. The distance between the pulses shown in Fig. 27b again corresponds to the nearly 10-ns spacing of the mode-locked pulses and served as a cross-calibration of the streaking rate used in the streak camera.

Figure 27c shows the time history of one of the pulses, which has been derived from microdensitometer data. As can be seen, the apparent pulsewidth is about 180 ps. Taking into account the contributions to the recorded data due to a finite slit width of the camera, inherent camera response, etc., the true pulsewidth is 164 ps.

The pressure-dependence of the FWHM pulsewidth, between 1000 and 6500 torr pressure, is shown in Fig. 28. No observable differences in the pulsewidth data were measured for the two mixtures: 80:1 and 60:1; hence, these data points are not differentiated in Fig. 28. The error bars were arrived at by scanning different portions of a given streak photograph and measuring the resultant pulsewidth. These errors arise because of several factors, including non-uniform photocathode response, etc., across the image. As is evident from Fig. 28, the pulsewidth decreases with increasing pressure.

The expression for the FWHM pulsewidth τ of an acousto-optic mode-locked laser oscillator in terms of the various laser parameters is:[5]

$$\tau = \frac{\sqrt{2\ell n2}}{\pi} g_o^{1/4} \theta^{-1/2} \left[\nu_m \Delta\nu_a\right]^{-1/2}, \qquad (2)$$

where g_o is the saturated scillator gain, θ is the modulation index, ν_m = 49.4 MHz is the modulation frequency of the acousto-optic

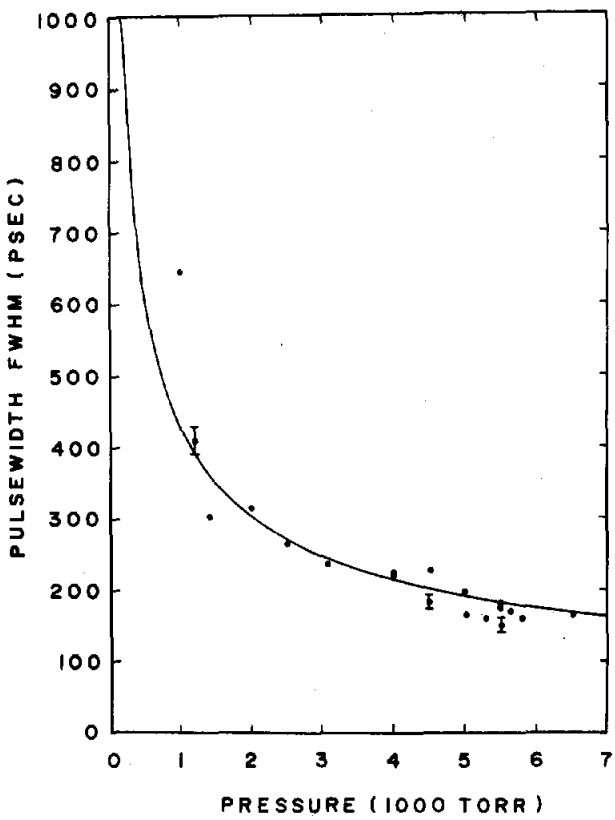

Fig. 28. Pressure-dependence of the deconvolved FWHM pulsewidths for the iodine photodissociation laser. The C_3F_7I-Ar pressure is in units of 1000 torr. The solid line shown in the figure is given by Eq. (2) (see text for details).

mode-locker, and $\Delta\nu_a$ is the frequency bandwidth of the lasing media. The gain factor g_o can be estimated from the relationship $g_o \simeq -1/2\ \ell n\ R \simeq 0.11$ for $R \simeq 0.8$. The modulation index $\theta = 0.93$ was experimentally determined as previously mentioned.

Measurements of the pressure broadening of the $5^2P_{1/2} \rightarrow 5^2P_{3/2}$ iodine transition by Ar have been reported in Refs. 8 and 9.

In order to further test the validity of Eq. (2) as applied to the iodine photodissociation laser, pulsewidth measurements were made at a fixed pressure of 4000 torr with variable rf power, i.e., varying θ in a known manner. These results were also in agreement with Eq. (2), i.e., the pulsewidth τ was proportional to $\theta^{-1/2}$. A similar confirmation of this predicted dependence has been reported[6] for the acousto-optic mode-locked Nd:YAG system. The pulsewidth data presented here are found to be in agreement with the theoretical calculation for an acousto-optic mode-locked homogeneously broadened laser medium. The various approximations which led to the derivation of Eq. (2) may not be valid for $P \leqslant 1000$ torr, where the conditions that the pulsewidth $\tau << 1/2\pi\nu_m$ and $\tau << 1/\Delta\nu_a$,[10] are not satisfied.

Since good agreement between experiment and theory is found for the iodine photodissociation laser, speculations regarding the ultimate pulsewidth are appropriate. Experimentally, for the acousto-optic mode-locker used in these measurements, the maximum value of θ at 1.315 μ is about 1.52 and is limited by rf breakdown in the driving transducer which occurred for powers near 80 W (corresponding to a peak-to-peak voltage of about 1000 V on the driving transducer). At this maximum rf power, the pulsewidth would be reduced by a factor of about 0.8. Increasing the mirror reflectivity will also decrease the pulsewidth [see Eq. (2)], but at an expense of output energy. These data indicate that, for Ar pressures up to 1500 torr, $\Delta\nu_a \alpha P$ with broadening coefficients of 5.8±0.5 MHz/torr[8] and 5.1±0.5 MHz/torr.[9] The data do not extend to the higher Ar pressures used in this experiment; but it is assumed for purposes of comparison that $\Delta\nu_a \alpha P$ in the range of 1000 to 6000 torr and the coefficient is 5.5 MHz/torr. Because of the relatively low C_3F_7I pressure, the contribution to $\Delta\nu_a$ by C_3F_7I pressure broadening has been ignored (the broadening coefficient for C_3F_7I is about 26 MHz/torr[8]). Thus, Eq. (1) becomes, in terms of the pressure:

$$\tau = 428\ P^{-1/2}\ \text{ps}\ , \qquad (3)$$

where P is in units of 1000 torr. It is interesting to note that the cross section σ has been reduced from about 6×10^{-18} cm^2 ($\Delta\nu_a \simeq 250$ MHz) to 6×10^{-20} cm^2 ($\Delta\nu \simeq 25$ GHz) by pressure broadening at 5000 torr.

The solid line shown in Fig. 28 is the calculated value of τ as given by Eq. (3) [or equivalently Eq. (2)]. As can be seen, the agreement is remarkably good, since there were no adjustable parameters used in the calculation of the curve shown in Fig. 28. This agreement also substantiates the assumption of the linear dependence $\Delta\nu_a$ upon pressure P to these higher pressures.

Using reflectivities approaching 98% and assuming no other contributions to the cavity losses, the pulsewidth would decrease, according to Eq. (2), by a factor of two. The third alternative is to increase the bandwidth $\Delta\nu_a$ by further pressure broadening. Again, assuming a linear dependence of $\Delta\nu_a$ on P, Ar pressures of $\sim$ 25,000 torr are needed in order to reduce the pulsewidth by a factor of two. However, it is not clear that, at these pressures, there would be enough gain in the system to sustain lasing, since $\sigma \simeq 10^{-20}$ cm^2 for P_{Ar} = 25,000 torr. Finally, the modulation frequency could be increased, either by working in an overtone mode of the cavity[5] or by decreasing the cavity length. Either of these schemes would decrease the pulsewidth as is evident from Eq. (2). It is obvious that by optimizing all of the parameters mentioned above, it would be reasonable to assume that pulsewidths of 100 ps could be obtained.

A measurement of the beam divergence of this oscillator system was made by directly photographing the output using the streak camera in the "focus" mode of operation. The output beam profile was photographed at a distance of 6.5 m from the oscillator output mirror. The aperture in the oscillator cavity for these measurements had a diameter of 3 mm corresponding to a Fresnel number ($a^2/\lambda L$) of about one. The measured beam divergence was about 0.5 milliradian; hence, the output can be considered to be diffraction-limited.

Large-Iodine-Laser System

The 3-inch-diameter iodine laser amplifier has been fully assembled and initial tests have been completed. To obtain an estimate of the stored energy, the amplifier was run as an oscillator. With 100% and 30% reflecting mirrors forming the oscillator cavity, the output energy was $\approx$ 65 joules in 200 ns. The flashlamp reflectors were made of aluminum foil with 68% reflectivity at 2700 Å. An increase of the order of a factor of 1.5 to 2 in output energy is expected when improved reflectors are installed. Evaluation of barium-sulfate reflectors and MgF_2-Aℓ reflectors is in progress; both are > 90% reflecting at 2700 Å.

The oscillator, pulse cutter, preamplifier, and beam expander have been relocated in the room where the amplifier is located. Figures 29 and 30 show a layout of the system. The short-pulse oscillator currently produces 200-ps pulses (FWHM) for the initial experiments. The preamplifier is fully assembled and tests have begun to determine the maximum gain at which it can be operated. Should it be found that the preamplifier can be operated at a gain of 1000 or more, a second Pockels cell gate will be placed between the preamp and the 3-inch-diameter amplifier.

The primary emphasis of experiments to be begun shortly on the iodine system will be to evaluate potential problems pertaining to iodine and other saturated gas lasers as well as to determine the maximum efficiency of the iodine laser system. A major consideration is evaluation of pulse distortion. Experiments will be done to determine what bandwidth is required to faithfully amplify a 200-ps pulse and the extent of the pulse distortion at smaller bandwidths. Iodine may have a potential problem of upper-level relaxation, leading to pulse distortion similar to CO_2 if the two upper hyperfine levels are not mixed or pressure broadened to obtain sufficient overlap. Experiments will be performed to evaluate this upper-level mixing, which is also critical to the extraction efficiency.

Another area of concern is beam quality. Experimenters at Max-Planck Institut Für Plasmaphysik[11] have observed shock waves in their iodine laser. It is planned to

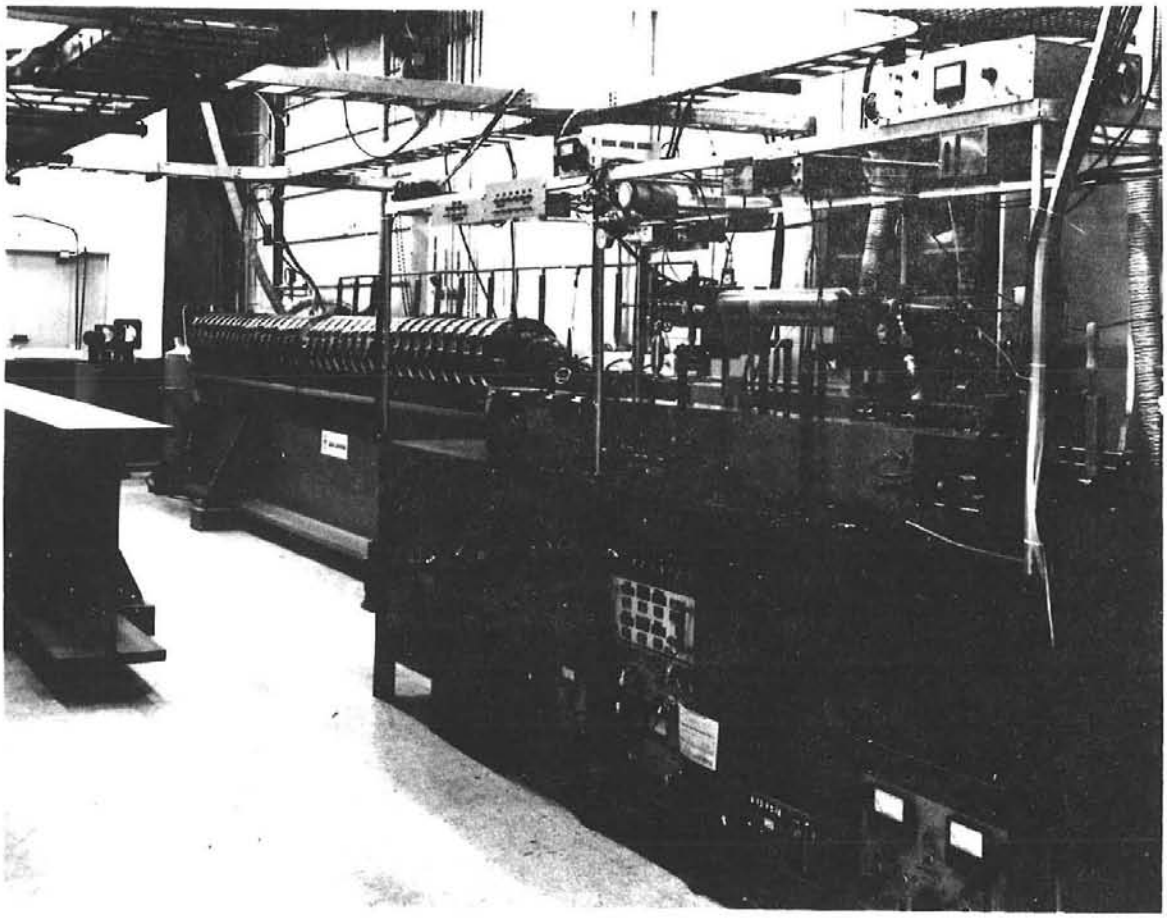

Fig. 29. Photograph of iodine system with the oscillator in the foreground and the large amplifier in the background.

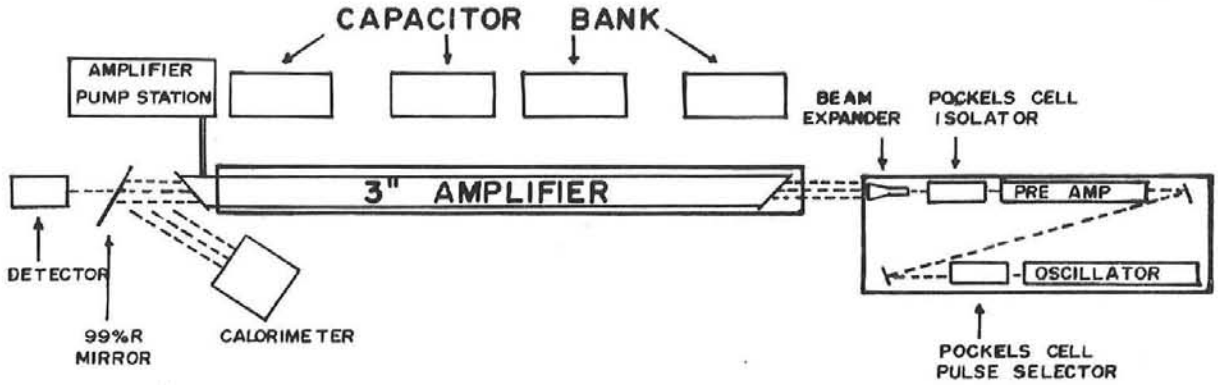

Fig. 30. Schematic drawing of iodine laser system.

investigate turbulence in the Sandia system and its effect on beam quality. A problem of more general concern is the effect of anomalous dispersion on beam quality under saturated-gain conditions. This and other nonlinear effects will be evaluated in the 3-inch-diameter amplifier by removing the beam expander. The latter will insure saturation intensity for most of the 4-m-long path length of the amplifier.

Using standard flashlamps, the maximum efficiency of the amplifier for short-pulse-width applications will be less than one-half of 1%. The maximum efficiency should approach this value if the two upper hyperfine levels are mixed at a sufficiently rapid rate. If a doped-lamp-development program is successful, then an efficiency of about 1% should be possible. An efficiency higher than 1% will require the development of a different type of photosource that does not have blackbody restrictions (noble-gas halide radiation could possibly increase the efficiency to a few percent).

Chemical Kinetic Studies of the Iodine-Photodissociation Laser

In an effort to improve the efficiency of the atomic-iodine-laser system, we have been investigating the compounds listed in Table II in order to present the broadest pump band to the broadband pump radiation. However, these compounds must have a high quantum yield of exited iodine (I^*) and must not rapidly deactivate I^*. We have developed a technique which allows the determination of the fraction of iodine atoms produced as I^* and rate constants for the decay of I^* by various alkyl iodides. In the technique used, the gain of an atomic-iodine laser amplifier is monitored as a function of time. The gain-vs-time data are then fit to a set of rate equations. The fitting routine uses as parameters the fraction of iodine dissociated to I^* and rate constants to the following reactions

$$RI + I^* \xrightarrow{k_1} R + I_2 \qquad (4)$$

$$RI + I^* \xrightarrow{k_2} RI + I \quad , \qquad (5)$$

where R is one of several radicals to be discussed below.

The first compound investigated was CH_3I. While it was not expected to be a candidate for use in an iodine laser system, much of the chemistry was known and it was an ideal system to check the technique. The results of the measurements are shown in Table III. It was also possible to determine the rate constant for deactivation of I^* by CH_3 radicals (k_3). The rate constants obtained (k_1 and k_2) and the fraction to I^* were in agreement with the other recent literature values.

We next investigated $(CF_3)_2AsI$. Birich et al.[12] had used this compound in an oscillator experiment because its absorption spectrum was broader, more intense, and shifted to longer wavelengths from the absorption spectrum of C_3F_7I. The results shown in Table III indicate that it has an attractive quantum yield for I^* but that the deactivation rate of I^* by the parent compound is too large to make the compound useful in a large iodine system.

The next molecule studied was CD_3I. Its absorption maximum is shifted about 200 Å from that of C_3F_7I. Also, one recent report in the literature[13] indicated that the deactivation rate was about two orders of magnitude lower than CH_3I. Table III lists the results for CD_3I. Both the quantum yield and the deactivation rate are acceptable for use in a large iodine amplifier. However, analysis of the absorption spectrum of C_3F_7I and CD_3I indicates that addition of CD_3I to C_3F_7I would increase the amount of absorbed pump light by only a few percent because of the already broad absorption band of C_3F_7I.

Additional experiments will study C_3F_7I, i-C_3F_7I, and CF_3I. It is also planned to investigate the possibility of obtaining multiple shots on a single fill of gas for each of the above compounds. This later experiment may be dependent on whether the amplifier has been chemically saturated due to the different chemical reactions involving I^* and I.

TABLE II

Compounds Which Produce Atomic Iodine Laser Transition and Their Absorption Properties

Compound	Wavelength at Peak (Å)	Peak Absorption Cross Section (10^{-18} cm^2)	Bandwidth at Base (Å)
CH_3I	2575	1.14	700
CD_3I	2575	1.14	700
C_2H_5I	2580	1.39	700
C_3H_7I	2600	1.52	750
CF_3I	2690	0.65	800
C_2F_5I	2690	0.68	900
C_3F_7I	2700	0.84	1000
i - C_3F_7I	2750	0.60	1000
$(CF_3)_2AsI$	2880	2.9	1350

TABLE III

Summary of Results from Computer Fitting of Data
(All rate constants are in units of cm^3 $molecule^{-1}$ sec^{-1}.)

	Fraction to I^*	k_1	k_2	k_3
CH_3I	0.76	$< 5 \times 10^{-15}$	2.0×10^{-13}	6.4×10^{-12}
$(CF_3)_2AsI$	≥ 0.99	$<< k_2$	1.7×10^{-13}	---
CD_3I	≥ 0.98	$<< k_2$	2.8×10^{-15}	---

NOBLE-GAS-HALIDE LASER PROGRAM

High-Power Ultraviolet Lasers

Less than a year ago Setser[14] at Kansas State and Golde and Thrush[15] at Cambridge postulated that the ultraviolet emissions they observed after mixing rare-gas-metastables with halogen-containing compounds were produced by diatomic rare-gas-halide molecules in their lowest excited state radiating to their ground state. Since the ground state of these molecules had been previously calculated[16] to be repulsive, they appeared to be ideal laser candidates. The fact that the lowest excited state was believed to be produced by reactive scattering of a rare-gas-metastable off of a halogen-containing compound suggested that electron beams would be efficient pumps for these lasers.[17]

Work was started in May 1975, using Sandia's electron-beam facilities, with the goal of observing laser action on at least one, and possibly more, of the rare gas-halide molecules. To date, we have successfully observed laser action on four rare gas-halides (KrF, XeF, XeCl, and XeBr) and one halogen (I_2). Three of these lasers have potential as high-power lasers (KrF, XeF, and I_2). During this period, attention has been primarily focussed on KrF. The goals have been twofold: (1) to scale the KrF laser to 100 joules and a power of 10^9 watt, and (2) to design and build a KrF laser with a repetition rate of one pulse per second with an energy of 1 to 10 joules and a power of 10^6-10^7 watt.

The experimental setup used on the e-beam facility is shown in Fig. 31. These mixtures generally consisted of high-pressure argon (2000-4000 torr), a low-pressure halogen-containing compound (1-10 torr) and, in the case of the rare-gas-halides, a few hundred torr of Xe or Kr.

The electron beam used to excite these mixtures entered the cell transverse to the optical axis. The beam was 6.0 cm high and 40.0 cm wide. It had a peak current of 140 kA, an initial electron energy of 1.2 MeV, and a pulse width of 50 ns (FWHM). Two laser-cavity configurations were used. Cavity I consisted of two high-reflectance (97%), dielectrically coated mirrors with a diameter of 2.5 cm and a radius of curvature of 2.0 m. Cavity II consisted of an aluminum flat and a flat quartz output-coupling window, each with a diameter of 5.0 cm. Both cavities were 65.0 cm long.

The laser-energy outputs, efficiencies, and wavelengths obtained are given in Table IV, along with a description of the emission observed. The spontaneous and stimulated-emission spectra of the various lasers are shown in Figs. 32 through 36. The time histories of the laser pulses versus the e-beam current are shown in Figs. 37 through 41.

Two facts stand out in the results presented: (1) in the series, XeF, XeCl, and XeBr, the energy of the laser is rapidly decreasing as a function of the weight of the halogen, and (2) molecular iodine is reported to lase using a variety of iodine-bearing compounds but never using I_2 itself. These facts suggest answers to two important questions: (1) what rare gas-halides have potential as high-power lasers, and (2) can other molecular halogen lasers be produced?

In answer to the first question, consider that as the atomic number of the halogen attached to the rare gas "increases," the energy difference between the lowest excited state of the rare gas-halide and its higher excited states "decreases." This implies that absorption of the rare-gas-halide laser radiation by the excited rare-gas-halide becomes more probable, and if the appropriate energy resonance occurred, then depopulation of the upper laser state would take place and constitute a potentially large loss to the system. In this case, rare-gas-chlorides, -bromides, and -iodides would have limited potential as high-power lasers. It is important to note that attempts to make a molecular-iodine laser, using I_2 itself, were unsuccessful. If the upper laser state of I_2 is produced by a three-body ion recombination, $I^- + I^+ + M$, the rate determining step in the formation of the ions is slow-electron attachment to the halogen-

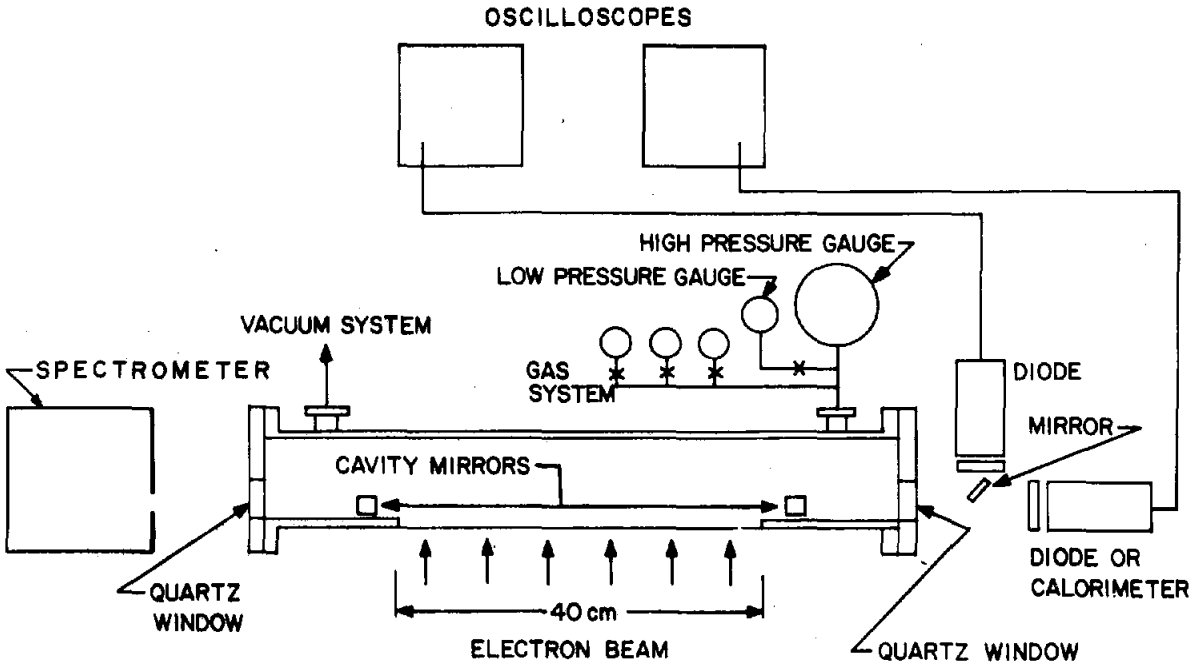

Fig. 31. Schematic diagram of experimental setup.

TABLE IV

Laser Energies, Powers, Efficiencies, Wavelengths, and Descriptions Obtained Using Sandia's 893 e-Beam Facility

	Maximum Energy (joules)	Maximum Power (watts)	Efficiency (%)	Wavelength (nm)	Transition
KrF	5.6	1.1×10^8	2-3	248.4, 249.1	Continuous
XeF	1.0	2.0×10^7	0.3-0.5	351.1, 353.2	Discrete
XeCl	-	$\sim 1.5 \times 10^4$	-	307.9, 308.1	Discrete
XeBr	-	$\sim 1.0 \times 10^3$	-	282.8	Continuous
I_2	1.0	2.5×10^7	0.3-0.5	342.0, 342.4	Discrete

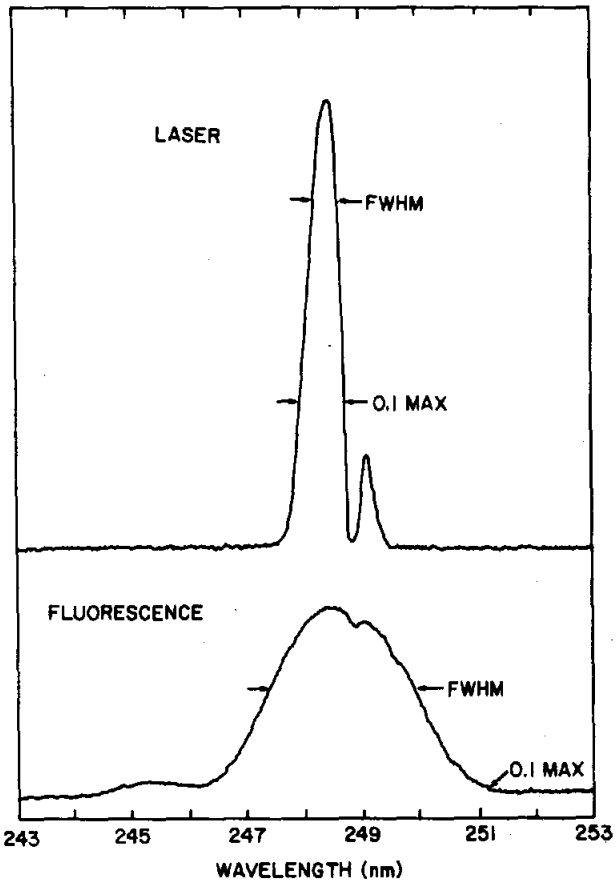

Fig. 32. Laser (top) and fluorescence (bottom) spectra of KrF.

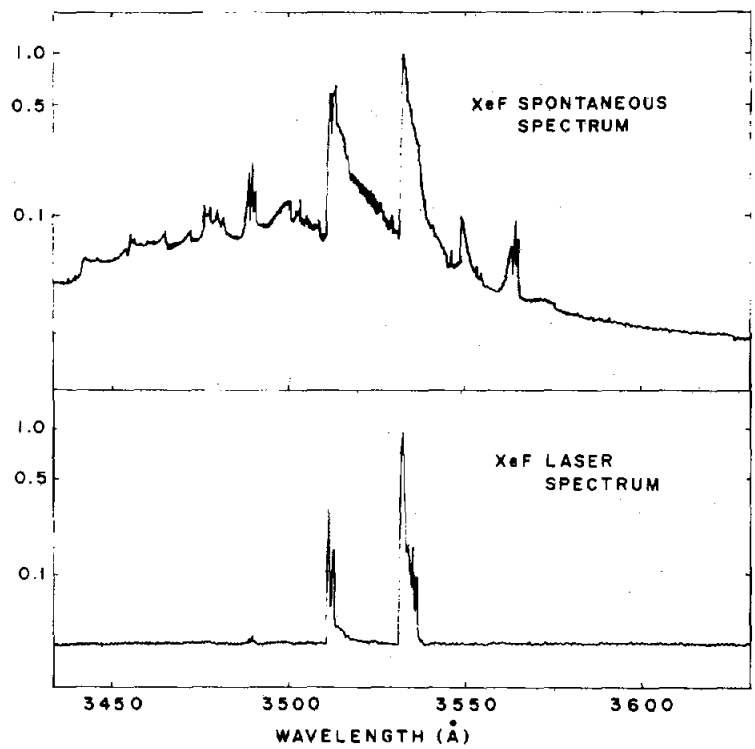

Fig. 33. Spontaneous (top) and laser (bottom) spectra of XeF.

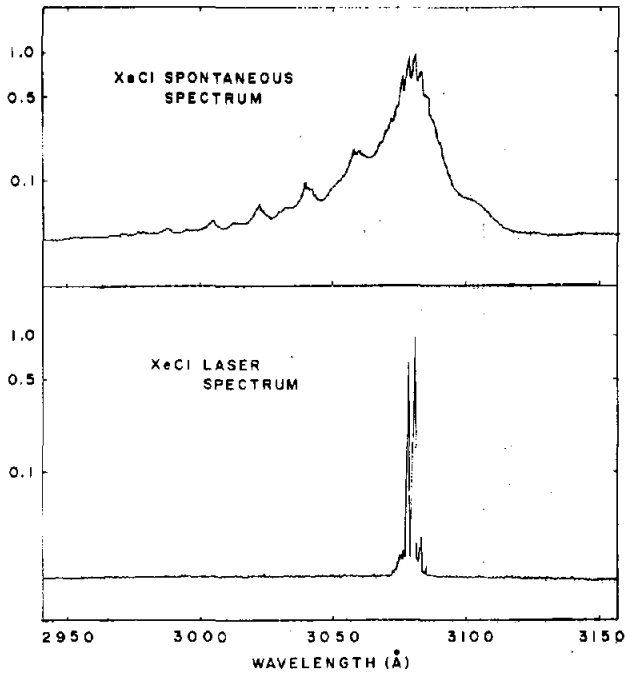

Fig. 34. Spontaneous (top) and laser (bottom) spectra of XeCl.

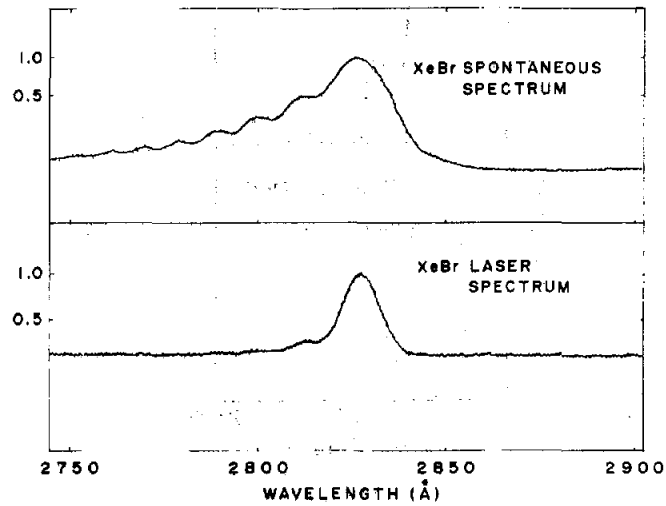

Fig. 35. Spontaneous (top) and laser (bottom) spectra of XeBr.

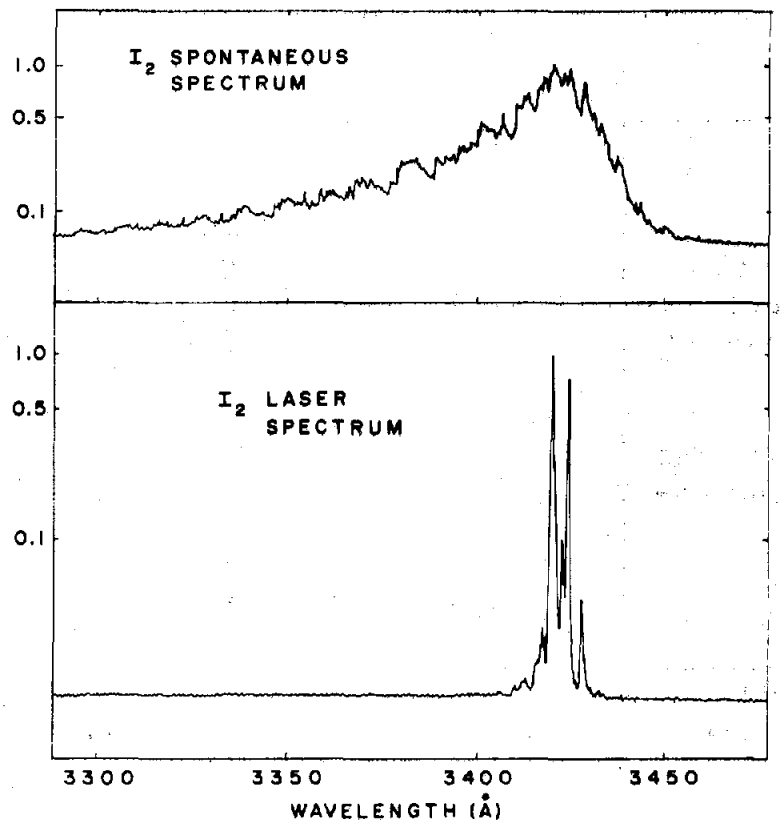

Fig. 36. Spontaneous (top) and laser (bottom) spectra of I_2.

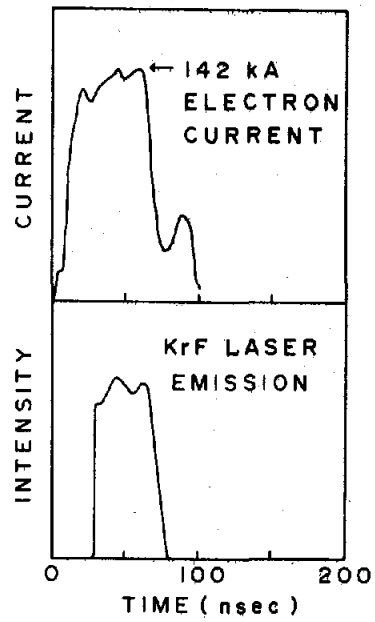

Fig. 37. Time history of electron-beam current (top) versus the KrF laser pulse (bottom).

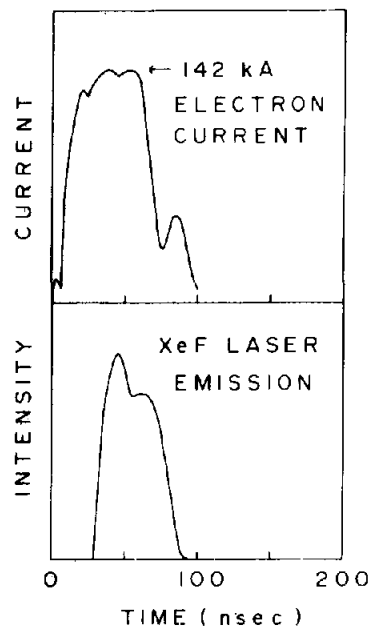

Fig. 38. Time history of electron-beam current (top) versus the XeF laser pulse (bottom).

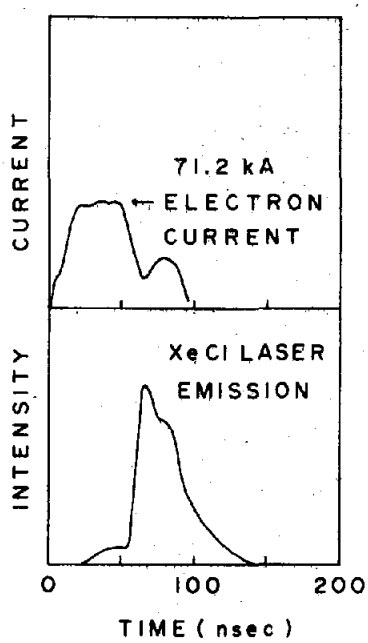

Fig. 39. Time history of electron-beam current (top) versus the XeCl laser pulse (bottom).

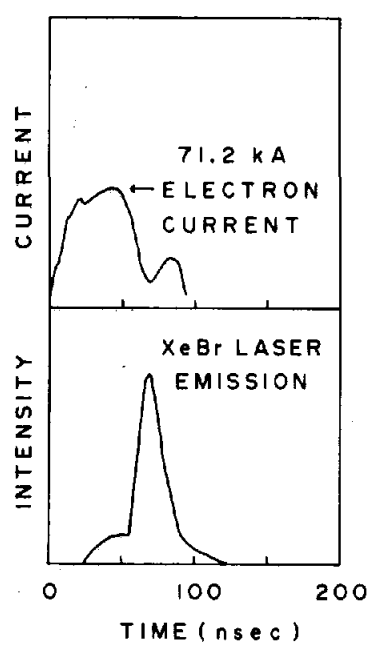

Fig. 40. Time history of electron-beam current (top) versus the XeBr laser pulse (bottom).

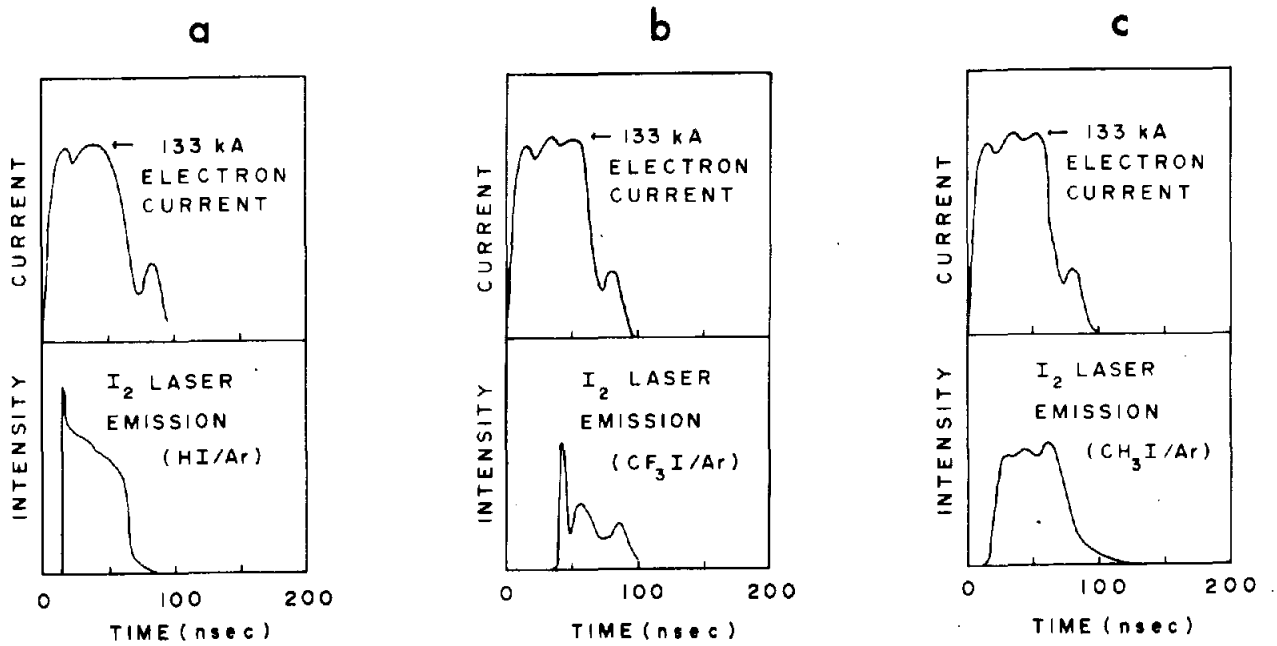

Fig. 41. Time history of electron-beam current (top) versus the I_2 laser pulse (bottom) for mixtures of (a) Ar/HI, (b) Ar/CF_3I, and (c) Ar/CH_3I.

containing compound to form I^-. The slow-electron attachment rates[18] of HI, CF_3I, and CH_3I are one to three orders of magnitude larger than the same rate[19] for I_2. This may explain why Ar/HI, Ar/CF_3I, and Ar/CH_3 mixtures lase and Ar/I_2 mixtures do not lase. This discussion suggests that other molecular-halogen lasers may be produced by selecting halogen-containing compounds with large electron-attachment rates.

In conclusion, it would seem that KrF, XeF, and I_2 are potential high-power, high-efficiency lasers. Self-absorption may exclude the rare gas-chlorides, -bromides, and -iodides from this category. At the same time, Br_2, Cl_2, and F_2 lasers, similar to the molecular I_2 laser, may be produced by selecting halogen donors with large electron-attachment rates.

Since this class of lasers utilizes allowed transitions, the gain cross section is large and they do not offer energy storage capability. Thus, they are not attractive for laser-fusion applications. However, their use as efficient photon sources to photoexcite other lasers could be attractive, and this is being studied as a pump source for the iodine laser. Also the potential of these lasers for use in isotope separation is great.

Spectroscopic Studies of Diatomic Noble Gas Halides: Analysis of Spontaneous and Stimulated Emission from XeCl

In their lowest excited configuration, $up^5(u+1)s$, the heavier noble-gas atoms display properties similar to those of the corresponding alkali metal atoms. One such similarity is their tendency to react with halogen-containing molecules to produce diatomic noble-gas-halide molecules in strongly bound ionic states.[20, 21] Unlike the analogous alkali-halide states, however, these are excited states which can radiate as they decay to lower electronic states. For the various AX molecules (A = Ar, Kr, Xe; X = F, Cl, Br, I), transitions are observed over the spectral range 1500 to 5000 Å.[20-24]

The observed AX spectra are attributed to transitions from one or more of the manifold

of excited states, $^2\Sigma^+$ and $^2\Pi$ in Hund's case (a), or 1/2, 1/2, and 3/2 in case (c) which correlate with A^+ (^2P) and X^-(^1S), to lower states of the same symmetry which correlate with the neutral atoms in their ground and metastable ($^2P_{1/2}$) state. All these excited states tend adiabatically toward somewhat lower $A^* + X$ or $A + X^+$ neutral-atom correlation limits. However, in many of the AX molecules, the predicted crossing of the neutral and ionic curves occurs at large internuclear distances so that the excited states are expected to be dominated by ionic character in the binding region. In general, the lower states are predicted to be only weakly bound van der Waals-type states, so that the AX emission transitions are predominantly bound-free. However, in at least two cases--XeF and XeCl--the spectrum is mainly bound-bound for emission from low v′ levels.

In this report we discuss the high-pressure XeCl spectrum which shows peak intensity near 3080 Å. The vibrational analysis of this spectrum is straightforward, as the violet-degraded bands group into clear v′′ progressions. The $^{35}Cl/^{37}Cl$ isotopic splitting evident in some of the bands supports our analysis. From the observed intensities and vibrational data we are able to derive reliable relative potential curves for upper and lower states. In addition, we discuss the laser experiments on this transition because the spectrum obtained under lasing conditions proved useful in deriving the potential curves.

The XeCl emission was produced by electron-beam excitation of Xe/HCl and Xe/Cl_2 mixtures having typical concentration ratios of 50:1 and total pressures of 300 torr. A Febetron Model 706 was used as the e-beam source. The spectrum was photographed on Kodak Tri-X 4164 film, using a Jarrell-Ash 1-meter Czerny-Turner spectrometer equipped with a 1180-grove/mm grating blazed at 7500 Å. Employed in the third order with 20-μm slits, this instrument gave a reciprocal dispersion of 2.2 Å/mm and a resolution of 0.05 Å. For calibration we used Hg lines from a low-pressure discharge lamp and Th and Ne lines from a Varian hollow-cathode thorium source.

Laser action in XeCl was produced by e-beam excitation of $Ar/Xe/Cl_2$ or $Ar/Xe/CH_2Cl_2$ mixtures. The mixtures had typical concentration ratios of 800:50:1 and total pressures of approximately 2000 torr. The optical cavity consisted of two mirrors separated by 65 cm. Each mirror had a 2-meter radius of curvature and 99.9% and 97% reflectances. The reflectances of these two mirrors covered the wavelength range 2500 to 3150 Å.

The e-beam accelerator used in the laser experiments operated at 1.2 MV with a peak electron current of 142 kA. The pulse duration of the electron beam was 50 ns.

Figure 42 illustrates the XeCl emission spectrum and, for comparison, a spectrum obtained with the laser mirrors in place. It is clear that lasing is occurring on the 0 to 1 and 0 to 2 bands, which also appear to be the strongest bands in the emission spectrum. The first 7 bands of the v′ = 0 progression are discernible, and 6 bands of the v′ = 1 progression can be identified. In the v′ = 2, 3, and 4 bands at shorter wavelengths, the $^{35}Cl/^{37}Cl$ isotopic splitting is evident, with the bands of the less-abundant (24.5%), heavier isotope occurring at slightly longer wavelengths.

The measured wavelengths and frequencies of the assigned bands are presented in Table V, together with their deviations from the frequencies calculated using the vibrational parameters described below.

Vibrational parameters for the upper and lower states were obtained from a least-squares fit of the measured frequencies to the double polynomial expression.

$$\nu_i = \Delta T_e + \sum_{j=1}^{m} c_j'[e(v' + 1/2)]^j - \sum_{k=1}^{n} c_k''[e(v'' + 1/2)]^k ,$$

where ν_i is the measured frequency for the $(v' - v'')_i$ band, ΔT_e is the electronic

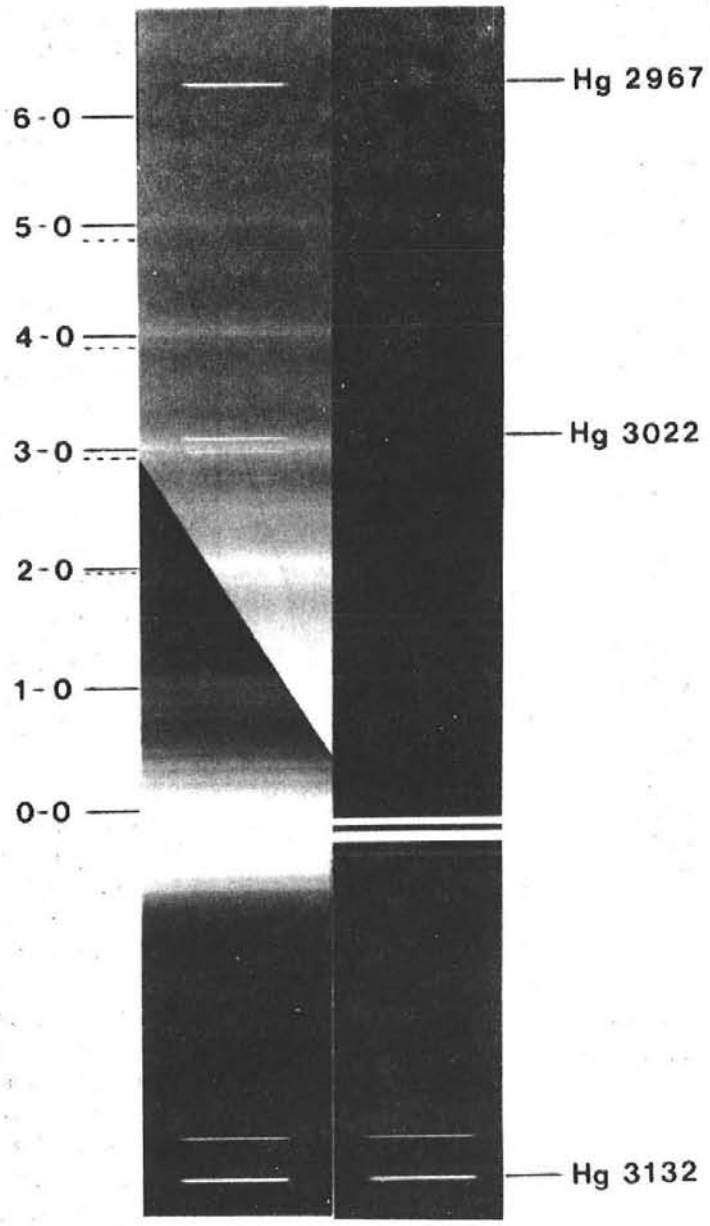

Fig. 42. Spontaneous emission (lower) and laser (upper) spectra of XeCl, obtained as described in text. Bands in the $v'' = 0$ progression are identified, with the $^{35}Cl/^{37}Cl$ isotopic splitting noted in several of these (broken lines).

TABLE V

Assigned Xe - ^{35}Cl and Xe - ^{37}Cl Vibrational Bands

v′ - v″	λ(A in air)	ν(cm^{-1})	Δν(cm^{-1})[a]
0-6	3091.44	32 338.0	0.4
0-5	89.24	361.0	-0.3
0-4	86.98	384.7	0
0-3	84.59	409.8	0.1
0-2	82.10	436.0	0
0-1	79.61	462.2	0.4
0-0	77.04	489.3	-0.1
1-7	74.87	512.3	-0.1
1-6	72.98	532.3	0.2
1-5	70.82	555.1	-0.3
1-4	68.61	578.6	0.2
1-1	61.25	656.9	-0.2
1-0	58.72	683.9	-0.6
2-1 (b)	44.06	841.3	-1.1
2-1	43.27	849.8	-0.1
2-0 (b)	41.83	865.4	0.8
2-0	40.81	876.4	-0.1
3-4	32.75	963.8	-0.1
3-3	30.46	988.7	0.2
3-0 (b)	24.65	33 052.1	1.9
3-0	23.24	067.5	0.7
4-0 (b)	07.34	242.3	-1.5
4-0	05.83	259.0	0
5-0	2988.77	448.9	-0.1

[a] Deviations of measured values from calculated values obtained using parameters in Table VI.

[b] Xe - ^{37}Cl bands.

energy difference, and the $\{c_j'\}$ and $\{c_k''\}$ are the vibrational parameters. The mass ratio factor e allows inclusion of the Xe^{37}Cl measurements, under the assumption that the usual isotopic relationship holds.[25] The number of coefficients, m and n, were varied to obtain an optimum (minimum variance) fit. Best results were obtained for m = 2, n = 3, yielding the parameters given in Table VI.

It is worth noting that c'' $(-\omega_e x_e'')$ is positive, contrary to usual diatomic behavior. We attach no particular significance to this result, in view of the small number (8) of v″ levels included in the analysis and the possibility of impaired precision from isotopic blending in some bands.

The lower-state vibrational parameters in Table VI imply a dissociation energy (D_e'') of 250 cm^{-1} and a total of 12 bound levels in this state.

TABLE VI

Xe ^{35}Cl Vibrational Constants (Standard errors in parentheses)

$$\Delta T_e = 32405.0\ (0.5)\ \text{cm}^{-1}$$

Upper State (cm^{-1})		Lower State (cm^{-1})
195.17 (0.31)	(ω_e)	26.27 (0.55)
-0.543 (0.063)	$(-\omega_e x_e)$	0.278 (0.17)
	$(\omega_e y_e)$	-0.0672 (0.14)

Extensive work on the alkali-halide molecules has shown that their ionic ground-state potential curves can be represented with fair accuracy by the Rittner potential[26] or one of its variants.[27] By analogy, the same analytical form should be useful in describing the AX excited states, particularly those (like XeCl) which have a crossing between the ionic and covalent states at large internuclear separation. We have chosen to represent the excited XeCl potential energy curve by a truncated Rittner potential of the following form:

$$U(R) = a + b \exp[-\beta R] - C_1 R^{-1} - C_4 R^{-4} .$$

Here the R^{-1} term represents the ion-ion attraction ($C_1 = 1.1614 \times 10^5$ cm^{-1} Å), and the R^{-4} term arises from ion-induced dipole interactions, with C_4 a function of the ion polarizabilities, $C_4 = 1/2\ e^2(\alpha_+ + \alpha_-) = 5.807 \times 10^4\ (\alpha_+ + \alpha_-)$ (cm^{-1} · Å). The exponential term is an ad hoc representation of the repulsive forces which must dominate at overall R. It contains two parameters which can be adjusted to give

correctly two known spectroscopic quantities, in our case D_e and ω_e. This procedure then fixes R_e, the position of the curve minimum.

For the Cl^- polarizability, we have used the value 3.0 $Å^3$ of Dalgarno.[28] We could locate no estimate of the Xe^+ polarizability. However, from the trend of the values for the A, A^+, X and X^- species and the alkali ions given by Dalgarno[28] and by Teachout and Pack,[29] we surmise that the value $\alpha_+ = 3.0$ $Å^3$ is reasonably close to the true value and certainly sufficient for our purpose. These polarizabilities yield $C_4 \approx 3.5 \times 10^5$ cm^{-1} $Å^4$, which, together with the spectroscopically derived values for ω_e' and D_e', gives b = 1.5124×10^7 cm^{-1}, $\beta = 2.5814$ $Å^{-1}$, and $R_e' = 2.9380$ Å. With the upper curve thus determined, it is possible to derive a reliable lower curve from the vibrational data and the observed v′ - v″ intensity distribution.

The violet-degraded character of the bands in Fig. 42 implies that $R_e'' > R_e'$, in which case the vibrational intensity distribution is determined mainly by the shape of the lower curve's repulsive wall in the Franck-Condon region ($R \approx 2.7 - 3.1$ Å). The turning-point difference ($R_{max} - R_{min}$) can be determined from the vibrational parameters, through one of the RKR relationships. These differences were evaluated by means of the Gauss-Mehler quadrature scheme[30,31] and were used to adjust the lower curve's attractive branch, as the repulsive branch was varied in a trial-and-error procedure of comparing calculated Franck-Condon factors (FCF) with the observed v′ - v″ intensities. A satisfactory match was obtained for a repulsive branch which, for $2.7 \leq R \leq 3.0$ Å, could be represented, relative to the curve minimum, as an exponential, 3.46×10^{15} exp (-11.022 R). The minimum was then located at $R_e'' = 3.18$Å.

In Fig. 43 we illustrate the two XeCl potential curves. The FCF's calculated with these curves are given in Table VII. Note particularly that as v′ increases beyond 3, the only bands predicted to be strong are the v′ - 0 bands, as observed. This trend correlates with a progressive increase in the bound-free/bound-bound intensity ratio for a given v′ level. In this regard, it is worth noting that, even for v′ = 2, about 60 percent of the total emission is bound-free.

In Table VIII we compare some properties of the XeCl excited state with the same quantities for the $^{133}C_s$ ^{35}Cl ground state. Note that both ω_e' and D_e' are somewhat smaller for XeCl, as would be expected for the larger and "softer" Xe^+ ion.

The vibrational frequency and the dissociation energy for the XeCl ground state are roughly in line with expectations for a van der Waals state. However, compared with ArXe (the nearest true van der Waals molecule),[32] the XeCl well is about twice as deep and is "drawn in" on the R-axis by ~ 0.9 Å. A similar displacement of the $^2\Sigma^+$ ground state of XeF was obtained in ab initio computation by Liskow et al.,[33] with the effect clearly evident in the configuration-interaction calculations. Thus, we conclude that both dispersion interactions and chemical bonding effects are significant in the $^2\Sigma^+$ ground state of XeCl.

The XeCl laser spectrum is shown in Fig. 42 (upper). As noted before, lasing is occurring strongly on the 0 to 1 and 0 to 2 vibrational bands and weakly on the 0 to 3 band. A peak power output of 1.5×10^4 watts was obtained using a mixture of 2300 torr of Ar, 100 torr of Xe, and 3 torr of CH_2Cl_2.

It has been suggested that stimulated emission from Xe Cl formed by e-beam excitation of $Ar/Xe/Cl_2$ mixtures is weak because of Cl_2 absorption at the laser wavelength. In our experiments, the maximum laser power output achieved with such mixtures was ~ 80% of that obtained with the $Ar/Xe/CH_2Cl_2$ mixture given above. Since CH_2Cl_2 does not absorb significantly near 3080 Å, it appears that absorption by Cl_2 is not a major factor limiting the power output of the XeCl laser. However, it is conceivable that other absorption processes play a role, in particular self-absorption by the excited molecules in transitions to one or more of the many predicted higher lying states of the XeCl molecule.

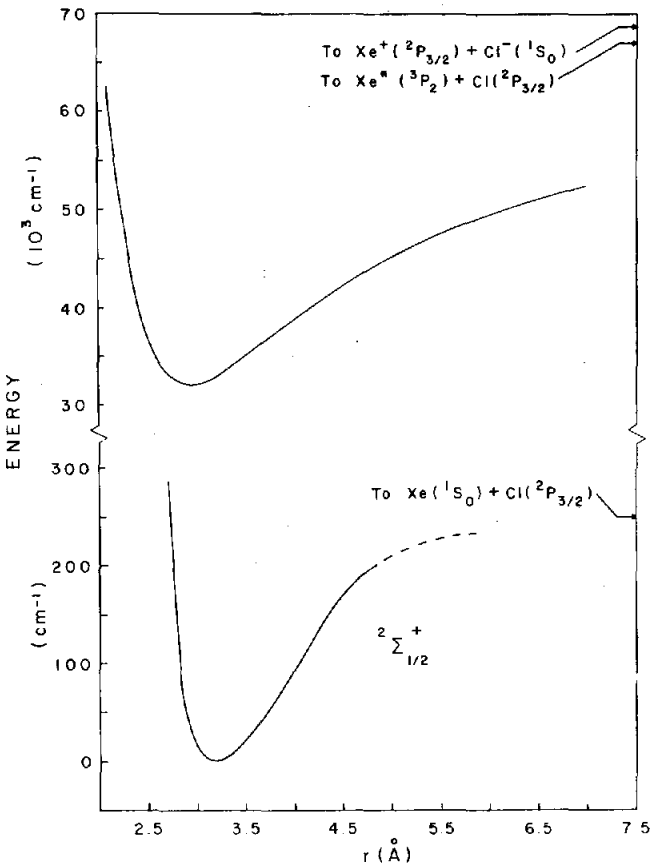

Fig. 43. Potential curves of upper and lower states involved in Spectrum I (~ 300 - 3090 Å) of XeCl. (Note different energy scales for upper and lower curves.)

TABLE VII

Xe ^{35}Cl Franck-Condon Factors Calculated for Potential Curves of Figure 2

v'' \ v'	0	1	2	3	4
0	0.120	0.078	0.103	0.092	0.094
1	0.248	0.061	0.062	0.019	0.008
2	0.253	0.005	0.004	0.009	0.016
3	0.179	0.017	0.006	0.049	0.031
4	0.098	0.079	0.016	0.051	0.010
5	0.042	0.131	0.009	0.025	0.000
6	0.013	0.146	0.000	0.005	0.014
7	0.002	0.127	0.004	0.000	0.030
8	0.000	0.094	0.018	0.001	0.034
9	0.000	0.062	0.032	0.002	0.028
10	0.002	0.037	0.039	0.002	0.019
11	0.002	0.020	0.037	0.001	0.011
12	0.002	0.010	0.028	0.000	0.006
13	0.000	0.005	0.015	0.000	0.003

TABLE VIII

Spectroscopic Properties of the Xe ^{35}Cl Excited State, Compared with the Same Quantities for the ^{133}Cs ^{35}Cl Ground State.[a] (D_e values for dissociation to ions.)

	ω_e (cm^{-1})	$\omega_e x_e$ (cm^{-1})	R_e (Å)	D_e (cm^{-1})
Xe ^{35}Cl	195.17	0.65[b]	2.938[b]	36540
^{133}Cs ^{35}Cl	214.22	0.74	2.9064	39300

[a] Values for CsCl taken from summary in Ref. 21.

[b] From truncated Rittner potential. Experimental $\omega_e x_e$ for Xe^{35}Cl was 0.54 (Table VI).

LASER-DEVELOPMENT-RELATED STUDIES

Electron Beam Excitation of Neon/D_2 Mixtures

A series of experiments has been performed using the Febetron 706 (2 ns, 440 keV) to examine the suitability of electronically excited molecular deuterium as a potential lasing medium near 3000 Å in e-beam excited gas mixtures. Typical mixtures contain from 0.1 to 10 torr D_2 and from 500 to 20,000 torr neon. Deposition of the e-beam energy occurs in the neon with subsequent energy transfer to D_2. The temporal behavior of the $a^3\Sigma_g$ (bound) $\rightarrow$ $b^3\Sigma_u$ (repulsive) emissions, which occur over a broad continuum from 1600 Å to 3500 Å, was observed with both a monochromator/multiplier arrangement and a calibrated filter/photodiode system.

Figure 44 shows the dependence of the peak emission intensity (circles) and the emission decay time (dashed line) on wavelength. The emission feature near 1350 Å originates from the $B^1\Sigma_u^+$ state. For the experimental conditions of this figure, about 40 percent of the radiated energy comes from the $B \rightarrow X$ transition and 60 percent from the $a \rightarrow b$ transition.

The radiative lifetime of the $a^3\Sigma_g$ state is so short (~ 30 ns) that the effective lifetime, which decreases with increasing neon or deuterium pressures, is determined primarily by the Ne* to D_2 energy transfer rates. Figure 45 contains a plot of the inverse decay time of the $a \rightarrow b$ emission as a function of neon pressure for several D_2 pressures.

It appears that the excitation scheme is roughly as follows:

$$Ne^* + D_2 \rightarrow D_2^{\ddagger} + Ne \ (\approx 10^{10}\ cm^3/sec) \qquad (6)$$

$$D_2^{\ddagger} + D_2 \rightarrow D_2\left(a^3\Sigma_g\right) + D_2 (\approx 10^{-10}\ cm^3/sec) \qquad (7)$$

$$D_2^{\ddagger} + Ne \rightarrow D_2\left(a^3\Sigma_g\right) + Ne \ (\approx 5 \times 10^{-14}\ cm^3/sec) \ . \qquad (8)$$

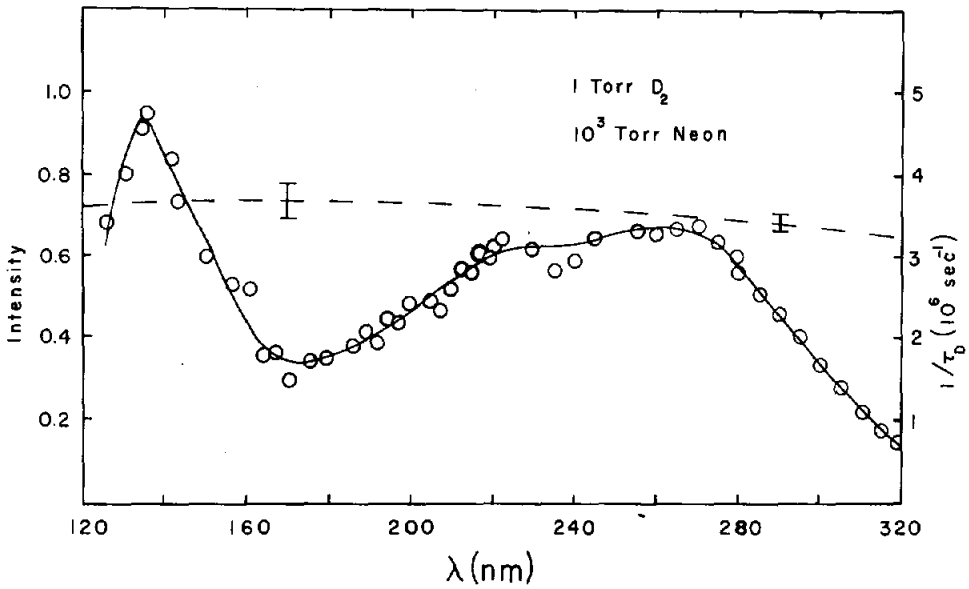

Fig. 44. Relative intensity (circles) and inverse decay times (dashed line) of the $a^3\Sigma_g \rightarrow b^3\Sigma_u$ emissions of D_2 versus wavelength. The intensity data have been corrected for variations in the instrument sensitivity.

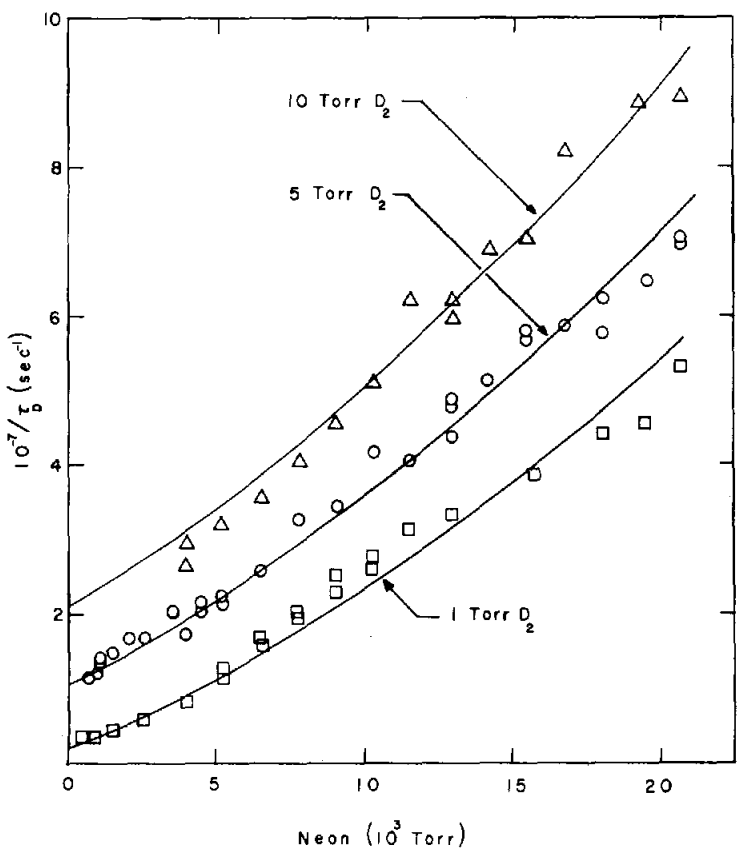

Fig. 45. Inverse decay times versus neon pressure for the $a^3\Sigma_g \rightarrow b^3\Sigma_u$ emission of D_2 for λ = 2600±125 Å.

The ‡ indicates an assumed excited state of D_2 which is higher in energy than the "a" state and is collisionally coupled to it. At higher neon pressures, the Ne_2^* formation competes with reaction (6) for the available excitation energy. For suitable conditions (0.1 to 0.2 torr D_2 and 1000 to 1500 torr neon), the quantum transfer efficiency from e-beam excited neon to the "a" state of D_2 reaches 40%. This efficiency decreases with increasing neon of D_2 pressure. The peak optical gain, calculated from the absolute emission intensity, increases with increasing pressure, attaining a value of 0.2% per cm in the present study for 10 torr D_2 and 20 ktorr neon.

Hg-Noble Gas Spectra

Fluorescence emissions from mixtures of Hg (~ 1 torr) with high pressures (10-150 psi) of Xe, Kr, and Ar have been studied for possible application as laser systems. The relativistic electron beam from Febetron 706 (12 J, 400 keV, 4 ns half-width) was used as an excitation source. In these experiments, the noble gas absorbed the e-beam energy, forming excited noble gas atomic and molecular states. The excitation was then transferred from these states to the Hg-noble gas molecular states of interest.

Three basic sets of molecular spectra were observed in all of these mixtures. First, an ~ 200 Å-wide band was observed on the red side of the Hg ($7^1S \rightarrow 6^1S_0$) 1849 Å line. This band was centered near 2100, 1970, and 1920 Å for mixtures of HgXe, HgKr, and HgAr, respectively, and is assigned to radiations for an Hg-noble gas molecule with Hg in the 7^1S_0 state and a ground-state noble gas atom. These emissions were produced with a quantum efficiency of ~ 1/2 percent (quantum efficiency ≡ photons radiated in band/e-beam energy deposited in the gas). The decay time of these emissions was very fast (5 to 100 ns, depending on noble gas pressure) and essentially followed the decay of the vuv noble-gas dimer radiation.

A second set of bands was observed on the red side of the Hg ($6^3P_1 \rightarrow 6^1S_0$) 2537 Å line, again, with a quantum efficiency of the order of 1/2%. In HgXe, this band was ~ 200 Å wide (full width), was peaked at 2650 Å, and had a number of well-defined absorption lines arising from transitions from the 6^3P to higher states. In HgKr, this band was ~ 50 Å wide and was peaked close to 2537 Å. In HgAr the band was only about 10 Å wide and was peaked very close to 2537 Å. These bands are assigned to transitions to the repulsive ground state from Hg-noble gas atoms containing an Hg 6^3P_1 atom and a noble gas atom in the ground state. These bands had a much slower decay rate (50 to 700 ns) than the above-discussed emission and were dependent on Hg and noble gas pressures. This slow decay rate is attributed to a slow formation rate of the Hg-noble molecules. The lifetime of the Hg-noble gas molecules giving rise to these bands was inferred from studies of the rise times of these emissions and was determined to be somewhat shorter than 100 ns.

A third set of bands was observed very close to the positions of the Hg atomic lines arising from transitions from the 7^3S to $6^3{}_{0,1,2}$ states. These bands, which were essentially identical in all of the Hg-noble gas mixtures, were a few angstroms on the red side of the Hg atomic lines and were about 10 Å wide. The rise and decay times of these emissions were very fast, essentially following the vuv noble gas dimer radiation. These bands were produced with fluorescence efficiencies varying from 1/4% to 1%, depending on gas pressures.

The low fluorescence efficiencies of these three sets of bands argue against their being used for a high-efficiency, high-power laser system. Also, the slow formation rate and relatively fast decay time of the bands near 2537 Å argue against their use for any short-pulse laser applications. The low fluorescence efficiencies of these bands appear to be due to the fact that most of the absorbed e-beam energy is radiated as vuv noble gas dimer emissions and hence is lost to the system.

Flashlamp Research

During the course of this year, a comprehensive program has been under way to determine the factors that govern the spectral efficiency of high-current flashlamps for use in pumping lasers. Special emphasis has been placed on the iodine photodissociation laser. It has been found that, in high-current xenon lamps, line radiation plays an important role relative to the continuum processes of bremsstrahlung and recombination radiation. Experimentally, it was found that the spectrum from such a lamp was typically a factor of two to three below the blackbody limit (at the plasma electron temperature). It was determined that the addition of Cd or Zn to the lamp produced a significant enhancement in the spectral range centered about 2800 Å. The problem with such an arrangement is that the dopant (Zn or Cd) migrates with successive shots out of the discharge volume with a concomitant reduction of the enhancement. A contract has been let with a flashlamp manufacturer to try to cure this problem by utilizing proprietary seals (those of the manufacturer).

Pragmatically, a very important question concerns the question of lamp efficiency as a function of tube bore. For the example to follow, the circuit calculations follow the standard approaches documented in the literature. The lamp is assumed to radiate as a blackbody (it is also assumed that the emitted radiation is determined by the peak discharge current). Figure 46 shows results of calculations for a capacitor bank energy of 1000 joules and for several current pulse-widths. The flashlamp is 100 cm long and the circuit is critically damped. The circuit parameters are listed in Table IX. The highest efficiency for uv radiation is attained for fast-current pulses. It can be seen that, for the 10-μs pulse, the emission is optimized for tube bores in the range of 10 to 20 cm. In general, flashlamps do not radiate as perfect blackbodies, but only approach this as a limit. For a given capacitor bank energy, smaller bore tubes approach closer to the radiation limit than larger bore tubes. An example of this is shown in Fig. 47. The ratio of the integrated energies for the large-bore tube relative to that for the smaller-bore tube and for the conditions shown in Fig. 47 is predicted (by using the experimentally observed discharge current) to be 0.43, but experimentally the ratio is 0.15. This large deviation between the experiment and calculation is caused by the relatively large departure from the limiting (blackbody) brightness of the 16-mm tube compared with the 8-mm tube.

The equivalent blackbody temperature is calculated from[34]

$$T = 603(j\sqrt{R})^{4/11} , \qquad (9)$$

where T is the temperature in Kelvin, j is the current density in amps/cm^2, and R is the radius of the tube in cm.

The temperature that maximizes the radiation efficiency (energy) about a given wavelength λ_Δ is

$$\lambda_\Delta T = 5040 \text{ microns-K} . \qquad (10)$$

On the other hand, the peak energy flux occurs for

$$\lambda_m T = 2898 \text{ microns-K} . \qquad (11)$$

So, for example, for a capacitor bank energy of 1000 joules, a bore of 10 mm, and a pulse length of 10 μs, the peak current is 13 kA (Table IX). From Eq. (9), T = 18,200 K. From Eqs. (10) and (11), it is found that λ_m = 1590 Å and λ_Δ = 2770 Å. It is seen that this is spectrally ideal for the iodine photodissociation laser. In fact, for an amplifier using C_3F_7I, the absorption band extends from nominally 2200 to 3100 Å. This results in 20% of the blackbody photons being in the appropriate absorption band. It is to be noted that the maximum emission in the 2500 to 3000 Å band for the 10-μs pulse, shown in Fig. 46, occurs for a 14-mm tube and corresponds to a temperature of 16,600 K. For the band 2500 to 3000 Å, an "optimum" temperature of 17,700 K is

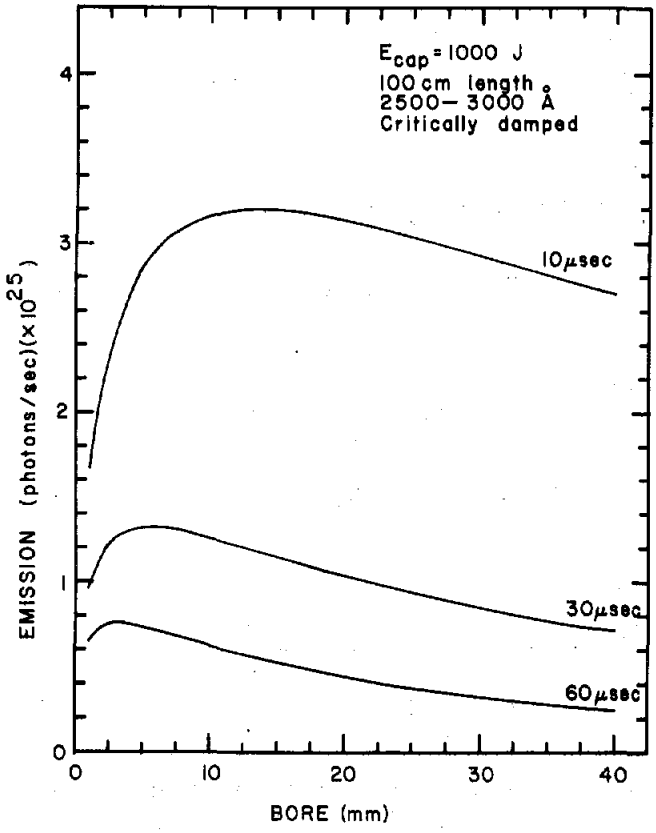

Fig. 46. The calculated photon emission (over the band 2500-3000 Å) for: E_{cap} = 1000 joules, pulse widths of 10, 30, and 60 μs, tube length of 100 cm, and a critically damped circuit.

TABLE IX

Circuit Parameters for Different Tube Bores*

Bore (mm)	C (μF)	L (μH)	V_{cap} (kV)	I_{peak} (kA)
4	0.8	10.0	49.4	7.1
8	2.1	3.9	31.1	11.1
10	2.8	2.9	26.8	13.0
12	3.5	2.3	23.8	14.7
15	4.7	1.7	20.5	17.1
20	7.1	1.2	16.8	21.0
32	12.9	0.6	12.4	28.6

*The capacitor energy is 1000 joules. The current pulse length is 10 μs (critically damped), and the tube length is 100 cm.

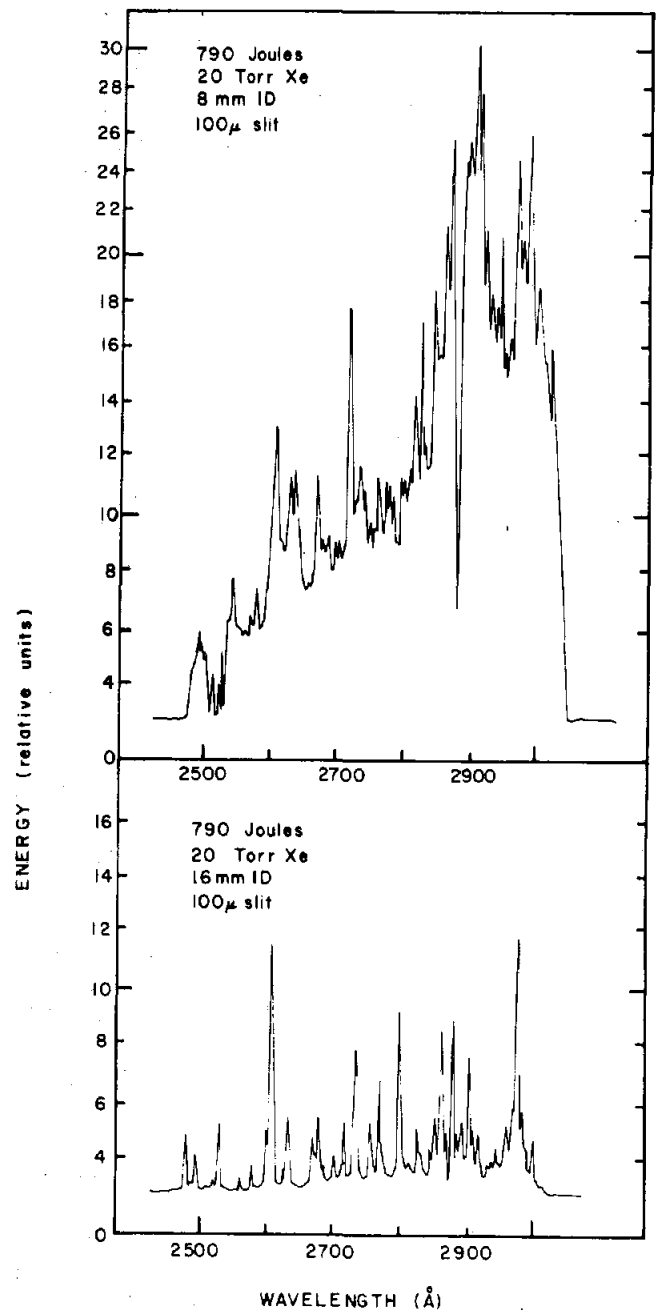

Fig. 47. The experimental time-integrated spectrum for 8- and 16-mm-ID flashlamps (30 cm long). The peak currents were 17 and 21 kA, respectively. These microdensitometer traces were obtained from photographs of the emitted spectra.

predicted, using Eq. (10), with 10.7% of the blackbody photon radiation falling in the absorption band. This small difference in determined optimum temperatures (17,700 and 16,600 K) shows that the estimate based on Eqs. (9) through (11) fairly accurately predicts the optimum flashlamp parameters for a given application.

Xenon-Excimer Formation Rates

Noble-gas excimers are important in the excitation scheme of many gas lasers, and they have been made to support laser action. Depending on the laser, excimer formation may be either desirable or undesirable. For example, the helium metastable atom, 2^1S, is essential in the excitation scheme of the 6328-Å He-Ne laser; but, if helium metastable atoms are converted to helium excimers, they can no longer serve as an energy pool for the He-Ne laser. Noble-gas excimer formation is also undesirable in some noble-gas halide lasers, the argon-nitrogen laser, and others. Excimer formation is, of course, necessary to achieve laser action in the noble-gas excimer lasers (Xe_2^*, Kr_2^*, and Ar_2^*, for example), and they have been used to excite other lasers by photolysis excitation and by collisional-energy-transfer excitation (for example, $O(^1D) \rightarrow O(^1D)$ laser). Whether excimer formation is desirable or undesirable, it is essential to laser modeling to know the reaction rates that are important for the formation and the decay of noble-gas excimers.

Reaction rates pertaining to the formation and decay of xenon excimers ($^3\Sigma_u$, $^1\Sigma_u$), both in pure xenon and in mixtures of xenon and other noble gases, were measured with the apparatus shown in Figure 48. The krypton-excimer laser radiation ($\lambda \approx 1465$ Å) excites ground-state xenon atoms, $^1S_0$, to the $^3P_1$ levels, and reaction rates are determined by analysis of the temporal behavior of the xenon-excimer radiation. An energy level diagram showing the energy levels of interest to this study is shown in Fig. 49, and the reaction scheme is shown in Fig. 50. The formation and decay of the xenon excimers is described by the following set of coupled differential equations, where the notation is explained in Fig. 50.

$$\frac{dN_1}{dt} = -(\nu_{13} + \nu_{14} + R_{12})N_1 + R_{21}N_2 \quad (12a)$$

$$\frac{dN_2}{dt} = -(\nu_{23} + \nu_{24} + R_{21})N_2 + R_{12}N_1 + \text{Source} \quad (12b)$$

$$\frac{dN_3}{dt} = \nu_{23}N_2 + \nu_{13}N_1 + R_{43}N_4 - (A_{35} + R_{34})N_3 \quad (12c)$$

$$\frac{dN_4}{dt} = \nu_{24}N_2 + \nu_{14}N_1 + R_{34}N_3 - (A_{45} + R_{43})N_4 \quad . \quad (12d)$$

It is convenient to express the rate coefficients in terms of partial pressures, p_{Xe}, p_{Kr}, etc.,

$$\nu_{\ell n} = \sum_K k_{\ell nK} p_{Xe} p_K \quad (13a)$$

$$R_{\ell n} = \sum_K R_{\ell nK} p_K \quad , \quad (13b)$$

where the summation is over all gas species. The radiative lifetimes, A_{35}^{-1} and A_{45}^{-1}, were measured by Ket et al.[35] and are given by $A_{35}^{-1} = (5.5 \pm 1.0)\ 10^{-9}$ sec and $A_{45}^{-1} = (96 \pm 5)\ 10^{-9}$ sec. The reaction rates were determined by comparing experimental excimer radiation intensities ($A_{35}N_3 + A_{45}N_4$) to numerical calculations. The observed waveshape of the laser was used to describe the source waveshape (since the equations are linear, the source intensity is not necessary). In some instances, approximate analytical solutions to Eqs. (12) are useful to determine coefficients and they are always useful to obtain an intuitive feeling for the effect of certain rates on the solution. If the source can be adequately described by a delta function at t = 0 and if R_{12} and R_{43} are set equal to zero, then

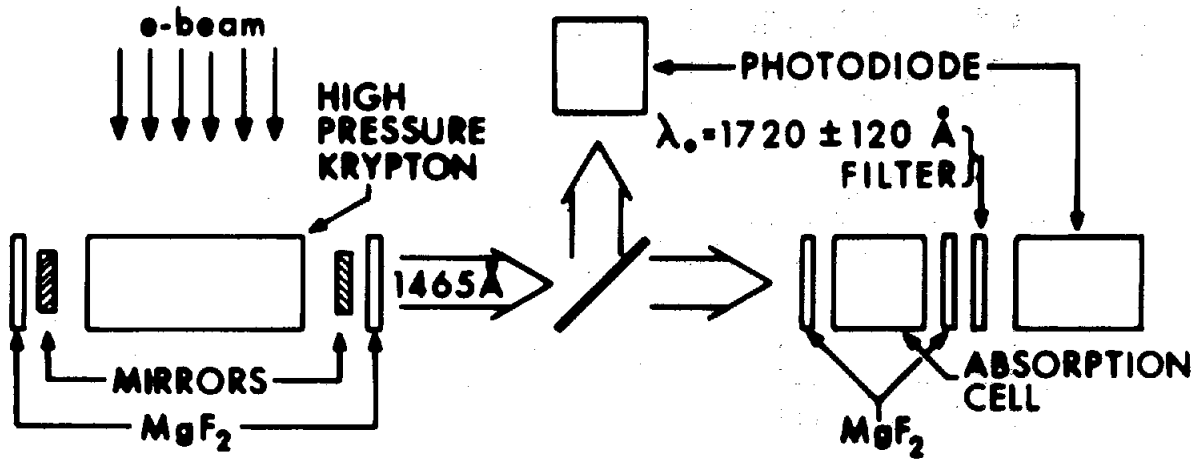

Fig. 48. Schematic of the experimental apparatus. The electron beam is from a Febetron 705.

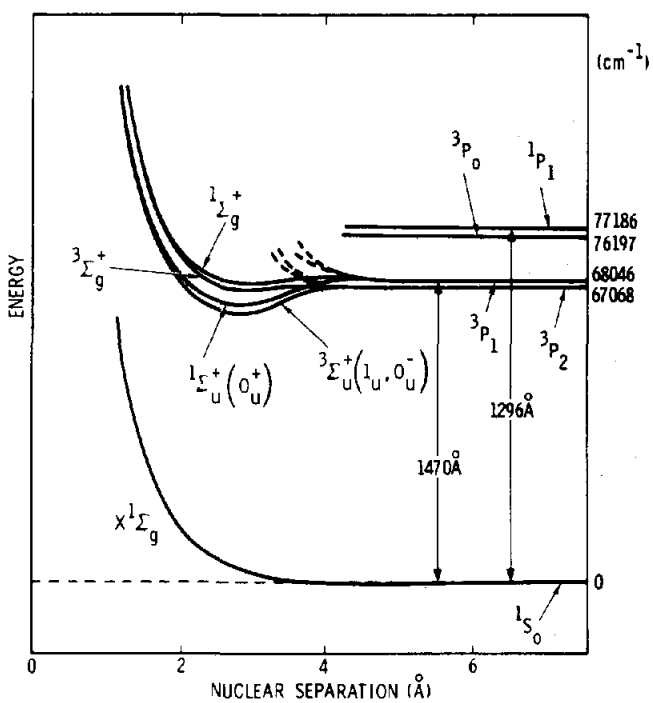

Fig. 49. Xenon energy levels of interest in this study. Krypton-excimer laser radiation is used to selectively excite the $^3P_1$ resonant level.

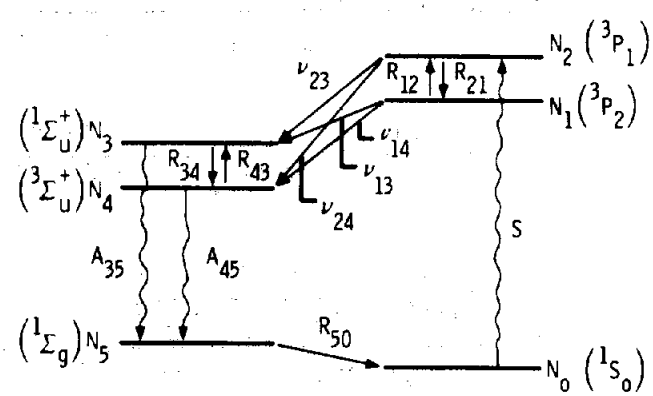

Fig. 50. Illustrates the reaction channels included in the model and the notation used in the text.

$$N_3 = N_{20}\left\{\frac{\nu_{23} + \dfrac{\nu_{13}R_{21}}{\nu_1 - \nu_2 - R_{21}}}{A_{35} + R_{34} - \nu_2 - R_{21}}\left[e^{-(\nu_1+R_{21})t} - e^{-(A_{35}+R_{34})t}\right]\right.$$

$$\left. - \frac{\nu_{13}R_{21}}{(\nu_1 - \nu_2 - R_{21})(A_{35} + R_{34} - \nu_1)}\left[e^{-\nu_1 t} - e^{-(A_{35}+R_{34})t}\right]\right\} \tag{14a}$$

$$N_4 = N_{20}\left\{\frac{H}{A_{45} - \nu_2 - R_{21}}\left[e^{-(\nu_2+R_{21})t} - e^{-A_{45}t}\right] - \frac{J}{A_{45} - \nu_1}\left[e^{-\nu_1 t} - e^{-A_{45}t}\right]\right.$$

$$\left. - \frac{K}{A_{45} - A_{35} - R_{34}}\left[e^{-(A_{35}-R_{34})t} - e^{-A_{45}t}\right]\right\} , \tag{14b}$$

where:

N_{20} = density of level N_2 at $t = 0$

$\nu_1 = \nu_{13} + \nu_{14}$

$\nu_2 = \nu_{23} + \nu_{24}$

$$H = \nu_{24} + \frac{\nu_{14}R_{21}}{\nu_1 - \nu_2 - R_{21}} + \frac{R_{24}\left(\nu_{23} + \dfrac{\nu_{13}R_{21}}{\nu_1 - \nu_2 - R_{21}}\right)}{A_{35} + R_{34} - \nu_2 - R_{21}}$$

$$J = \frac{\nu_{14}R_{21}}{\nu_1 - \nu_2 - R_{21}} + \frac{R_{34}\nu_{13}R_{21}}{(\nu_1 - \nu_2 - R_{21})(A_{35} + R_{34} - \nu_1)}$$

$$K = \frac{R_{34}\left(\nu_{23} + \dfrac{\nu_{13}R_{21}}{\nu_1 - \nu_2 - R_{21}}\right)}{A_{35} + R_{34} - \nu_2 - R_{21}} - \frac{R_{34}\nu_{13}R_{21}}{(\nu_1 - \nu_2 - R_{21})(A_{35} + R_{34} - \nu_1)} .$$

Various limits of this solution are useful to evaluate certain coefficients. For example, if $A_{45} < \nu_1$ and $A_{45} < \nu_2$, the final decay of the excimer radiation is given by A_{45}. Also, if $\nu_1 < R_{21}$ and $\nu_1 < A_{45}$, the final decay is given by ν_1. Also, if $(A_{35}+R_{34}) > (\nu_2 + R_{21})$, $(A_{35}+R_{34}) > \nu_1$ and $\nu_1 < (\nu_2+R_{21})$, the radiation will rise with a rate determined mainly by $(A_{35}+R_{34})$ and it will attain a value on this time scale that is determined mainly by ν_{23}. Clearly, by comparison of experimental excimer radiation waveforms to calculated intensities at many different pressures, several of the coefficients of interest can be determined. Some of the coefficients that we have determined are listed in Table X.

TABLE X

Some Reaction Rates That Determine the Formation and Decay of Xenon Excimers in Xenon and in Mixtures of Xenon with Other Noble Gases

K	$k_{13K} + k_{14K}$ (10^{-32} cm^6 sec^{-1})	k_{23K} (10^{-32} cm^6 sec^{-1})	R_{21K} (10^{-13} cm^3 sec^{-1})	R_{43K} (10^{-15} cm^3 sec^{-1})
Xe	7.9	1.2	9.1	< 17
Kr	4.9		2.2	
Ar	2.7			
Ne	1.8			
He	1.7			< 3.7

Electron-Beam Excitation of Rare Gas Mixtures

There is considerable interest in the electron-beam-excited xenon dimer (Xe_2^*) laser as a potentially efficient, tunable source of vuv radiation. The Xe_2^* dimers, which radiate in a broad continuum near 1720 Å, are formed primarily by the three-body association reaction

$$Xe^* + Xe + R \rightarrow Xe_2^* + R \qquad (15)$$

in typical e-beam-excited, high-pressure, rare-gas mixtures. We have performed a series of experiments in which mixtures of xenon with added helium and argon are excited by an electron beam from a Febetron 706 (2 ns, 440 keV). The added rare gas markedly increases the formation rate of Xe_2^* as shown in Fig. 51. In this figure the photodiode signal is directly proportional to the 1720 Å fluorescence intensity which is, in turn, a measure of the stored energy in the upper laser level. The peak intensity in Fig. 51 increased with the addition of 10^4 torr helium by more than a factor of 3, while the e-beam energy deposition increased by only 37 percent.

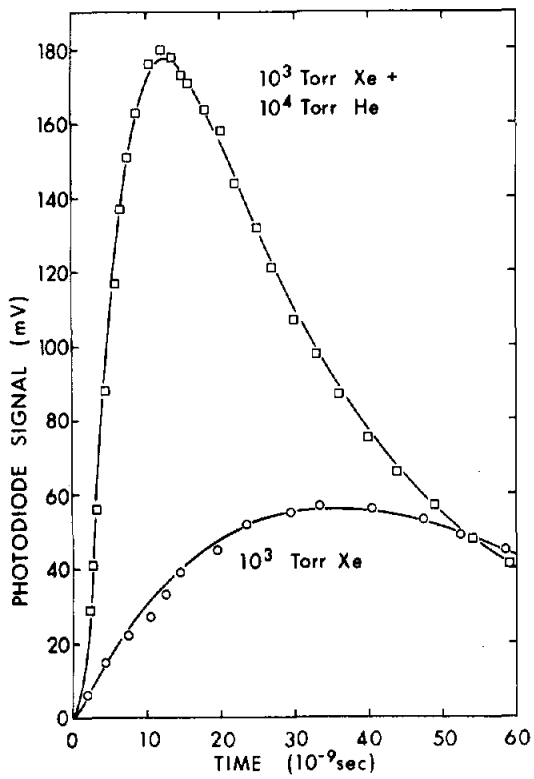

Fig. 51. Digitized photodiode signal of the 1720 Å fluorescence versus time for 103-torr xenon with and without added helium. The solid curves are the exponential fits to these data.

A considerable body of data similar to those of Fig. 51 for different pressures of xenon, helium, and argon was analyzed in terms of a phenomenological three-body formation rate constant. These rate constants are summarized in the following table:

R	k_1
Xenon	5.0×10^{-32} cm^6 sec^{-1}
Helium	1.4×10^{-32} cm^6 sec^{-1}
Argon	2.3×10^{-32} cm^6 sec^{-1}

In addition to decreasing the formation time of Xe_2^*, the present study showed that the addition of helium or argon to xenon does not quench any significant portion of the Xe_2^* fluorescence, even at the highest pressures examined (2×10^4 torr).

Relativistic E-Beam Energy Deposition in Gases

To model a laser with inversions produced by relativistic e-beam energy deposition, one wants a source term relating the production rate of slow electrons, ions, and metastables to the e-beam time history. To do this, one needs the atomic subshell ionization cross section and stopping power, both at the energy of the e-beam and at low (< 10 keV) energies. This latter is necessary to describe further ionization by secondaries. The available data are limited to either semiempirical fits to observations of semiclassical calculations. To remedy this, we have calculated generalized oscillator strengths for elements with $18 \leq Z \leq 54$, to supplement earlier calculations with $Z \leq 18$ (Phys. Rev., A3, 267, 1971). With suitable interpolation, the calculations are applicable to all elements with $Z \leq 54$. Our specific interest is argon, krypton, and xenon, and, for these elements, the calculations were done for all the subshells.

Gas Discharge Physics

Townsend Discharges - The traditional treatment of Townsend discharges examines the electron multiplication when an electron produced at the cathode crosses a planar diode and produces further ionization. For various gases there is a large body of experimental data relating various parameters to functions of E/P, the ratio of diode electric field to pressure. For systems with different initial conditions (e.g., volume production of low-energy electrons via transverse e-beams), it is assumed that the parametric dependence on E/P found in the traditional discharge is still applicable. To investigate this point, a model for the discharge was developed which uses only atomic parameters for the gas, i.e., realistic stopping power, ionization cross sections, and thresholds. The results, while still tentative, are interesting in that the model predicts both first and second Townsend coefficients, without recourse to a feedback mechanism, for the traditional Townsend discharge. Current efforts are directed to predicting Paschen breakdown curves from the basic atomic parameters, and extending the analysis to systems relevant to lasers.

Space Charge Effects in Gas Discharges

When space charge effects may be relevant to the physics of gas discharges, it is a common practice to invoke vacuum space charge results. To study the modifications of the vacuum results when positive ions are present, we are examining space charge flow in a vacuum diode with a positive ion background density. Currently the ions are treated as having infinite mass (no ion currents). The ion density can drastically modify the vacuum space charge results. For the planar vacuum diode, the potential must rise monotonically from cathode to anode. With positive ion density, the potential can both rise and fall, i.e., the potential can be zero at points other than the cathode. Further, for certain ranges of electron current density and net charge between the plates, the potential is not unique. We are examining the possibility that the boundaries, separating parameter regions where the potential is unique from those in which it is not unique, may provide a criterion for arcing.

Computer Modeling of Traveling-Wave-Excitation in the N_2 Laser

The implicit method of characteristics, developed to calculate amplification of probe beams and spontaneous emission in the H_2-F_2 laser, is also useful in systems where traveling-wave excitation is important. A brief investigation of traveling-wave effects in the electron-beam-excited superradiant N_2 laser has been completed. The purpose of this investigation was to demonstrate the utility of the implicit method of characteristics and to assess the validity of two assumptions used in a recently developed computer model of the N2 system (IEEE J. Quantum Electron., Vol. QE-11, November 1975, pp. 892-902). The assumptions were: (1) there is negligible radiation extracted in the direction opposite to the electron beam propagation, and (2) a quasi-equilibrium exists between pumping and stimulated emission at a point once the overall gain for a wave reaching that point reaches the value e^{13}. Using the implicit method of characteristics developed for the H_2-F_2 laser code and the same essential kinetics as used in the referenced paper, both assumptions have been confirmed for the regime they considered.

The Characterization and Calibration of Nonlinear Optical Susceptibilities

The observation of highly dispersive nonlinear propagation phenomena in the spectral region of a Raman active excitation suggests the importance of the ability to obtain a complete characterization of the third-order nonlinear susceptibility χ_3.[36] Although a variety of techniques have been applied to the study of nonlinear optical interactions that are cubic in the electric field strength, quantitative comparison of the available data on the nonlinear susceptibility χ_3 has been limited by the lack of: (1) an accurate common standard of calibration, (2) a full understanding of the dispersive character of χ_3, (3) the ability to obtain independent determinations of the real and imaginary parts of χ_3, and (4) a method which is capable of accurately discriminating between the electronic and molecular contributions to χ_3. Indeed, the latter point has precluded any meaningful comparison of nonlinear refractivity data with data obtained by frequency-mixing techniques.

We have developed a technique of nonlinear interferometry, whereby both the real and imaginary parts of the nonlinear susceptibility, χ_3, can be determined independently both in sign and absolute amplitude over a wide spectral region. Moreover, the technique has a unique capability of separating the electronic and molecular contributions to χ_3 to a high degree of accuracy, hence, suggesting that it may serve as a basis of calibration for a variety of measurements of χ_3 including nonlinear refractive index phenomena, frequency-mixing, Raman scattering, and two-photon absorption.

As shown in Fig. 52, the Jamin interferometer is central to the technique. A doubled Nd:YAG laser beam at 0.532 μ is injected into one arm of the interferometer to induce a phase shift due to nonlinear refractivity or a gain or loss arising from Raman activity or multiple photon processes, respectively, in the sample. A cw dye laser is used to probe the interferometer. Changes induced by the 0.532-μ pump pulse are thus manifested in a fringe shift or intensity change at the interferometer output and contain the information necessary to determining χ_3.

It is well known that an interferometer adjusted to give a nulled output will not discriminate between amplitude and phase changes induced in one of its paths. It merely responds to the squared amplitude of these changes. By operating the interferometer with a relative phase retardation of $\pm\pi/2$, however, one obtains an output intensity of the form

$$S_{\pi/2} \approx KE^2\ 1 \pm \Delta(t) + G(t)/2 \quad , \qquad (16)$$

where $\Delta(t)$ is the phase retardation produced by the pump in units of radians, $G(t)$ is the corresponding intensity gain in nepers, E is the unperturbed probe-beam field amplitude, and K contains geometric factors governed by beam overlap. Thus, the

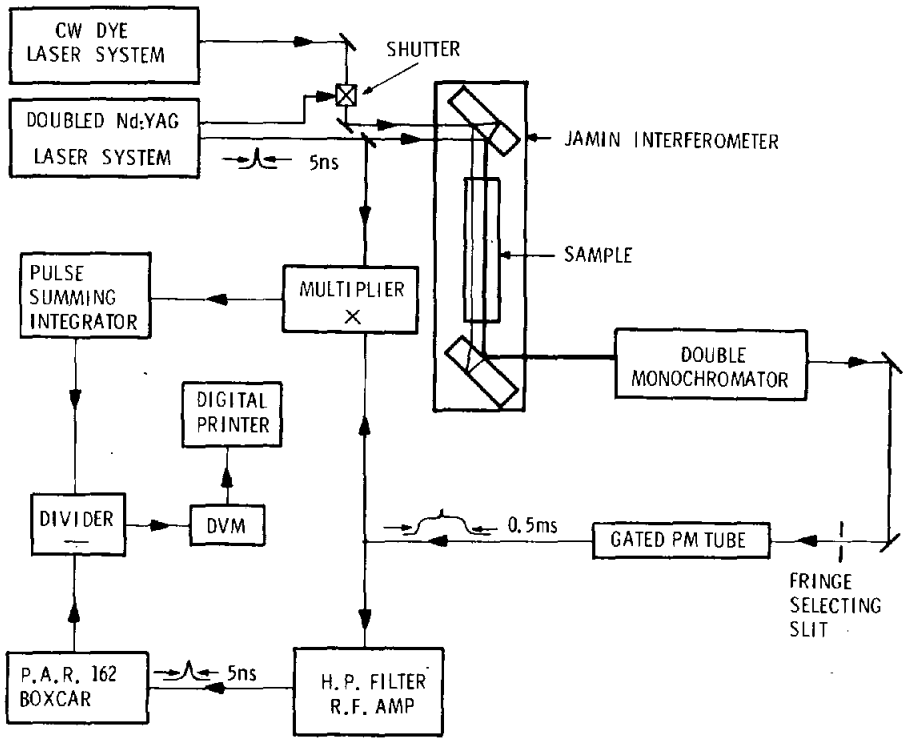

Fig. 52. Schematic representation of the experimental apparatus.

perturbation is optically heterodyned to produce an output signal with time-varying terms which are directly proportional to the induced gain and phase shift. Moreover, by blocking one path of the probe beam through the interferometer, the phase-information signal is lost and a simple gain signal is obtained. Adjustment of the interferometer for $\pm\pi/2$ phase delay changes the sign of the phase-shift term, thus providing a self-consistency check on the experiment. An output signal linearly proportional to input intensity considerably simplifies the signal processing, and the close proximity of the two paths in the interferometer makes for outstanding thermal stability.

A schematic representation of the experimental apparatus is shown in Fig. 52. The Jamin interferometer described above consists of two interferometer flats coated for total reflection on one surface and partial transmission (8% to 50%) in the range of interest on the opposite face. A TEM_{00q} single-mode Q-switched Nd:YAG laser system is frequency-doubled in KDP to provide the 5-ns pump pulse which is 92% reflected from the partially transmitting interferometer surface. A single-mode cw dye laser operating in the region from 0.52 to 0.69 μ is used as the probe source and is synchronously shuttered with the pump pulse to avoid thermal blooming in the samples. At the interferometer output, the two collinear beams are separated by a double monochromator, and a fringe-selecting slit is used to select a portion of the fringe display representing not more than ±3 degrees of variation from the desired ±90-degree relative phase retardation specified by Eq. (16). The interferometer output is shown in Fig. 53. The signal is detected by a gated photomultiplier (EMI Model 9818A) resulting in a gated cw background signal with a 5-ns perturbation superimposed on it. A high-pass filter eliminates the background signal, and the 5-ns signal is amplified and detected on a PAR Model 162 boxcar averager operating in a linear summing mode with a 10-ns gatewidth. Relative values for $\Delta(t)$ are obtained directly by taking the ratios of the boxcar output relative to the time-integrated

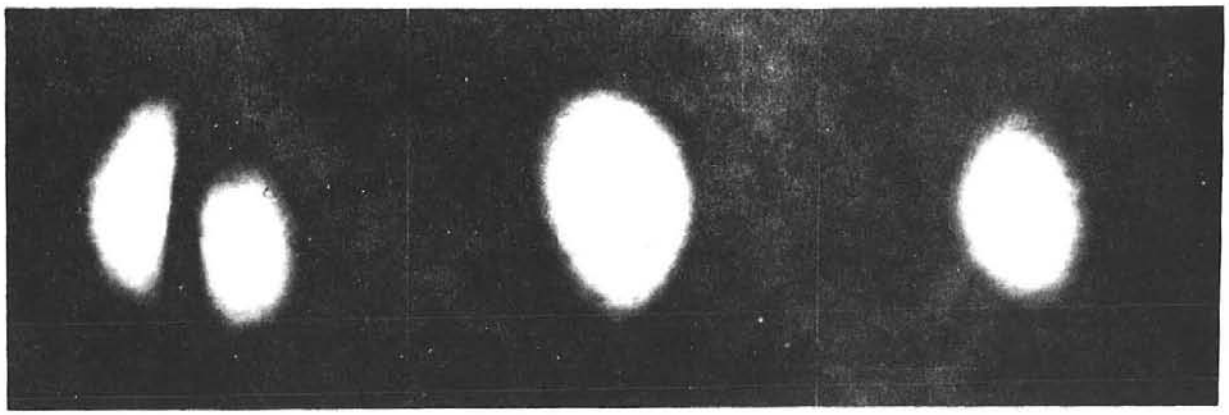

a b c

Fig. 53. Photographs of the interferometer output under the conditions where the two paths through the sample are (a) 180 degrees out of phase, (b) in phase, and (c) ±90 degrees out of phase. The entire spot size spans a phase traversal of approximately 180 degrees, while the fringe-selecting slit is adjusted to a maximum width of 350 μ and covers approximately 6 degrees of phase.

product of the pump and probe laser input intensities. The results are displayed on a digital printout with a reproducibility which is presently better than 3%, after averaging over 350 shots. Further improvement is expected by improving the amplitude stability of the pump source. At present, the instrumental resolution is 0.2-degree phase retardation or a gain of 3.5×10^{-3}. A typical signal fed into the boxcar integrator is shown in Fig. 54.

Although the technique described above may be applied to a variety of problems, it was felt that a pressing question was the large uncertainty in the available nonlinear refractive index measurements, which results from an almost complete lack of knowledge concerning the sizes of the various mechanisms contributing to n_2.[37] As shown in Fig. 55, a measurement of φ, which is the ratio of the induced refractive index change with the probe beam linearly polarized parallel and perpendicular to the pump beam, respectively, gives an extremely sensitive determination of ρ, the fractional electronic contribution to the optical Kerr constant. By measuring φ to be -3.25 and -3.8 in liquid CS_2 and C_6H_6,

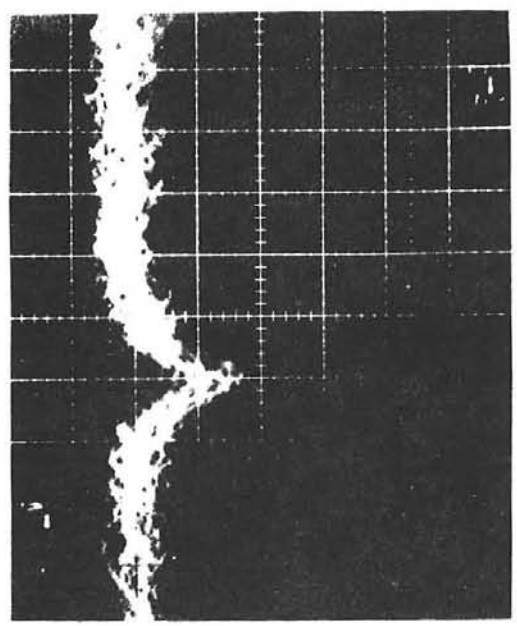

Fig. 54. A typical input signal into the boxcar integrator for approximately 3 degrees of induced phase retardation. Fluctuations arise primarily from shot noise and pose the basic limitation on detection sensitivity. The horizontal scale is 5 ns/div.

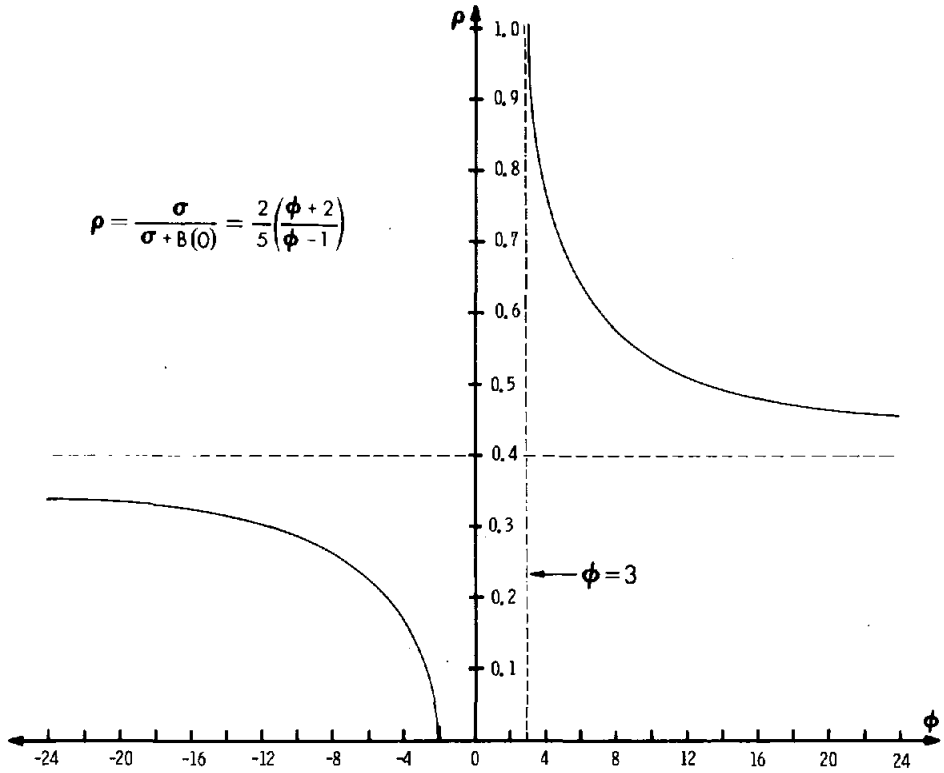

Fig. 55. Graph of the fractional electronic contribution to the optical Kerr constant ρ vs the measured ratio of nonlinear refractive index changes φ for a probe polarized parallel and perpendicular to the pump beam, respectively.

respectively, for a pump wavelength of 0.532 μ, we determine that 11.8±1.1% and 15.0±0.8% of the Kerr constants of these respective liquids arise from an electronic nonlinearity. Calibration to precise dc Kerr measurements in CS_2 yield values of $(8.05 \pm 0.87) \times 10^{-14}$ esu and $1.55(\pm 0.16) \times 10^{-14}$ esu for the electronic contributions to the nonlinear susceptibility $\chi_3^{1111}(-\omega_1, \omega_1, \omega_2, -\omega_2)$ in CS_2 and C_6H_6, respectively. These values provide a basis for comparison of nonlinear refractive index measurements with results obtained by frequency-mixing techniques.

LASER-EXCITATION-SOURCE DEVELOPMENT

Long Pulsewidth Electron Beams for Laser Excitation

Relativistic electron beams have been demonstrated to be useful to excite gas lasers. These e-beams have a number of advantages and unique applications in the excitation of many types of lasers including excimer lasers. In a large laser system, it is important that the excitation system be simple, inexpensive, and reliable. For this reason and others, we have developed and are presently testing an e-beam system that does not utilize a pulse line to form a short pulse. Instead of using a charged transmission line, the output from a modified Type C Guillemin pulse-forming network is used to form a nominally 1-μs pulse. A circuit schematic is shown in Fig. 56. Previous experience and tests have shown that an electron beam diode can be made that will not short out in less than 1 μs at current densities well above the operating level of our 10 Ω, 700-kV device. In Fig. 57, we present the computed (SCEPTRE circuit analysis program) output pulse across a 10-Ω load. Because of the long

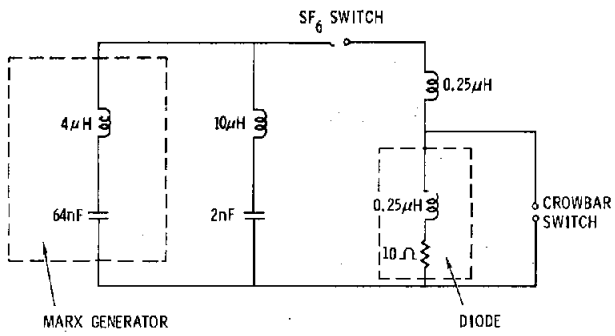

Fig. 56. Schematic diagram of 1-μs, 650-kV, 35-kJ electron beam accelerator.

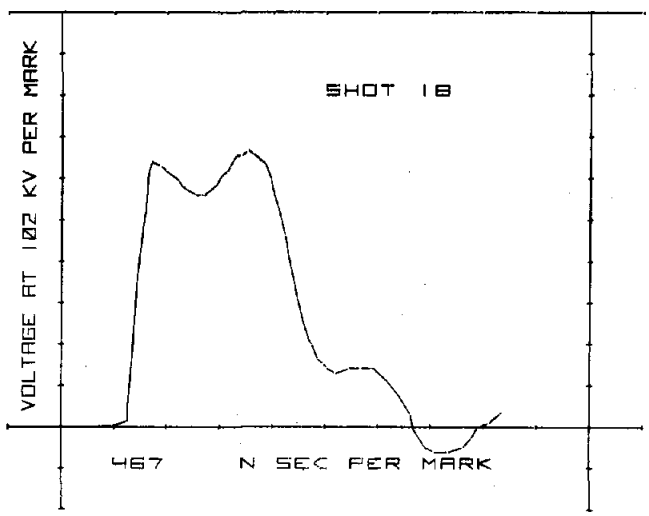

Fig. 57. LILI output voltage pulse with 15-ohm resistive load

tail on the pulse, we may have to short-circuit the diode at ~ 1 μs to prevent the destruction of the anode. The exact timing of the crowbar will be determined after a detailed study of the pulse shape. This study is now being performed.

The vacuum diode is a shortened version of the REBA diode, and the capabilities exist for either transverse or axial electron beam excitation of the laser gas. The measured diode inductance is 250 nH.

Radially Converging Electron Beams

Radially converging electron beams that enter the gas volume through the cylindrical walls of the chamber offer several advantages in pumping gas lasers. A preliminary design study of an accelerator capable of depositing 10 to 20 kJ of electrons in a 30-cm-diameter, 80-cm-long gas volume in 20 ns was completed.[38, 39] An experiment was constructed to generate radially converging electron beams, and initial diode experiments demonstrated that uniform current densities could be achieved on the anode.

Monte Carlo electron transport calculations with the CYLTRAN code[40] indicate that the most uniform deposition occurs when the range of the electrons equals the diameter of the gas chamber. For this study, a 30-cm-diameter chamber was selected, and for gas pressures in the 3- to 10-atm range (a standard HF mixture was used for the code calculations) the voltage should be in the 0.5- to 1-MV range. The uniform deposition depends upon a constant current density at the anode. Thus, the current must be limited in each diode such that pinching due to the self-magnetic field of the beam does not occur. Three to seven diodes will be required to generate the 1- to 2-MA current. An artist's sketch of the proposed accelerator is shown in Fig. 58. Each diode is fed by rapidly charged (< 100 ns) oil-dielectric transmission lines with untriggered rail switches.[41, 42] A Marx generator charges two or three water dielectric capacitors that subsequently discharge into the transmission lines.

The CYLTRAN calculations indicate that, at the optimum voltage and with a constant-current density at the anode, the electron beam energy deposition will be uniform within ±7% throughout the gas volume. Up to 75% of the beam energy will be deposited in the gas. If the range of the electrons is twice the diameter of the chamber, only slight changes in the uniformity of deposition

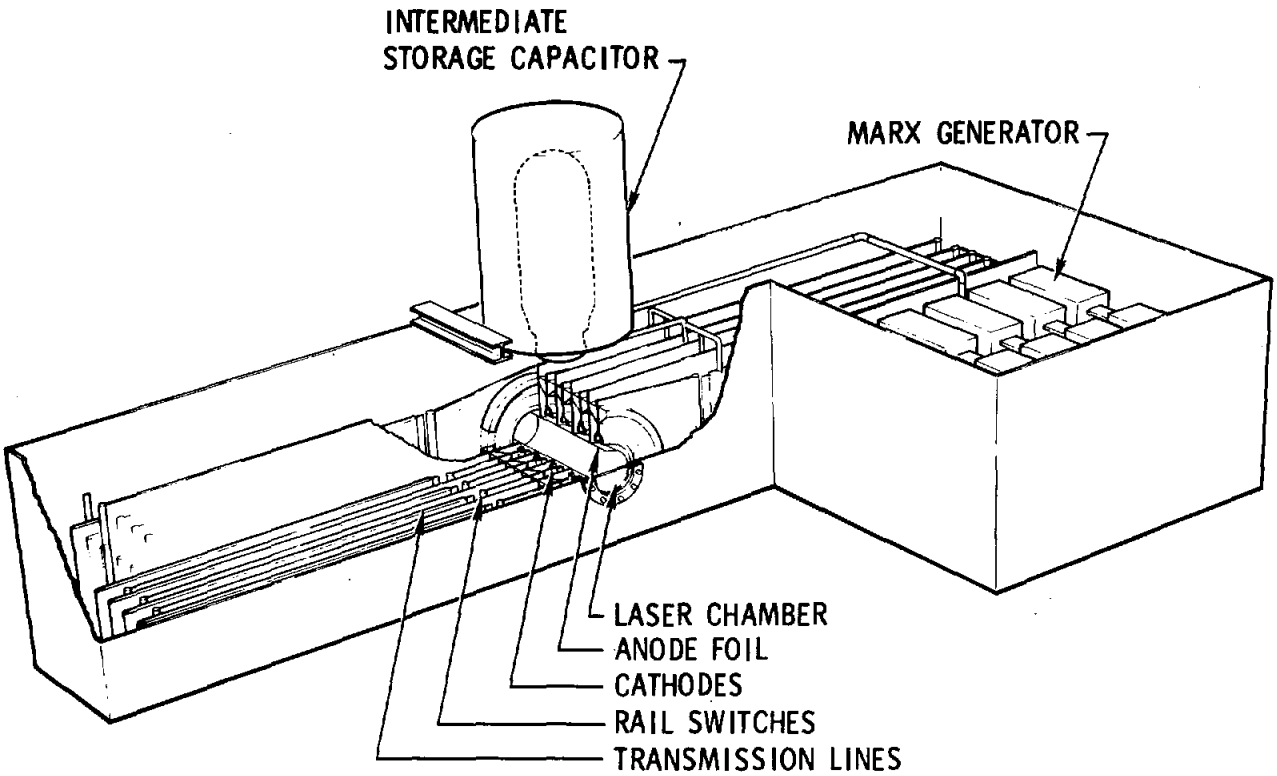

Fig. 58. Electron beam accelerator for generating 10 to 20 kJ of radially converging beam.

occur (variations always less than ±20%). In the region between the diodes, the scattering of the electrons creates uniform deposition except near the anode surface where the deposition is 20% lower.

The experiment was designed to generate a 1-MV, 200-kA, 20-ns electron beam in a cylindrical diode. An artist's sketch of a pulser is shown in Fig. 59. An existing Marx generator, intermediate storage capacitor, and test tank were used. The intermediate storage capacitor charges the oil-dielectric, pulse-forming transmission lines (PFL) to 2 MV in 100 ns. The PFL is discharged into the diode through two low-jitter, self-closing, oil-dielectric rail switches. Figure 60 is a sketch of the diode. The anode is 20 cm in diameter and 26 cm long. Initial tests were done with the diode operating at 600 kV and 70 kA. The most uniform current densities were obtained when the cathode consisted of three 5-μm-thick stainless-steel discs with a 30-cm inner diameter and spaced 5.5 cm apart. Figure 61 is a plot of the relative current density along the anode cylinder. The plot is an average of four measurements taken 90 degrees apart. The cathode blade locations are indicated. The current density (60 kA/cm^2) is constant to within ±20 percent over the desired 20-cm length and decreases very rapidly at the edges. Similar measurements in the azimuthal direction indicated variations in current density less than 10%.

Wire mesh or metal cathode cylinders 30 cm in diameter did not emit uniformly with the low electric fields (~ 100 kV/cm) and produced 30% higher current densities on the anode at the edges of the cylinder than the area inside the cylinder. These tests are continuing at the 1-MV level.

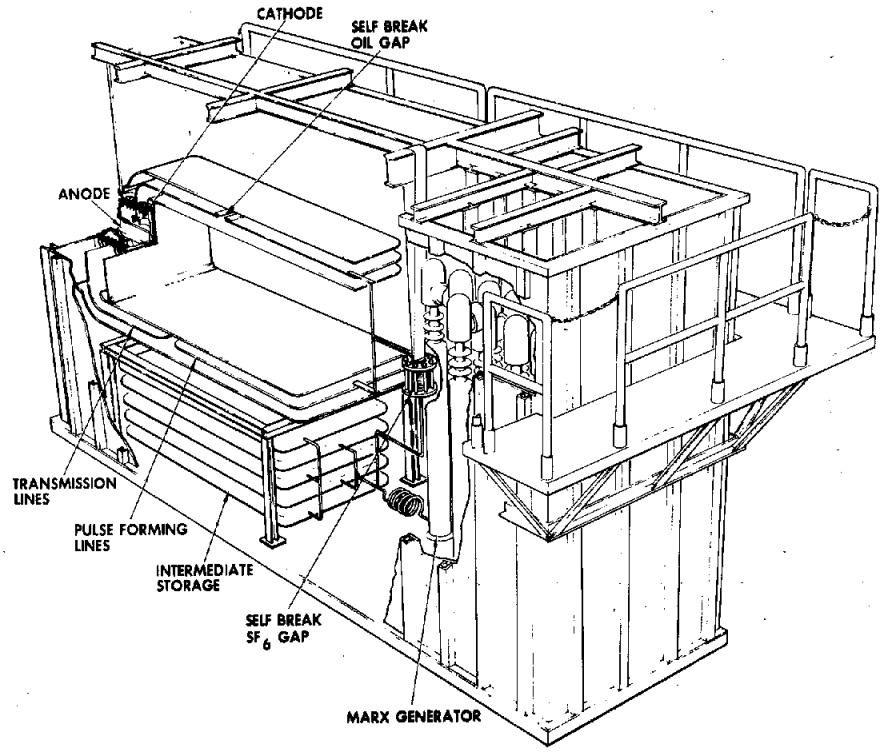

Fig. 59. Sketch of pulser constructed for cylindrical diode experiment.

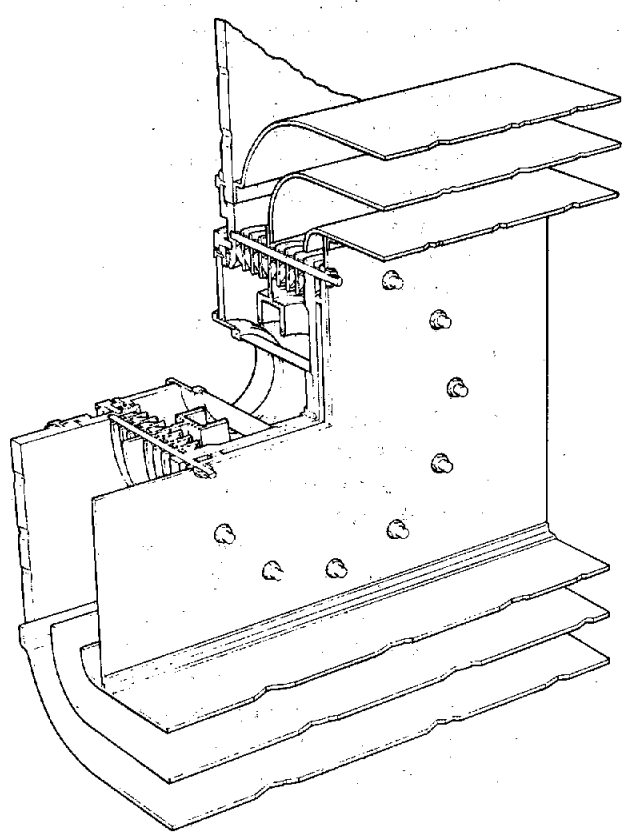

Fig. 60. Cylindrical diode with radially converging electron beams.

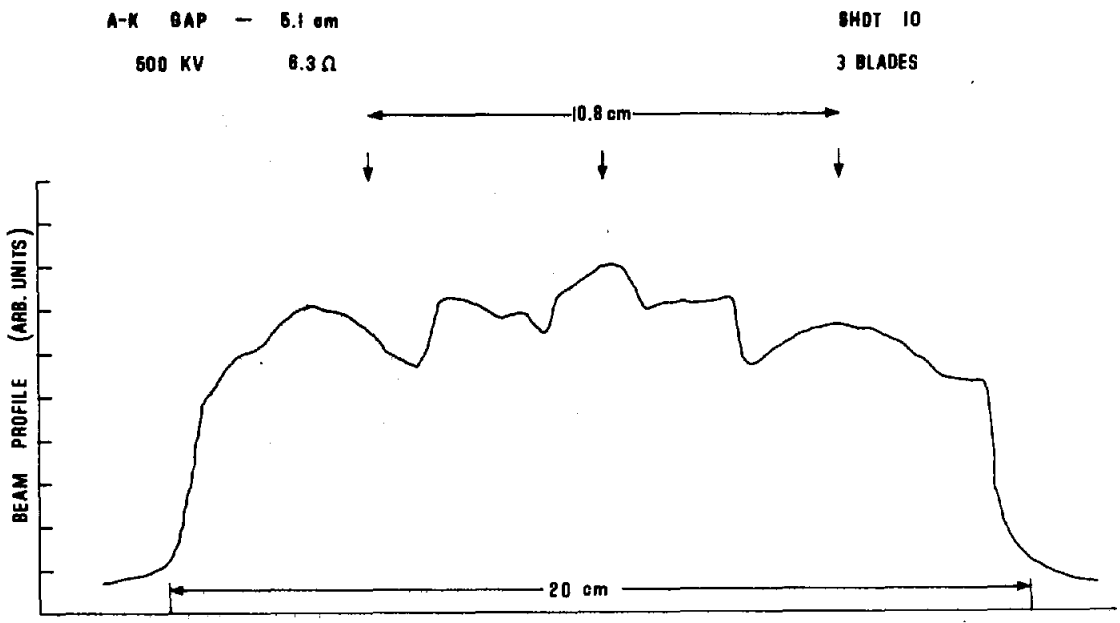

Figure 61. Relative current densities along cylindrical anode.

Excitation of Rare Gases in a High-Voltage, Electron-Beam-Controlled Discharge

Compared with pumping by high-energy electron beams, the excitation of rare gases by electron-beam-controlled discharges offers an important advantage: The apparatus required to produce the discharges is generally simpler and less expensive than high-energy beam machines. We are continuing to study the usefulness of such discharges in exciting electronic transitions in rare gases. These transitions are important not only in rare-gas lasers but also in lasers that involve transfer of energy from rare gases to other lasing atomic species.

The apparatus for this study consists of three major components. A stainless-steel chamber houses the rare gas at pressures up to 2.5 atm; inside this chamber is a polished anode, 10 cm wide and 100 cm long, to which high voltage may be applied. A switched capacitor bank, the second major component of the apparatus, supplies potentials up to 100 kV to this anode. A cold-cathode electron gun, driven by a 300-kV Marx generator, is the third component; it supplies a preionizing electron beam at intensities up to 0.5 A/cm^2 in the 1000-cm^2 area subtended in the gas chamber by the anode plate.

The first task required by this study was a determination that the anode could hold its potential for times longer than 1 μs without arc formation in the preionized gas. To make this determination, we fired the electron gun into the gas; then, after delays ranging from 0 to 4 μs, we switched the capacitor-bank potential onto the anode. At electric field strengths up to ~ 5 V/cm/torr, the field proved stable for times as long as 3 or 4 μs after application of the anode potential. Such times are long enough to permit significant passage of energy from the capacitor bank into the gas; in the system consisting of the capacitor bank and the cables connecting it to the discharge anode, there is enough inductance to produce a voltage risetime of 1 to 2 μs.

We next proceeded to observe the ultraviolet light emitted from the excited gas. In all our studies of uv emission, we found it necessary to crowbar the anode voltage a few μs after it appeared at the anode; otherwise, arcs invariably formed in the ionized medium. We have now observed

ultraviolet emission from argon and xenon at pressures up to 2.5 atm. As determined by a uv spectrometer viewing the excited volume, the radiation is the usual continuum radiation characteristic of each gas. The discharge has no easily observed effect upon the spectral shapes.

Our principal concern in these studies was to measure the effect of the applied electric field on the intensity of uv emission. A calibrated photodiode, sensitive to radiation in the range covered by the argon and xenon continua, viewed the entire excitation volume. The results for the two gases were very different. In argon we observed no experimentally significant difference in intensity of emission under excitation by the electric field. In tests at 2.5 atm of argon with no applied electric field, we measured up to 40 joules of emitted uv light from the 3.84-liter excited volume. Application of voltage to the anode had the effect of lengthening the total pulse width by ~ 50%, but the energy emitted in the added pulse duration amounted to only a few percent of the total emission. Within experimental uncertainty, the applied electric field contributed no enhancement of the radiation produced by the preionizing electron beam.

In xenon the electric field significantly increased the observed uv radiation. Typical data appear in Fig. 62. With no applied field, the total uv energy, as determined by the photodiode, was 0.4 joule. The energy supplied by the electron gun over the duration of this pulse was ~ 250 joules. With an applied field of intensity E/P = 2 V/cm/torr, the total energy was 9 joules. The energy supplied by the capacitor bank during this light pulse was only 70 joules; the pulse had terminated before the bank was able to deliver the majority of its stored energy. The absolute values of these two emitted-energy measurements may be uncertain by a factor of two, but their relative values should be accurate to ~ 20%.

These data indicate that it is possible to pump xenon gas by an electron-beam-controlled discharge and to excite electronic transitions. There are two important experimental areas

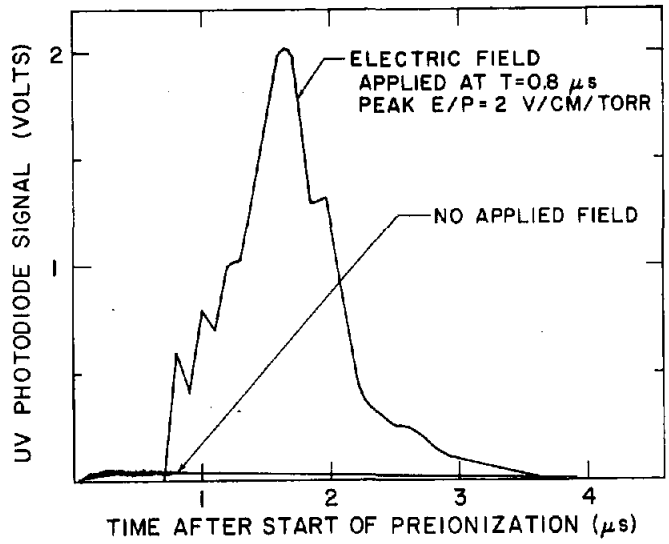

Fig. 62. Typical data exhibiting enhancement of xenon ultraviolet radiation by an applied electric field. The two curves represent the time behavior of ultraviolet intensity with and without an electric field applied to the discharge region.

for extension of these results: (1) further study to determine the discharge parameters that produce maximum enhancement and (2) determination of the feasibility of transferring the excitation energy to laser species such as $O(^1S)$ in the discharge.

2-MeV, 200-kA Electron-Beam Facility

A 2-MeV, 200-kA, 50-ns electron beam system was purchased from Maxwell Laboratories and became operational early in this reporting period. Two cathode-anode structures are available for excitation of gas lasers with electron-beam injection transverse to the optical axis, 50 cm long and 100 cm long. A 10-cm-diameter round cathode is also available; this cathode is used for axial excitation of laser media. Up to a 2-kG magnetic field can be applied for electron-trajectory control with either the 50-cm-long or 10-cm-diameter cathodes. Several segmented calorimeters are available

to study electron-beam transport and energy deposition. The calorimeter data are acquired, stored, and analyzed with a PDP-8E computer.

Over 2500 shots have been made with this system since it became operational. The maintenance time on the system was less than 3 weeks, once the machine became fully operational.

LASER-FUSION RELATED STUDIES

Sandia Glass Laser System

The reconfiguration of the glass-laser system for the amplification of picosecond pulses has been completed, and the spatial and temporal characteristics of the amplified pulse have been examined. Several thousand shots have been obtained since the last progress report.[43] A Quantel short-pulse 1.06-μm YAG oscillator generates the pulse which is beam-split to provide pulses to each of the four distinct laser legs in the glass laser area. The glass laser area is illustrated in Fig. 63. Leg A is a pulsed glass amplifier system for utilization in the X-ray laser experiment. Leg B has been used routinely for the laser-matter interaction studies. Leg C is a holographic laser to be used as a plasma probe in the laser-matter interaction experiment.

The Quantel short-pulse 1.06-μm YAG oscillator is alternately Q-switched or passively mode-locked to provide spatially filtered pulses of several different pulse lengths. Through the use of four separate laser-cavity etalons mounted on a rotating base, the mode-locked pulses are generated at nominally 25, 35, 100, or 200 ps. During Q-switched operation, the TEM_{00} 30-ns pulse can be variably pulse-sliced to provide pulses between 30 and 2 ns. The pulse-slicer can also extract a single pulse from the mode-locked train. Spatial filtering of the beam is accomplished via hard aperture to select the central portion of an Airy pattern. A YAG preamplifier can be adjustably pumped to provide 5-mJ minimum energy for any of the different pulse lengths. The YAG preamplifier was modified to a single-pass configuration when whole-beam self-focusing was discovered for the former double-pass configuration.

The finalized system design and construction of the Sandia glass laser has been realized and is illustrated in Fig. 64. Table 1 of Fig. 64 schematically depicts the Quantel oscillator, while Tables 2 through 4 comprise the Nd^{3+} glass amplifier chain. Using a nominal 3-mJ oscillator energy output, the pulse beam is sent through an expander-collimator and subsequently allowed to overfill a 17-mm-diameter (FWHM) photographic film "soft" aperture. The apodized beam is inserted along the axis of a 25- x 660-mm glass-rod amplifier, passes through a saturable dye cell to reduce the amplified spontaneous emission from the amplifier, and then is enlarged via a 2X expander-collimator. The beam is then sent through the indicated clean-up polarizers, a quartz half-wave plate, diagnostic beam splitter, two pulsed Faraday rotators,[44] another dye cell, and three 45- x 660-mm glass-rod amplifiers. The alignment telescope is inserted during routine servicing and utilizes the many adjustable iris alignment apertures, which were placed on the optic axis between each set of foldback mirrors. A cw YAG laser, located on Table 1 of Fig. 64, may be inserted just prior to the 100% reflector in the Quantel oscillator and transverses the entire system for experimental target alignment purposes. A removable mirror on Table 3 of Fig. 64 allows operation of either the single-beam experiment (leg B), or the three-beam experiment (leg D). The single beam has been split into three nearly equal-energy beams for subsequent amplification by three 45- x 660-mm glass-rod amplifiers arranged in parallel for the X-ray laser experiment. An upper average power flux of 3 GW/cm^2 has been used during operation to minimize self-focusing damage for the picosecond pulse lengths.

The amplifier chain has been operated up to 2.4 J in 50 ps, in compliance with the 3-GW/cm^2 constraint, with no apparent damage. The system has also been operated at 10 ns and up to 20 J. Dielectric mirror damage was experienced under those conditions and

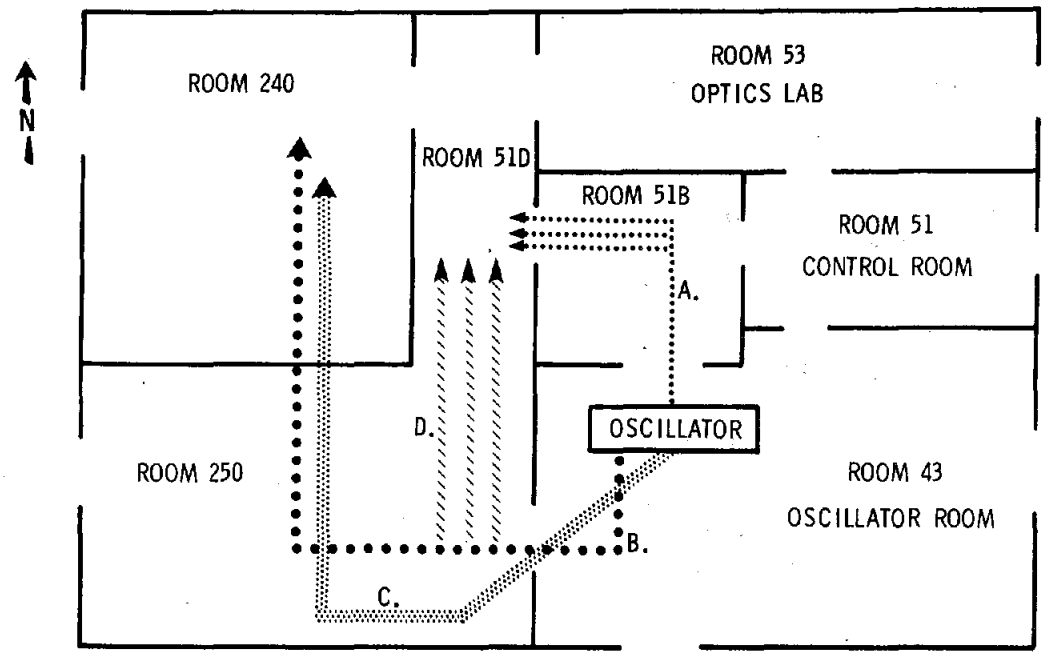

Fig. 63. There are four distinct and independent laser legs. Legs A and D are utilized in the X-ray laser experiment. Legs B and C are used in the laser-matter interaction studies.

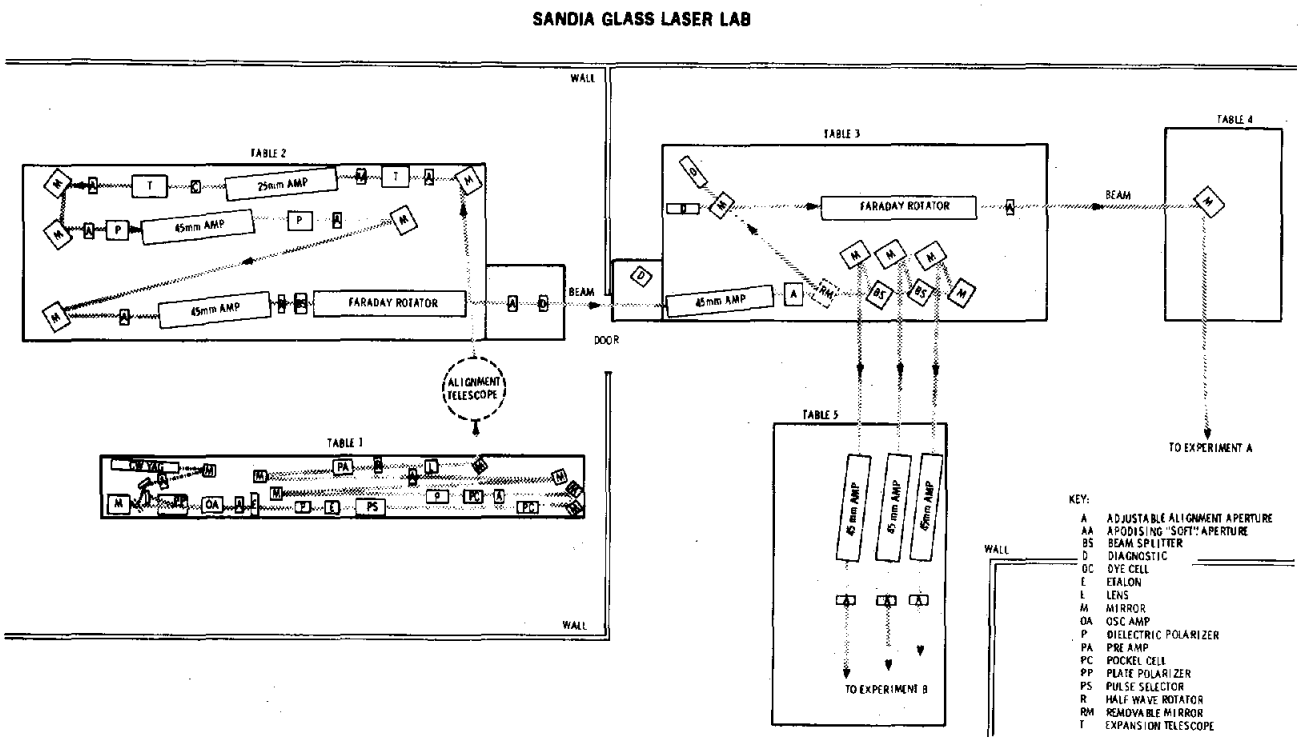

Fig. 64. The tables in this figure illustrate the Quantel short-pulse YAG oscillator and depict the Sandia glass laser amplifier system. The removable mirror on Table 3 of this figure defines the single-beam laser-matter interaction experiment (Leg C) or the three-beam X-ray laser experiment (Leg D).

was probably due to energy absorption with the corresponding average energy flux of 1.3 J/cm^2.

Using an f/4.3 aspheric-corrected lens to focus through several calibrated pinholes of varying diameter, the percentage of transmitted energy versus hole radius has been determined.[45] Figure 65a depicts the experimental results for a 10-ns pulse width operated at an energy up to 20 J. Approximately 60% of the energy was contained inside a pinhole with radius of 30 μm, while there appeared to be no additional energy outside a radius of 200 μm. The cutoff was determined by blocking 90% of the pulse beam, using a metal disk and allowing an accuracy of about 0.1% on the remaining 10%. The data curve of Fig. 65b may be differentiated to determine the intensity distribution of the lens focus. Figure 65b shows a gaussian fit to the differentiated intensity distribution. The gaussian radius R_o, as defined by $I = I_o \exp[-R/R_o]^2$, was found to be 29.8 μm. Figure 66a indicates the fractions of transmitted energy versus pinhole radius when the laser was operated at 50 ps and up to 2.4 J (3 GW/cm^2). Sixty percent of the energy incident on a 50-μm-radius pinhole was transmitted. The corresponding radial intensity distribution for the 50-ps experiment is illustrated by Fig. 66b. A gaussian fit was not attempted for the 50-ps data. The wider focal spot at 50 ps compared with 10 ns may be attributed to some small content of self-focusing for the shorter pulse length. Also, the 50-ps pinhole experiment was performed prior to the results obtained with the collimation tester that indicated the importance of thermal lensing as controlled by a 5-minute system repetition rate.

Facilities to study the extrinsic properties of dielectric material, gas-breakdown thresholds, and laser propagation in materials are being installed. When completed, the system will be useful to perform the above-mentioned studies at 1.06, 0.53, 0.35, and 0.177 μm. The 0.177-μm radiation will be obtained by generating the sixth harmonic of 1.06-μm laser radiation by frequency tripling a frequency-double output for the Nd:glass laser. It is estimated that 800 MW of 1770 Å radiation will be obtainable with our present glass laser as the driver.

This multiple-frequency laser facility will be used to perform propagation studies and evaluate component limitations at wavelengths of interest to and in materials of interest for future high-power laser systems.

Plasma and Solid Conductivity

One of the fundamental considerations in attaining efficient thermonuclear burn with laser-pellet fusion is the ability of plasmas to transport energy from the absorption region to the high-density pellet core. The behavior of these processes depends on wavelength and power density in ways that will clearly impact future laser designs and performance criteria. Preliminary measurements of X-ray emission and ion expansion from solid laser-irradiated targets have suggested the possibility of anomalously low thermal conductivity in laser-produced plasmas. Recently, a systematic measurement of plasma expansions from the front and rear of laser-irradiated thin films has determined the value of laser flux threshold for the onset of reduced thermal conductivity.

A 50-ps Nd:glass-laser pulse was focused with an f/4.3 aspheric lens onto an 1100-Å-thick polystyrene film. The laser energy was varied to provide an incident flux between 10^{13} watts/cm^2 and 3×10^{14} watts/cm^2. The expansion velocities from the front (irradiated side) and the rear of the film were monitored with Faraday cups. In addition, ion species and ion energies in the expanded plasma were monitored with a Thomson parabola. The temporal evolution of the Faraday-cup currents showed the existence of multiple peaks. The first low peaks from the front and first ion peak from the rear of the film had similar velocities for an incident laser flux greater than 7×10^{13} watts/cm^2. The second peaks from the front and the rear, characteristic of thermalized plasma expansions, had similar expansion velocities up to 6×10^{13} watts. Beyond this level, the front expansion velocity increased while that of the rear decreased. This phenomenon is indicative

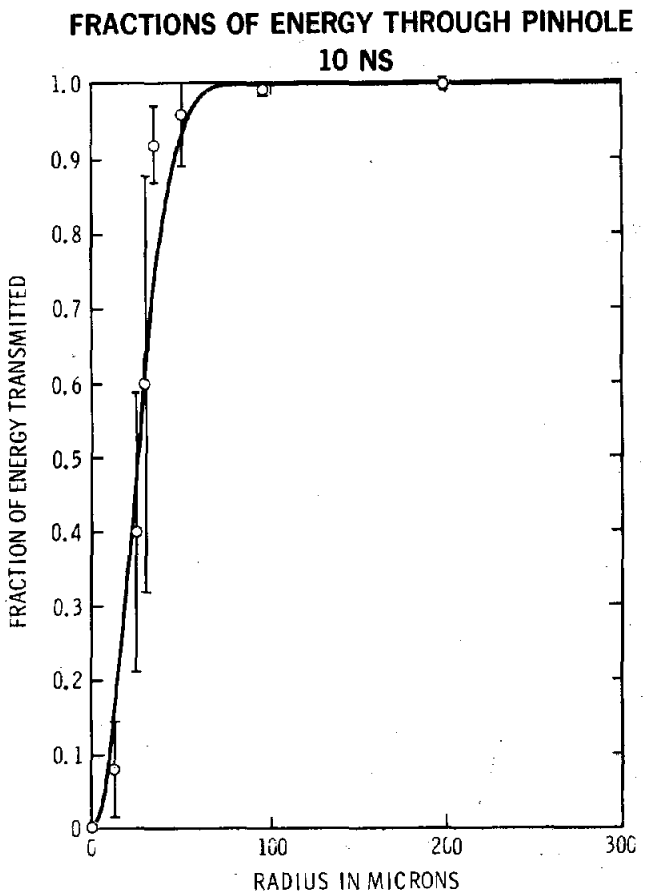

Fig. 65a. The focusability, using an f/4.3 33-cm focal length lens, was determined by monitoring the percentage of transmitted energy incident on a pinhole as a function of pinhole radius for a 10-ns pulse length. Figure 65a shows transmission versus pinhole radius with 60% contained inside a pinhole radius at 30 μm.

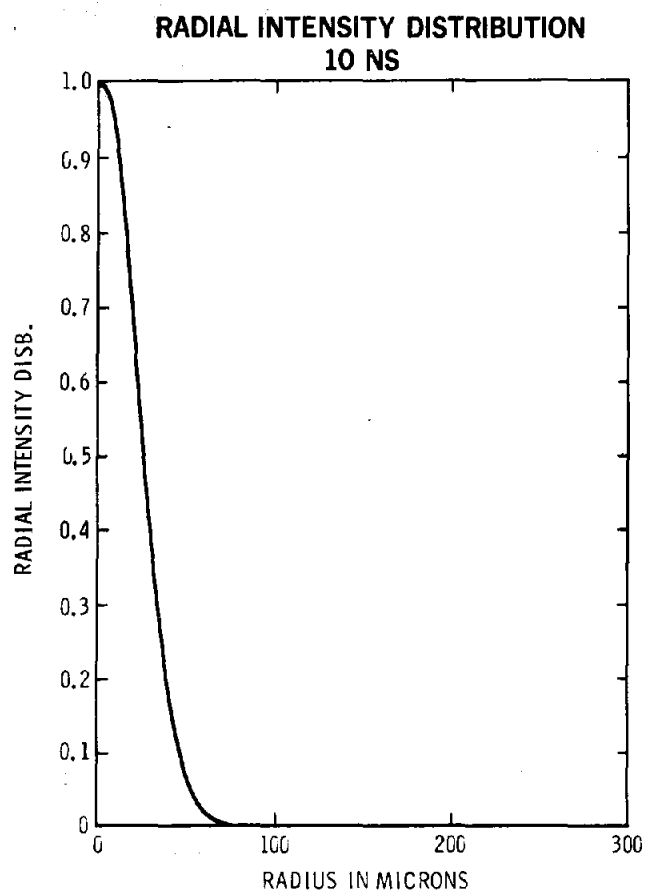

Fig. 65b. Differentiating the data of Fig. 65a yields the corresponding intensity distribution. The computer fit is Gaussian.

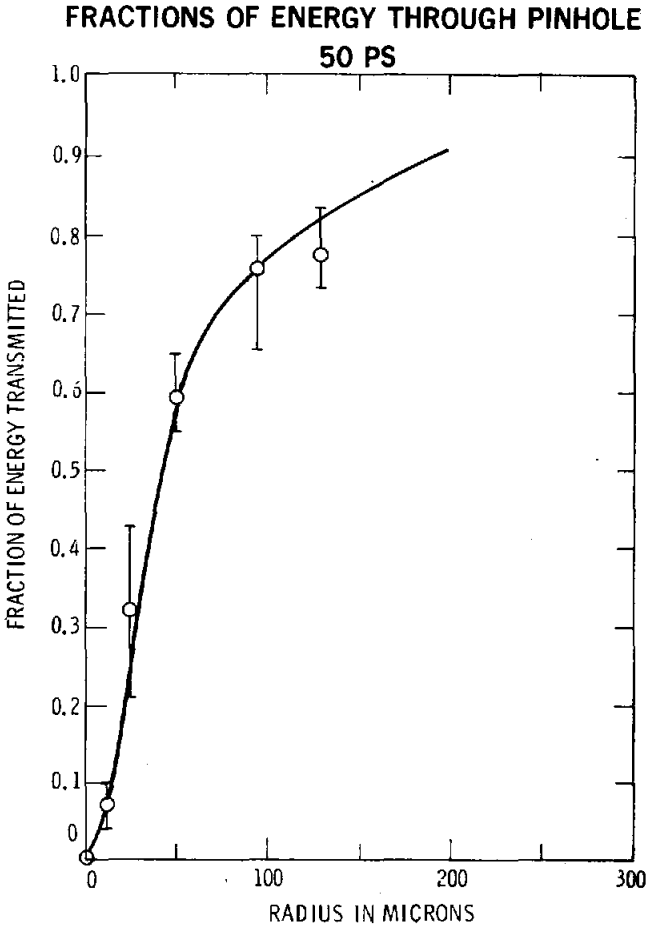

Fig. 66a. The focusability of a 50-ps pulse was also investigated using pinholes. Figure 66a shows that 60% of the incident laser beam was transmitted through a pinhole with 50-μm radius. The focusability degradation for a 50-ps pulse-length was ascribed to some content of small-scale self-focusing.

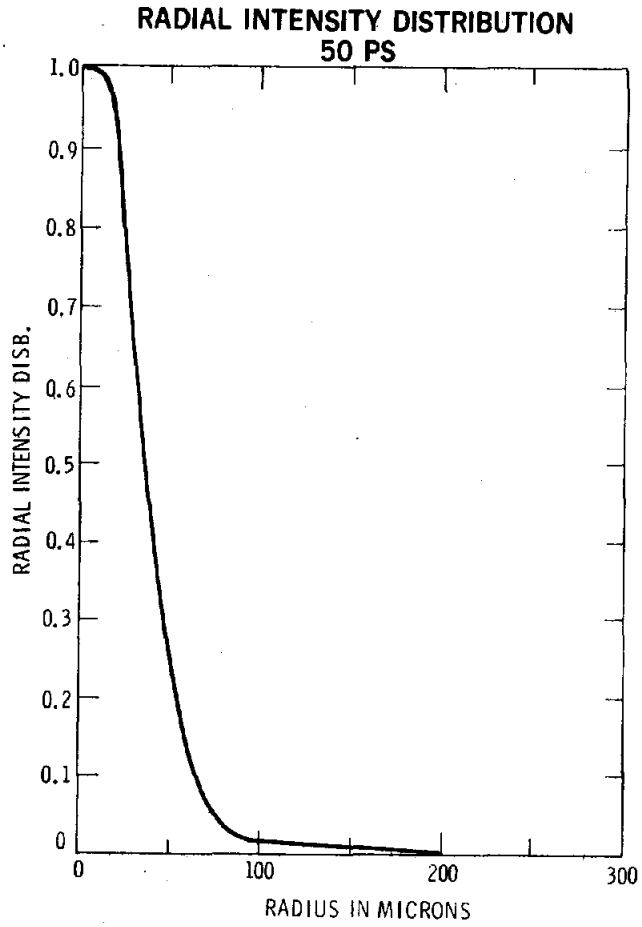

Fig. 66b. The differentiated data illustrate the corresponding intensity distribution for the 50-ps pulse duration.

of reduced thermal transport through the thin polystyrene film.

In a significant number of cases, Faraday-cup traces with triple-peaked current distributions were recorded. The existence of a third peak leads to the possibility of a new interpretation to the multiple-peak structure: an envelope of quasi-Maxwellian shape upon which a resonant oscillation is imposed. Further investigations are under way to evaluate this interpretation.

Energy measurements of the expanding plasmas showed that protons with energies above 200 keV and singly charged carbon ions with energies greater than 100 keV were generated. These high energies appear to be related to the acceleration processes connected with superthermal electrons which are generated by nonlinear absorption. The equal expansion velocities of the front and rear first-current peaks observed with the Faraday cups showed the ability of the superthermal electrons to penetrate through the thin film without significant energy loss. The fact that the first-peak velocities are unequal with laser fluxes below 5×10^{13} watts/cm^2 may imply that the fast electrons experience significant collisional losses in moving through the film at these laser fluxes.

Blast-Shutter Experiment

An experiment was undertaken to measure the opening time of the so-called "blast shutter" currently used as an isolator at Battelle. Pulses 50 ps in duration from an Nd:glass laser were gently focused in vacuum to a spot size of about 3 mm on the blast shutter. The latter consists of a 300 A film of aluminum on 2-mil Mylar. When the laser pulse energy density is between 0.5 and 2 J/cm^2 the aluminum film is clearly removed from the Mylar.

In order to measure how quickly the reflective aluminum film is turned into a gas by the laser pulse, a cw argon laser beam was made to impinge upon the blast shutter. The amount of argon laser light (at 4880 Å) transmitted by the film was monitored by a streak camera with a 50-ps resolution.

The fastest shutter opening time measured this way was ~ 800 ps, which occurred for power densities of the order of 2 J/cm^2. At lower power densities (~ 0.5 J/cm^2), the shutter may take as long as a few nanoseconds to open. After blasting away, the shutter transmission appears to be ~ 80%.

In conclusion, it appears that a blast shutter can open sufficiently fast to remove a "foot" that might precede a 1-ns-type laser pulse used for pellet fusion.

REFERENCES

1. C. M. Ferrar, Appl. Phys. Lett., 12, 381 (1968).

2. K. Hohla, W. Fuss, R. Volk, and K. J. Witte, Opt. Commun., 13, 114 (1975).

3. E. D. Jones and M. A. Palmer, Opt. Quantum Electron., 7, 520 (1975).

4. K. Hohla and K. L. Kompa, Appl. Phys. Lett., 22, 77 (1973).

5. A. E. Sigman and D. J. Kuizenga, Opto-Electron., 6, 43 (1974).

6. D. J. Kuizenga, D. W. Phillion, T. Lund, and A. E. Siegman, Opt. Commun., 9, 221 (1973).

7. W. G. Wagner and B. A. Lengyel, J. Appl. Phys., 34, 2040 (1963).

8. W. Fuss and K. Hohla, Max-Planck Institut Für Plasmaphysik, IPP Report Number IV/67 (1974).

9. T. D. Padrick and R. E. Palmer, J. Chem. Phys., 62, 3350 (1975).

10. D. J. Kuizenga and A. E. Siegman, IEEE J. Quantum Electron., QE-6, 694 (1970).

11. G. Brederlow, K. Hohla, and K. J. Witte, Max-Planck Institut Für Plasmaphysik, IPP Report Number N/74, June 1974.

12. G. M. Birich, G. I. Drozd, V. N. Sorokin, and I. I. Stuk, JETP Lett., 19, 27 (1974).

13. R. J. Donovan and C. Fotakis, J. Chem. Phys., 61, 2159 (1974).

14. J. E. Velasco and D. W. Setser, J. Chem. Phys., 62, 1990 (1975).

15. M. F. Golde and B. A. Thrush, Chem. Phys. Lett., 29, 486 (1974).

16a. B. Liu and H. F. Schaefer, III, J. Chem. Phys., 55, 2369 (1971).

16b. D. H. Liskow, H. F. Schaefer, III, P. S. Bogus, and B. Liu, J. Amer. Chem. Soc., 95, 4056 (1973).

17. D. C. Lorents and R. E. Olson, SRI Project PYU-2018, Semi-Annual Report, December 27, 1972.

18. Electronic Cross-Sections and Macroscopic Coefficients, Vol. 2, Editors: P. Laborie, J. M. Rocard, and J. A. Rees, Dunod, Paris, 1971.

19. F. K. Truby, Phys. Rev., 172, 24 (1968).

20. M. F. Golde and B. A. Thrush, Chem. Phys. Lett., 29, 486 (1974).

21. J. E. Velazco and D. W. Setser, J. Chem. Phys., 62, 1990 (1975).

22. J. J. Ewing and C. A. Brau, Phys. Rev., A12, 129 (1975).

23. M. F. Golde, J. Mol. Spectrosc. (in press).

24. L. A. Gundel, M. A. A. Clyne, J. A. Coxon, and D. W. Setser, Chem. Phys. Lett. (to be submitted).

25. G. Herzberg, Spectra of Diatomic Molecules, Van Nostrand, Princeton, 1950.

26. E. S. Rittner, J. Chem. Phys., 19, 1030 (1951).

27. P. Brumer and M. Karplus, J. Chem. Phys., 58, 3903 (1973).

28. A. Dalgarno, Adv. in Phys., 11, 281 (1962).

29. R. R. Teachout and R. T. Pack, Atomic Data, 3, 195 (1971).

30. J. Tellinghuisen, J. Mol. Spectrosc., 44, 194 (1972).

31. J. Tellinghuisen, Computer Phys. Comm., 6, 221 (1974).

32. J. M. Parson, T. P. Schafer, P. E. Siska, F. P. Tylly, Y. C. Wong, and Y. T. Lee, J. Chem. Phys., 53, 3755 (1970).
J. S. Cohen and R. T. Pack, J. Chem. Phys., 61, 2372 (1974).

33. D. H. Liskow, H. F. Schaefer, III, P. S. Bagus, and B. Liu, J. Am. Chem. Soc., 95, 4056 (1973).

34. M. A. Gusinow, Journal of Applied Physics, 44, 4567 (1973).

35. J. W. Keto, R. E. Gleason, Jr., and G. K. Walters, Phys. Rev. Lett., 33, 1365 (1974).

36. A. Owyoung, Appl. Phys. Lett., 26, 168 (1975).

37. A. Owyoung, Opt. Commun. (to be published).

38. K. R. Prestwich, "Pulse Power Technology Application to Lasers," Electro-Optics '75 International Laser Exposition, Anaheim, California, November 1975.

39. J. B. Gerardo, J. J. Ramirez, R. A. Gerber, E. L. Patterson, and K. R. Prestwich, "Electron-Beam Excitation of Gas Lasers," International Topical Conference on Electron Beam Research and Technology, Albuquerque, New Mexico, November 1975.

40. J. A. Halbleib and W. H. VanDevender, "CYLTRAN: A Cylindrical Geometry Multi-material Electron/Photon Monte Carlo Transport Code," Sandia Laboratories, Albuquerque, New Mexico, SAND74-0030, March 1975.

41. D. L. Johnson, "Untriggered Multichannel Oil Switching," Proceedings of the International Conference on Energy Storage, Compression and Switching, Asti, Italy, 1974 (to be published).

42. K. R. Prestwich, "Harp, a Short Pulse, High Current Electron Beam Accelerator," IEEE Transactions on Nuclear Science, Vol. NS-22, No. 3, June 1975, p. 975.

43. Laser Fusion and Electron-Beam-Fusion Progress Report (U), Sandia Laboratories, Albuquerque, New Mexico, SAND75-0262, July-December 1974.

44. P. J. Brannon and E. D. Jones, Pulsed Faraday Rotator, Sandia Laboratories, Albuquerque, New Mexico, SLA-73-0092, March 1973.

45. P. J. Brannon, J. P. Anthes, G. L. Cano, and J. E. Powell, "Laser Focal Spot Measurements," J. Appl. Phys., 46, 1975, p. 3577.

PUBLICATIONS

RELATIVISTIC ELECTRON BEAM EXCITATION OF GAS LASERS, J. B. Gerardo, R. A. Gerber, E. L. Patterson, and A. Wayne Johnson, Annals of the New York Academy of Sciences 251, 590 (1975).

COMMENT ON "DYNAMIC MODEL OF HIGH-PRESSURE RARE-GAS EXCIMER LASERS," J. B. Gerardo and A. Wayne Johnson, Applied Physics Letters 26, 582 (1975).

XENON-DIMER-LASER NET-GAIN MEASUREMENTS, J. B. Gerardo and A. Wayne Johnson, J. Appl. Phys. 46, 4870 (1975).

ELECTRON-BEAM EXCITATION OF GAS LASERS, J. B. Gerardo, R. A. Gerber, E. L. Patterson, J. J. Ramirez, and K. R. Prestwich, Proceedings of the First International Topical Conference on Electron Beam Research and Technology, Albuquerque, New Mexico, November 3-6, 1975.

MULTIPLET AUGER TRANSITION RATES FOR PARTIALLY FILLED SHELLS, E. J. McGuire, Phys. Rev. A12, 330 (1975).

AUGER SPECTRA OF THE NOBLE GASES, II ARGON, E. J. McGuire, Phys. Rev. A11, 1880 (1975).

AUGER CASCADES IN ALUMINUM, E. J. McGuire, Phys. Rev. A11, 1889 (1975).

SOFT X-RAY AMPLIFIED SPONTANEOUS EMISSION VIA THE AUGER EFFECT, E. J. McGuire, Phys. Rev. Lett. 25, 844 (1975).

N-SHELL AUGER, COSTER-KRONIG TRANSITION RATES IN j-j COUPLING, E. J. McGuire, SAND75-0443, November 1975.

THE DIFFUSION IN ISOTOPIC MIXTURES OF POLYATOMIC GASES I: THE THERMAL DIFFUSION COEFFICIENT, M. K. Matzen, J. Chem. Phys. 62, 500 (1975).

THERMAL DIFFUSION IN ISOTOPIC MIXTURES OF POLYATOMIC GASES II: MODEL CALCULATIONS, M. K. Matzen, J. Chem. Phys. 62, 509 (1975).

TEMPERATURE DEPENDENCE OF THERMAL DIFFUSION IN CO ISOTOPIC GAS MIXTURES, M. K. Matzen with Jerome D. Verlin and D. K. Hoffman, J. Chem. Phys. 62, 4151 (1975).

COLLISION INTEGRALS FOR SOFT, NONSPHERICAL MOLECULES IN TERMS OF SPHERICAL Ω^* INTEGRALS, M. K. Matzen with J. D. Verlin and D. K. Hoffman, J. Chem. Phys. 62, 4146 (1975).

NON-MAXWELLIAN H AND F VELOCITY DISTRIBUTIONS IN AN H_2-F_2 REACTION, M. K. Matzen and M. E. Riley, J. Chem. Phys. 63, 4787 (1975).

THEORETICAL ELECTRON ATOM ELASTIC SCATTERING CROSS SECTIONS FOR SELECTED ELEMENTS FROM 1 keV TO 256 keV, M. E. Riley, C. J. MacCallum, and Frank Biggs, Atomic Data and Nuclear Data Tables 15, 443 (1975).

APPROXIMATIONS FOR THE EXCHANGE POTENTIAL IN ELECTRON SCATTERING, M. E. Riley and Donald G. Truhlar, J. Chem. Phys. 63, 2182 (1975).

CHARACTERISTICS OF A HIGH ENERGY HF LASER INITIATED BY AN INTENSE ELECTRON BEAM, R. A. Gerber and E. L. Patterson, IEEE J. of Quantum Electronics, Vol. QE.-11, No. 8, 642 (1975).

HIGH-ENERGY HF LASER INITIATED BY AN INTENSE ELECTRON BEAM, R. A. Gerber and E. L. Patterson, Sandia Laboratories, Albuquerque, NM, SAND75-0255, August 1975.

ABSOLUTE EMISSION CROSS SECTION FOR N_2^+ (3913 Å) FOR PROTONS INCIDENT ON N_2 GAS, J. M. Hoffman, G. J. Lockwood, and G. H. Miller, Phys. Rev. A11, 841 (1975).

100 MW, 248.4 nm, KrF LASER EXCITED BY AN ELECTRON BEAM, G. C. Tisone, J. M. Hoffman, and A. K. Hays, Optics Communications 15, 188 (1975).

STUDIES OF RARE-GAS HALOGEN MOLECULAR LASERS EXCITED BY AN ELECTRON BEAM, J. M. Hoffman, G. C. Tisone, and A. K. Hays, Proceedings of the Second Summer Colloquium on Electron Transition Lasers, Woods Hole, Mass., September 17-19, 1975.

SIMULTANEOUS Q-SWITCHING AND ACOUSTO-OPTIC MODE-LOCKING OF THE 1.318 μ TRANSITION IN Nd:YAG, E. D. Jones and M. A. Palmer, Opt. Quantum Electron. 7, 520 (1975).

SATURABLE ABSORBERS, E. D. Jones, Sandia Laboratories, Albuquerque, NM, SAND74-0359, January 1975.

EFFICIENT RUBY LASER PUMPED DIFFRACTION LIMITED DYE LASER, A. Owyoung, Opt. Commun. 11, 14 (1974).

INDUCED FOCUSING AND DEFOCUSING OF OPTICAL BEAMS VIA A RAMAN TYPE NONLINEARITY, A. Owyoung, Appl. Phys. Lett. 26, 168 (1975).

A PINHOLE CAMERA FOR PHOTOGRAPHING X RAYS FROM LASER-PRODUCED PLASMAS, J. J. Hohlfelder and M. A. Palmer, Advances in X-Ray Analysis, 18, 136 (1975).

LASER-PLASMA STUDIES OF SOLID PELLETS IRRADIATED WITH THE SANDIA-FOUR-BEAM LASER, J. E. Powell, E. H. Beckner, P. J. Brannon, G. L. Cano, J. J. Cuderman, K. M. Glibert, and M. A. Palmer, Plasma Physics and Controlled Nuclear Fusion Research, 1974, Vol. II, International Atomic Energy Agency, Vienna, 1975.

LASER FOCAL SPOT MEASUREMENTS, P. J. Brannon, J. P. Anthes, G. L. Cano, and J. E. Powell, J. Appl. Phys. 46, 3577 (1975).

REDUCTION OF CLASSICAL THERMAL CONDUCTIVITY UNDER THE INFLUENCE OF HIGH POWER LASERS, Jay S. Pearlman and John P. Anthes, Appl. Phys. Lett. (accepted October 10, 1975).

THOMSON SCATTERING FROM A CO_2 LASER HEATED MAGNETICALLY CONFINED PLASMA, J. S. Pearlman, Z. Pietrayk, and G. Vlases, Appl. Phys. Lett. 26, 3 (1975).

ELECTRO-OPTICS, Encyclopedia of Science and Technology, Revised Edition (McGraw-Hill, New York, 1976), M. A. Duguay (accepted August 19, 1975).

KERR SHUTTERS, Encyclopedia of Science and Technology, Revised Edition (McGraw-Hill, New York, 1976), M. A. Duguay (accepted August 19, 1975).

OBSERVATION OF PICOSECOND X-RAY PULSES, M. A. Duguay and J. N. Olsen, IEEE J. Quantum Electron. QE-10, 642 (1974).

SOFT X-RAY LASERS PUMPED BY PHONOIONIZATION, M. A. Duguay, Proceedings of the Physics of Quantum Electronics Conference, Santa Fe, NM, June 23-July 4, 1975.

THE ULTRAFAST OPTICAL KERR SHUTTER, Progress in Optics (Pergamon Press, New York, 1976, Vol. 14).

SUBNANOSECOND HIGH-PRESSURE IODINE PHOTODISSOCIATION LASER OSCILLATOR, E. D. Jones, M. A. Palmer, and F. R. Franklin, Opt. Quantum Electron (accepted for publication December 1, 1975).

RELATIVE YIELD AND RATE CONSTANTS FOR DECAY OF I^* PRODUCED BY AKYL IODIDE PHOTOLYSIS, T. D. Padrick and R. E. Palmer, Proceedings of the Second Summer Colloquium on Electron Transition Lasers, Woods Hole, Mass., September 17-19, 1975.

STABILITY STUDIES OF H_2-F_2-O_2 MIXTURES AT PRESSURES ABOVE ONE ATMOSPHERE (U) F. K. Truby, Sandia Laboratories, Albuquerque, NM, SAND75-0513, 1975.

POWER FAILURE PROTECTION FOR VACUUM SYSTEMS (U), Gary S. Schuster, RS 5215/003, 1975.

THE ENHANCEMENT OF THE NEAR UV FLASHLAMP SPECTRA WITH SPECIAL EMPHASIS ON THE IODINE PHOTODISSOCIATION LASER, M. A. Gusinow, Opt. Commun. 15, 190 (1975).

NEAR UV SPECTRAL EFFICIENCY OF HIGH-CURRENT XENON FLASHLAMPS, M. A. Gusinow, IEEE J. Quantum Electron (accepted for December 1975 publication).

THE SPECTRAL ENHANCEMENT OF NEAR UV XENON FLASHLAMPS, M. A. Gusinow, Appl. Opt. 14, 2645 (1975).

THE SPECTRAL EFFICIENCY OF PULSED HIGH-CURRENT FLASHLAMPS, M. A. Gusinow, J. Appl. Phys. 46, 4847 (1975).

PRESSURE BROADENING OF THE ATOMIC IODINE $5^2P_{1/2}$ - $5^2P_{3/2}$ TRANSITION, T. D. Padrick and R. E. Palmer, J. Chem. Phys. 62, 3350 (1975).

KINETIC MASS SPECTROMETRY: THE LIMITING EFFECT OF VELOCITY DISTRIBUTIONS ON MEASURED REACTION RATES, J. K. Rice and F. K. Truby, Dynamic Mass Spectrometry, Vol. IV (Heyden & Sons, Lts., London, 1976), Editor: Dennis Price.

ENHANCEMENT BY HELIUM AND ARGON OF THE FORMATION RATE OF THE 1720-Å-RADIATING STATES OF Xe_2 EXCITED BY AN E-BEAM, A. Wayne Johnson and J. K. Rice, accepted for publication in J. Chem. Phys.

CALORIMETRIC DETERMINATION OF BEAM ENERGY, G. H. Miller and G. J. Lockwood, IEEE Trans. on Nucl. Sci., NS-22, No. 3 (June 1975).

SIMULTANEOUS INTEGRAL MEASUREMENT OF ELECTRON ENERGY AND CHARGE ALBEDOES, G. H. Miller, G. J. Lockwood, and J. A. Halbleib, Sr., IEEE Trans. on Nucl. Sci., NS-22, December 1975.

ABSOLUTE DETERMINATION OF BREMSSTRAHLUNG DEPOSITION (HYDRA), G. H. Miller and G. J. Lockwood, Sandia Laboratories, Albuquerque, NM, SAND75-0005, June 1975.

RESPONSE OF IMPROVED HYDRA CALORIMETERS TO BREMSSTRAHLUNG DEPOSITION, G. H. Miller and G. J. Lockwood, Sandia Laboratories, Albuquerque, NM, SAND75-0587, December 1975.

EXPERIMENTAL DETERMINATION OF THE SINGLE PHOTON $2^3S_1 \rightarrow 1^1S_0$ TRANSITION RATE IN HeI, J. R. Woodworth and H. W. Moos, Phys. Rev. A12, 2455 (1975).

PRESENTATIONS

ELECTRON-BEAM-DRIVEN HIGH-POWER HYDROGEN FLUORIDE LASERS, J. B. Gerardo, IIII Quantum Electronics Council & Optical Society of America, Conference on Laser Engineering and Applications, Washington, DC, May 28-30, 1975 (Invited paper).

VUV NOBLE-GAS-DIMER LASERS, J. B. Gerardo, Gordon Research Conference on Nonlinear Optics and Lasers, Plymouth, NH, August 18-22, 1975 (Invited paper).

FORMATION AND DECAY OF XENON DIMERS IN PHOTOEXCITED XENON AND XENON-NOBLE GAS MIXTURES, J. B. Gerardo and A. Wayne Johnson, 28th Annual Gaseous Electronics Conference, University of Missouri, Rolla, MO, October 21-24, 1975.

ELECTRON-BEAM EXCITATION OF GAS LASERS, J. B. Gerardo, R. A. Gerber, E. L. Patterson, K. R. Prestwich, and J. J. Ramirez, The First International Topical Conference on Electron Beam Research and Technology, Albuquerque, NM, November 3-6, 1975.

COLLISION INTEGRALS FOR SOFT, NONSPHERICAL MOLECULES IN TERMS OF SPHERICAL Ω^* INTEGRALS, M. K. Matzen, J. D. Verlin, and D. K. Hoffman, Eighth Midwest Theoretical Chemistry Conference, Madison, WI, May 2, 1975.

TEMPERATURE DEPENDENCE OF THERMAL DIFFUSION IN CO ISOTOPIC GAS MIXTURES, M. K. Matzen, J. D. Verlin, and D. K. Hoffman, Eighth Midwest Theoretical Chemistry Conference, Madison, WI, May 2, 1975.

THE EFFECTS OF NON-MAXWELLIAN H AND F VELOCITY DISTRIBUTIONS IN AN H_2-F_2 REACTION, M. E. Riley and M. K. Matzen, Research Seminar, Los Alamos Scientific Laboratory, Los Alamos, NM, May 1, 1975.

THE EFFECTS OF NON-MAXWELLIAN H AND F VELOCITY DISTRIBUTIONS IN AN H_2-F_2 REACTION, M. K. Matzen and M. E. Riley, 28th Annual Gaseous Electronics Conference, University of Missouri, Rolla, MO, October 21-24, 1975.

APPROXIMATIONS FOR THE EXCHANGE POTENTIAL IN ELECTRON SCATTERING, M. E. Riley and D. G. Truhlar, 8th Midwest Theoretical Chemistry Conference, Midwestern Universities, University of Wisconsin, Madison, WI, May 1-3, 1975.

EULAR-LAGRANGE OPTIMIZATION OF TRANSLATIONAL FACTORS, M. E. Riley and T. A. Green, ICPEAC, Seattle, WA, July 1975.

CHARGE-TRANSFER EXCITATION OF THE N_2^+ - 3914 Å BAND BY VARIOUS IONS, J. M. Hoffman, G. H. Miller, and G. J. Lockwood, Division of Electron and Atomic Physics Meeting of the American Physical Society, Tucson, AZ, December 3-6, 1975.

STUDIES OF RARE-GAS HALOGEN MOLECULAR LASERS EXCITED BY AN ELECTRON BEAM, G. C. Tisone, J. M. Hoffman, and A. K. Hays, Second Summer Colloquium on Electronic Transition Lasers, Woods Hole, MA, September 17-19, 1975.

COLLISIONAL DEACTIVATION OF THE 3427 Å VIBRATIONAL BAND OF THE 3460-3015 Å BAND SYSTEM OF I_2 BY VARIOUS INERT GASES, G. C. Tisone and A. K. Hays, Molecular Spectroscopy Symposium, Ohio State University and the National Science Foundation, Ohio State University, Columbus, OH, June 16-20, 1975.

FUSION: BACKGROUND AND PROSPECTS, J. S. Pearlman, Physics Department Seminar, University of New Mexico, Albuquerque, NM, February 21, 1975.

DISCUSSION OF SOFT X-RAY LASERS PUMPED BY PHOTOIONIZATION, M. A. Duguay, Advanced Research Project Agency, Naval Research Laboratory, Special Seminar, Washington, DC, May 27, 1975 (Invited paper).

DISCUSSION OF SOFT X-RAY LASERS PUMPED BY PHOTOIONIZATION, M. A. Duguay, Research Center on Energy, University of Quebec, Varennes, Montreal, Candada, June 4, 1975 (Invited paper).

SOFT X-RAY LASERS PUMPED BY PHOTOIONIZATION, M. A. Duguay, Physics of Quantum Electronics Conference, Santa Fe, NM, June 23-July 4, 1975 (Invited paper).

REDUCTION OF CLASSICAL THERMAL CONDUCTIVITY UNDER THE INFLUENCE OF HIGH POWER LASERS, J. S. Pearlman, Physics Department Seminar, University of Hull, Hull, England, August 15, 1975 (Invited presentation).

A TWO-BEAM INTERFEROMETRIC TECHNIQUE FOR STUDYING THE NONLINEAR SUSCEPTIBILITY, χ_3, A. Owyoung, Gordon Conference on Nonlinear Optics and Lasers, Plymouth, NH, August 18-22, 1975.

SOFT X-RAY LASERS, M. A. Duguay, Gordon Research Conference on Laser Interaction with Matter, Tilton School, Tilton, NH, August 18-22, 1975 (Invited paper).

DISCUSSION OF SOFT X-RAY LASERS PUMPED BY PHOTOIONIZATION, M. A. Duguay, Gordon Research Conference on Nonlinear Optics, Plymouth, NH, August 18-22, 1975 (Invited paper).

REDUCTION OF CLASSICAL THERMAL CONDUCTIVITY UNDER THE INFLUENCE OF HIGH POWER LASERS, J. S. Pearlman, XIIth International Conference on Phenomena in Ionized Gases, Eindhoven, The Netherlands, August 23, 1975.

REDUCTION OF CLASSICAL THERMAL CONDUCTIVITY UNDER THE INFLUENCE OF HIGH LASERS, J. S. Pearlman, Special Seminar, Max-Planck Institut Für Physik, Garching, Germany, September 8, 1975 (Invited paper).

LASER INTERACTION WITH POLYSTYRENE FILMS, J. S. Pearlman, Special Seminar, Los Alamos Scientific Laboratory, Los Alamos, NM, October 2, 1975.

INTERACTION OF HIGH-POWER LASER RADIATION WITH THIN POLYSTYRENE FILMS, Jay S. Pearlman and John P. Anthes, Seventeenth Annual Meeting of the American Physical Society, Division of Plasma Physics, St. Petersburg, FL, November 10-14, 1975.

SUBNANOSECOND HIGH-PRESSURE IODINE PHOTODISSOCIATION LASER OSCILLATOR, E. D. Jones, Special Seminar, Physics Department, University of Michigan, Ann Arbor, MI, November 17, 1975 (Invited paper).

MODE-LOCKING AND THE IODINE-PHOTODISSOCIATION LASER, E. D. Jones, Special Seminar, Physics Department, Naval Research Laboratory, Washington, DC, December 4, 1975 (Invited paper).

MODE-LOCKING AND THE IODINE-PHOTODISSOCIATION LASER, E. D. Jones, Special Seminar, Division of Physics, National Research Council of Canada, Ottawa, Canada, December 5, 1975 (Invited paper).

APPLICATION OF MOLECULAR BEAM TECHNIQUES TO THE STUDY OF ENERGY TRANSFER IN UNIMOLECULAR SYSTEMS, G. A. Fisk, American Chemical Society Meeting, Chicago, IL, August 24-29, 1975 (Invited paper).

MOLECULAR IODINE LASER NEAR 3400 Å, A. K. Hays, J. M. Hoffman, and G. C. Tisone, Second Summer Colloquium on Electronic Transition Lasers, Marine Biology Laboratory Conference Center, Woods Hole, MA, September 17-19, 1975.

100 M WATT KrF LASER AT 2484 Å, A. K. Hays, G. C. Tisone, and J. M. Hoffman, Gordon Conference on Nonlinear Optics and Lasers, Plymouth, NH, August 18-22, 1975.

RELATIVE YIELD AND RATE CONSTANTS FOR DECAY OF I^* PRODUCED BY ALKYL IODIDE PHOTOLYSIS, T. D. Padrick and R. E. Palmer, Second Summer Colloquium on Electronic Transition Lasers, Marine Biology Laboratory Conference Center, Woods Hole, MA, September 17-19, 1975.

LASING AT 5578.5 Å IN E-BEAM EXCITED Kr/O_2 MIXTURES, A. Wayne Johnson, F. W. Bingham, and J. K. Rice, IEEE/OSA Conference on Laser Engineering and Applications, Washington, DC, May 28-30, 1975.

PROBLEMS IN THE PRODUCTION OF HIGH-POWER VACUUM-ULTRA-VIOLET LASERS, A. Wayne Johnson, IV Vavilov Conference on Nonlinear Optics, Novosibirsk, USSR, June 10-13, 1975.

ELECTRON-BEAM-EXCITED GAS LASER RESEARCH, A. Wayne Johnson, J. B. Gerardo, R. A. Gerber, E. L. Patterson, F. W. Bingham, and J. K. Rice, Second All-Union Symposium on Gas Laser Physics, Novosibirsk, USSR, June 16-18, 1975.

FORMATION OF XENON DIMERS IN ELECTRON-BEAM-EXCITED XENON AND XENON-NOBLE-GAS MIXTURES, A. Wayne Johnson and J. K. Rice, Twenty-Eighth Annual Gaseous Electronics Conference, University of Missouri, Rolla, MO, October 21-24, 1975.

SIMULTANEOUS INTEGRAL MEASUREMENT OF ELECTRON ENERGY AND CHARGE ALBEDOES, G. H. Miller, G. J. Lockwood, and J. A. Halbleib, Sr., Annual Conference on Nuclear and Space Radiation Effects, Arcata, CA, July 14-17, 1975.

THE OBSERVATION OF Kr:S(^{1}S) EMISSION NEAR 7725 Å IN ELECTRON-BEAM-EXCITED MIXTURES OF HIGH-PRESSURE KRYPTON AND COS, J. K. Rice, Washington Meeting of the American Physical Society, Washington, DC, April 28-May 1, 1975.

ELECTRON-BEAM EXCITATION OF RARE-GAS-HYDROGEN MIXTURES, J. K. Rice and A. Wayne Johnson, 28th Annual Gaseous Electronics Conference, University of Missouri, Rolla, MO, October 21-25, 1975.

FLUORESCENCE EMISSIONS FROM MIXTURES OF MERCURY AND XENON, J. R. Woodworth, 28th Annual Gaseous Electronics Conference, University of Missouri, Rolla, MO, October 21-24, 1975.

DISTRIBUTION:
TID-4500-R64 UC-21 (189)

ERDA (16)
USERDA/NS
Washington, DC 20545
Attn: Lt. Gen. A. D. Starbird
C. Martin Stickley (10)
Dr. L. E. Killion
R. Schriever
G. W. Kuswa
Maj. Gen. J. K. Bratton
Dr. F. C. Gilbert

ERDA (4)
USERDA/AE
Washington, DC 20545
Attn: R. L. Hirsch
Bennett Miller
K. Moses
J. Decker

ERDA
Albuquerque Operations Office
P.O. Box 5400
Albuquerque, NM 87115
Attn: H. E. Roser, Mgr.

ERDA
San Francisco Operations Office
University of California
Lawrence Berkeley Laboratory
Berkeley, CA 94720

Los Alamos Scientific Laboratory (5)
P.O. Box 1663
Los Alamos, NM 87544
Attn: K. Boyer

University of California (7)
Lawrence Livermore Laboratory
P.O. Box 808
Livermore, CA 94550
Attn: C. Haussmann
J. Emmett (5)
J. Nuckolls

B. D. Fried, Dept. of Physics
University of California
Los Angeles, CA 90024

W. P. Kovacik,
Laser Fusion, Westinghouse Elec. Corp.
Research Laboratories
Pittsburgh, PA 15235

J. Dawson
University of California
Los Angeles, CA 90024

N. Rostoker
University of California
Irvine, CA 92664

R. Sudan
Cornell University
Ithaca, NY 14850

R. Gould
California Institute of Technology
Pasadena, CA 91109

K. Brueckner
University of California at La Jolla
La Jolla, CA 92037

G. Pimental
University of California
Berkeley, CA 94720

J. Marburger
University of Southern California
Los Angeles, CA 90007

A. Yariv
Cal Tech
Department of Physics
Pasadena, CA 91109

Robert Cooper
Office of Director of Defense
Research and Engineering
Room 3E1006, The Pentagon
Washington, DC 20301

Robert B. Watson
Chief, Research and Development
Department of the Army
The Pentagon
Washington, DC 20301

Advanced Research Projects Agency (3)
1400 Wilson Blvd.
Arlington, VA 22209
Attn: Dr. E. Gerry
Dr. P. Clark
Lt. Col. R. Sullivan

DISTRIBUTION (cont):

P. Haas (3)
Defense Nuclear Agency
Washington, DC 20305
Attn: G. Soper

Col. R. K. Parson
Hq. USAF (RDCCO)
DCS/Research and Development
Washington, DC 20330

Col. O. R. Cunningham, USAF (2)
Air Force Weapons Laboratory (DOUA)
Kirtland AFB, NM 87117
Attn: Col. J. Rich

A. H. Guenther
Air Force Weapons Laboratory (DOUA)
Kirtland AFB, NM 87117

C. Longmire
Mission Research Institute
Santa Barbara, CA 93102

M. Lubin (5)
University of Rochester
Rochester, NY 14627

Henry Gomberg (2)
KMS Fusion, Inc.
Ann Arbor, MI 48106

John P. Hallowes
Physical Sciences Director
U.S. Army Missile Command
Redstone Arsenal, AL 35809

Capt. J. G. Wilson
USN (PMO-405)
Naval Ordnance Systems Command
Department of the Navy
Washington, DC 20360

Walter R. Sooy
U.S. Naval Research Laboratory
Washington, DC 20390

A. Javan
Massachusetts Institute of Technology
Cambridge, MA 02139

R. Gross
Columbia University
New York, NY 10027

S. J. Buchsbaum
Bell Laboratories
Murray Hill, NJ 07974

A. M. Clogston
Bell Laboratories
Murray Hill, NJ 07974

Joseph A. Giordmaine
Bell Laboratories
Murray Hill, NJ 07974

C. K. N. Patel
Bell Laboratories
Holmdel, NJ 07733

Electric Power Research Institute (3)
3412 Hillview Avenue
Palo Alto, CA 94306
Attn: R. E. Bolzhiser
N. Amherd
W. Gough

P. Persiani
Argonne National Laboratory
Argonne, IL 60439

A. J. DeMaria
United Aircraft Research Labs.
East Hartford, CT 01608

W. B. Bridges
Hughes Research Labs.
Malibu, CA 90265

A. Schawlow
Physics Department
Stanford University
Stanford, CA 94305

A. Siegman
Microwave Laboratory
Stanford University
Stanford, CA 94305

Mrs. Margaret King, Culham Laboratory
UKAEA Research Group
Abingdon Oxfordshire OX14 3DB
England

DISTRIBUTION (cont):

S. E. Harris
Microwave Laboratory
Stanford University
Stanford, CA 94305

M. D. Scully
University of Arizona
Tucson, AZ 85721

Bruce J. Mann, Chief
Evaluation Branch
Office of Radiation Programs, LVF
Nat'l Environmental Research Center
P.O. Box 15027
Las Vegas, NV 89114

LaMoyle Masters, AEC Library
Battelle Laboratories
505 King Avenue
Columbus, OH 43201

P. Mallozzi
Battelle Laboratories
505 King Avenue
Columbus, OH 43201

O. M. Friedrich, Jr., Ass't Dir.
Electronics Research Center
College of Engineering
University of Texas at Austin
Austin, TX 78712

W. Drummond
University of Texas
Austin, TX 78712

J. Verdeyn
University of Illinois
Urbana, IL 61801

Harry Diamond Laboratories (2)
Washington, DC 20438
Attn: Dr. Robert Oswald
Mr. S. Greybill

Director
Naval Research Laboratory (2)
Washington, DC 20375
Attn: R. Shanny
G. Cooperstein

Maxwell Laboratories (2)
9244 Balboa Avenue
San Diego, CA 92123
Attn: A. Kolb
P. Korn

Pacific-Sierra Research Corporation
1456 Cloverfield Blvd.
Santa Monica, CA 90404
Attn: Mr. J. Wyatt

Physics International (3)
2700 Merced Street
San Leandro, CA 94577
Attn: I. Smith
S. Putnam
J. Bailey

R&D Associates (2)
P.O. Box 3580
Santa Monica, CA 90403
Attn: Dr. B. Hartenbaum
Dr. C. McDonald

D. J. Bradley
Imperial College of Science and Technology
London, England

S. A. Ramsden
University of Hull
Hull, England

F. T. Arecchi
C.I.S.E. Laboratories
Milano, Italy

W. Kaiser
Technische Universitat
Munchen, Germany

C. Yamanaka
Institute of Laser Engineering
Osaka University
Osaka 565, Japan

Atomic Weapons Research
Establishment (2)
Aldermasten, England
Attn: J. C. Martin
John Weale

DISTRIBUTION (cont):

1	M. Sparks
1000	G. A. Fowler
1100	C. D. Broyles
1200	W. A. Gardner
1300	D. B. Shuster
2000	E. D. Reed
2100	W. J. Spencer
2300	L. D. Smith
2500	J. C. King
2600	L. E. Hollingsworth
3145	L. S. Ostrander
3600	L. J. Heilman
4010	C. Winter
4300	R. L. Peurifoy
5000	A. Narath
5100	J. K. Galt
5110	F. L. Vook
5120	G. J. Simmons
5130	G. A. Samara
5150	J. E. Schirber
5160	W. Herrmann
5200	E. H. Beckner (30)
5210	J. B. Gerardo (10)
5211	E. J. McGuire
5212	R. A. Gerber
5214	E. D. Jones
5215	M. A. Gusinow
5216	A. W. Johnson
5230	M. Cowan
5231	J. H. Renken
5232	L. D. Posey
5233	M. J. Forrestal
5240	G. Yonas (30)
5241	J. R. Freeman (20)
5242	A. J. Toepfer
5245	T. H. Martin
5260	K. J. Touryan
5261	T. A. Green
5262	R. A. Hill
5400	A. W. Snyder
5420	J. V. Walker
5421	H. R. Schmidt
5422	R. L. Coats
5423	J. E. Powell
5424	J. A. Reuscher
5700	J. H. Scott
5800	R. S. Claassen
8000	T. B. Cook, Jr.
8100	L. Gutierrez
8200	C. H. DeSelm
8300	B. F. Murphey
8334	W. Bauer
9000	R. A. Bice
9300	L. H. Hopkins, Jr.
8266	E. A. Aas (2)
3141	C. A. Pepmueller (Actg) (5)
3151	W. L. Garner (3)
	For ERDA/TIC (Unlimited Release)